ornl

ORNL/TM-12967

OAK RIDGE NATIONAL LABORATORY

MARTIN MARIETTA

Neutronic Analysis of Three-Element Core Configurations for the Advanced Neutron Source Reactor

J. C. Gehin

August 1995

Advanced Neutron Source

MANAGED BY
MARTIN MARIETTA ENERGY SYSTEMS, INC.
FOR THE UNITED STATES
DEPARTMENT OF ENERGY

ORNL/TM-12967

Computational Physics and Engineering Division

NEUTRONIC ANALYSIS OF THREE-ELEMENT CORE CONFIGURATIONS FOR THE ADVANCED NEUTRON SOURCE REACTOR

J. C. Gehin

Date Published—August 1995

Prepared by the
OAK RIDGE NATIONAL LABORATORY
Oak Ridge, Tennessee 37831
managed by
LOCKHEED MARTIN ENERGY SYSTEMS, INC.
for the
U.S. DEPARTMENT OF ENERGY
under contract DE-AC05-84OR21400

CONTENTS

LIST OF FIGURES

LIST OF TABLES

ABSTRACT

Calculations of several important neutronic parameters have been performed for ten different three-element configurations considered for the Advanced Neutron Source (ANS) Reactor. Six of these configurations (labeled ST, SB, MT, MB, LT, and LB) are the result of the permutations of the same three elements. Two configurations (ST-MOD and SB-MOD) have the same element configuration as their base core design (ST and SB) but have slightly different element dimensions, and two configurations (ST-OL1 and ST-OL2) have two overlapping elements to increase the neutron fluxes in the reflector. For each configuration, in addition to the conceptual two-element design, fuel-cycle calculations were performed with calculations required to obtain unperturbed fluxes. The element power densities, peak thermal neutron flux as a function of position throughout the cycle, fast flux, fast-to-thermal flux ratios, irradiation and production region fluxes, and control rod worth curves were determined. The effective multiplication factor for each fuel element was also computed to assess the impact that changing to a three-element design has on fuel element criticality. A comparison shows that the ST core configurations have the best overall performance, and the fully overlapping core configuration ST-OL2 has the best performance by a large margin. Therefore, on the basis of the neutronics results, the fully overlapping configuration is recommended for further consideration in using a three-element ANS reactor core. Other considerations such as thermal-hydraulics, safety, and engineering that are not directly related to the core neutronic performance must be weighed before a final design is chosen.

ACRONYMS

ANS	Advanced Neutron Source
BOC	beginning of cycle
CPBT	core pressure boundary tube
EOC	end of cycle
HFIR	High Flux Isotope Reactor
MOC	middle of cycle
ORNL	Oak Ridge National Laboratory
pcm	percent mille
ST, SB MT, MB LT, LB	Three-element core configurations; the first letter indicates the size of the element in the central location (small, medium, large), second letter indicates the location (top, bottom) of the larger of the two remaining elements
ST-MOD	Three-element core configuration with the same layout as ST but with modified element dimensions
SB-MOD	Three-element core configuration with the same layout as SB but with modified element dimensions
ST-OL1	Three-element core configuration with the same basic configuration as ST but with the upper element lowered to a half-overlap position with the central element
ST-OL2	Three-element core configuration with the same basic configuration as ST but with theupper element lowered to a full-overlap position with the central element

1. INTRODUCTION

The Advanced Neutron Source (ANS) is a neutron research facility being designed at Oak Ridge National Laboratory (ORNL). This facility's purpose is to provide unprecedented experimental capabilities in the areas of neutron scattering, materials research, and isotope production. The primary goals of the ANS project are to obtain neutron flux levels for beam experiments 5 to 10 times larger than available at the current best existing facilities and to provide isotope irradiation facilities that are at least as good as the High Flux Isotope Reactor (HFIR) at ORNL.

The ANS conceptual design[1] consists of a 330-MW_f nuclear reactor with highly enriched fuel that is cooled, moderated, and reflected with heavy water. Throughout the evolution of the project, however, many different designs have been considered. The current two-element configuration was chosen as a compromise design that optimizes the neutron flux and the safety margins.

In recent ANS fuel enrichment studies,[2,3] three-element core configurations were considered as a means of increasing the core volume to allow the use of lower-enriched fuels. In the course of the analysis, certain potential advantages of a three-element configuration became apparent. If the core power is held constant, an increase in the core volume may allow the use of lower-enriched fuels, an increased cycle length, and a lower power density. The heated length of each element can be shortened, thereby lowering the coolant exit temperatures and improving thermal-hydraulic conditions. Increasing the number of elements will also lower the possibility of fuel-element criticality during the refueling procedures. In addition, the in-core isotope production and irradiation regions may be placed downstream of the fuel elements, lowering the possibility of a flow blockage. In general, the flexibility and safety margins will be improved.

There are, however, severe disadvantages to the three-element configuration. The primary disadvantage is that an increase in the core volume directly leads to a decrease in the neutron flux that can be obtained. In addition, an increase in the size of the core may lead to changes in the size of the core pressure boundary, the control rod designs, and experimental facility placement.

This report presents the results of the analysis of several different three-element core configurations to determine the configuration that has the best neutronic performance characteristics. In Chap. 2 the two-element conceptual design is presented, and the three-element core configurations are discussed. The calculational methods that were used are presented in Chap. 3, and the results are given in Chap. 4. The conclusions of this study are given in Chap. 5.

2. CORE GEOMETRY DESCRIPTIONS

2.1 INTRODUCTION

This chapter presents the descriptions of the core geometries. First, the conceptual two-element core geometry and parameters are given. Next, the different three-element configurations are discussed, and finally, an overlapping core concept is presented.

2.2 TWO-ELEMENT CONCEPTUAL DESIGN

The ANS conceptual design baseline[1] was the two-element core configuration presented in Fig. 2.1. The core consists of two offset annular fuel elements containing involute-shaped fuel plates, as shown in Fig. 2.2, attached to inner and outer side plates. The upper element contains 432 such plates, and the lower element contains 252 plates. The plates are 1.27 mm thick and are separated by 1.27-mm coolant channels. The individual plates consist of highly enriched uranium- silicide/aluminum fuel, an aluminum filler region, and 0.254-mm-thick aluminum cladding. The thickness of the fuel meat is continuously graded in both the axial and radial directions to minimize power peaking. The 10-mm unfueled endcap regions at the top and bottom of each element contain boron carbide burnable absorber to hold down the core reactivity at the beginning of the cycle and to provide power shaping throughout the 17-d fuel cycle. The reactor operates at a power of 330 MW_f and is cooled by heavy water.

Reactivity is controlled by three hafnium control rods located in the central hole of the fuel elements. In the two-element configuration, the hafnium is 1.2 m long and is attached to a support rod. The central control rods are driven from below and are withdrawn in an upward direction during the fuel cycle. At full insertion, the active hafnium region is symmetrically positioned about the midplane of the core. In addition to reactivity control, the central control rods also serve as the primary shutdown system. An additional independent shutdown system, consisting of eight hafnium rods, is located in the heavy water reflector.

The high-pressure core inlet (3.2 MPa) is separated from the heavy water reflector by a double-walled aluminum core pressure boundary tube (CPBT). The reflector contains experimental facilities and irradiation positions. Figure 2.3 shows a horizontal view of the reflector facilities layout. In addition, in-core irradiation facilities are located inside the upper fuel element, and in-core transuranic isotope production facilities are positioned outside the lower fuel element.

2.3 THREE-ELEMENT CORE CONFIGURATIONS

In this study, several different three-element core configurations were considered with elements that are similar in design to the elements of the two-element configuration. The heated length, however, is decreased from 507 to 418 mm, the optimal length for a three-element configuration.[4,5] The basic configuration is identical to that used in the ANS fuel-enrichment study[2] and a recent parameter study[3] and is shown in Fig. 2.4. In this design the active core volume is increased from the two-element size of 67.6 to 82.6 L, which is the optimal volume (in terms of maximizing flux and safety margins) for this core configuration.[4,5] The three elements are sized so that, viewed axially, they do not overlap, and so each element has its own coolant stream. The radial dimensions of the elements were chosen to ensure fuel-plate stability. Because a fuel grading has not been developed for the three-element configuration, a

uniform grading was used. This is acceptable because calculations show that fuel grading has only a small impact on reactivity and neutron flux.

With three fuel elements there are six different possible element configurations. In this study all six configurations are examined. The nomenclature adopted for the different core configurations is a two-letter name in which the first letter indicates the size of the element located in the center (small, medium, or large—S, M, or L), and the second letter indicates the location of the larger of the two remaining elements (top or bottom—T or B). Therefore, the configuration that was studied in the ANS fuel enrichment study is characterized as configuration ST. The six different configurations and their two-letter names are shown in Fig. 2.5. Note that three of the configurations (SB, MB, and LB) are mirror images of other configurations (ST, MT, and LT) and would give identical results in the absence of the central control rods and the reflector components. However, since the control rods and reflector components are not situated in axially symmetric locations, all six configurations will actually have differing behaviors during the fuel cycle.

Because of the wider and taller core, the CPBT is larger, and the hafnium length was increased to 1.5 m. All other aspects of the core, besides those mentioned previously remain unchanged from the two-element conceptual core design.

2.4 ALTERNATE THREE-ELEMENT CORE CONFIGURATIONS

In addition to the six basic three-element configurations (ST, SB, MT, MB, LT, LB), the ST and SB core configurations with element sizes slightly modified to increase the fuel-plate stability were also considered. These configurations are labeled ST-MOD and SB-MOD. The core dimensions for the ST-MOD configuration are shown in Fig. 2.6. The SB-MOD configuration has the same element dimensions as ST-MOD, but it has the top and bottom elements reversed. These alternate element dimensions result in a very slightly larger core volume of 82.8 L.

As previously mentioned, as the core volume increases, the thermal flux in the reflector decreases, and the peak thermal flux in the reflector of the three-element core configuration is lower than that of the two-element design. For a given power level, the thermal flux in the reflector is approximately inversely proportional to the core surface area. Therefore, if the effective surface area of the three-element core can be reduced, the thermal flux in the reflector will increase. This can be accomplished in the ST configuration by lowering the upper element so that it overlaps the middle element, as shown in Fig. 2.7. Therefore, two additional core configurations, based on the ST configuration, with the upper element halfway (ST-OL1) and fully overlapping (ST-OL2) the middle element were analyzed. Note that overlapping the elements in this fashion is mechanically possible only in configurations in which the overlapped elements do not have a common wall. The midplane of the overlapping core configuration is at the axial center of the central element, the same position as the nonoverlapping configurations.

2.5 SUMMARY

In this chapter descriptions of the two-element conceptual core configuration and ten different three-element core configurations were presented. The three-element designs consist of six different configurations of elements (ST, SB, MT, MB, LT, and LB), two additional configurations with slightly different element dimensions (ST-MOD and SB-MOD), and two overlapping configurations (ST-OL1 and ST-OL2).

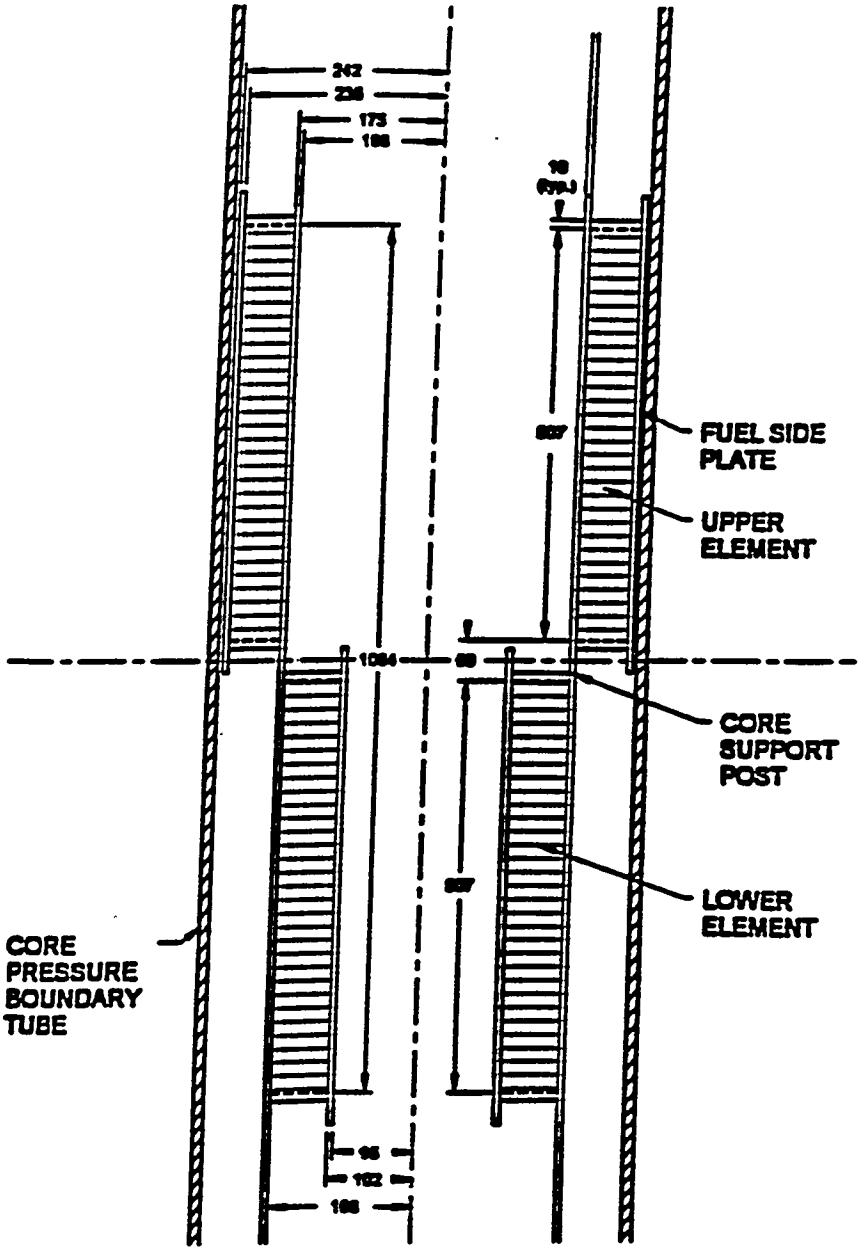

Fig. 2.1. ANS conceptual two-element core configuration.

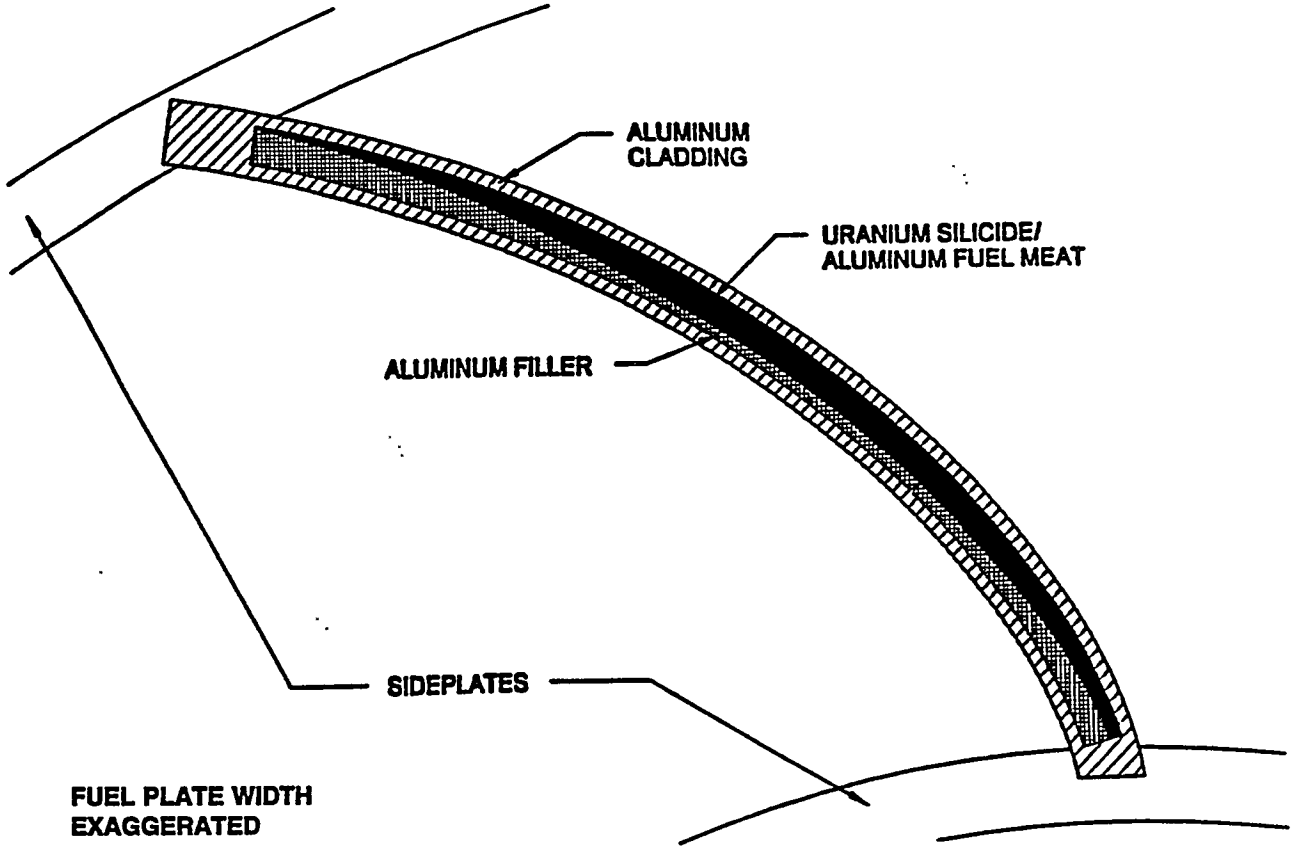

Fig. 2.2. Cross section of an ANS fuel plate.

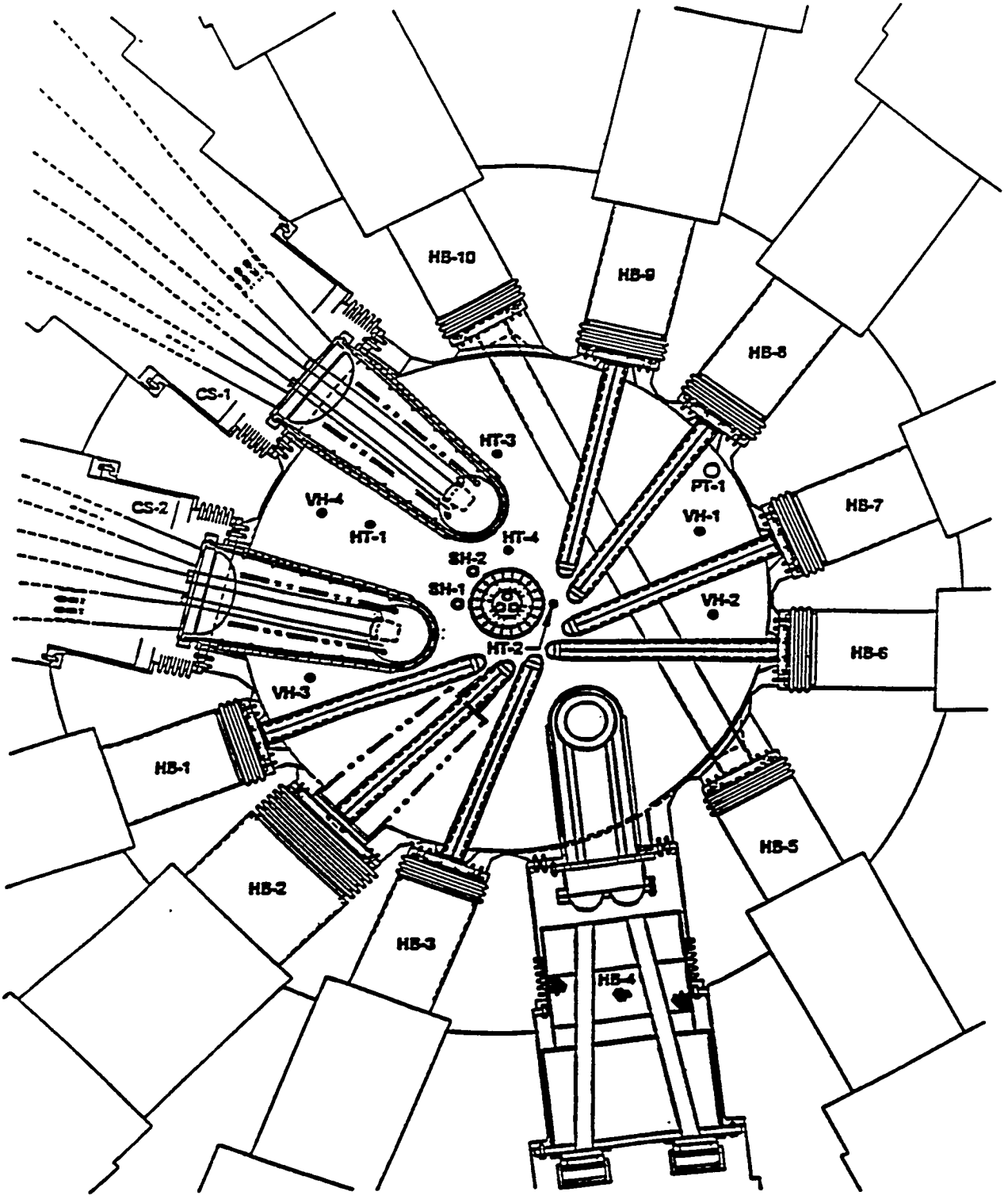

Fig. 2.3. Horizontal cross-sectional view of conceptual design showing the layout of the reflector components.

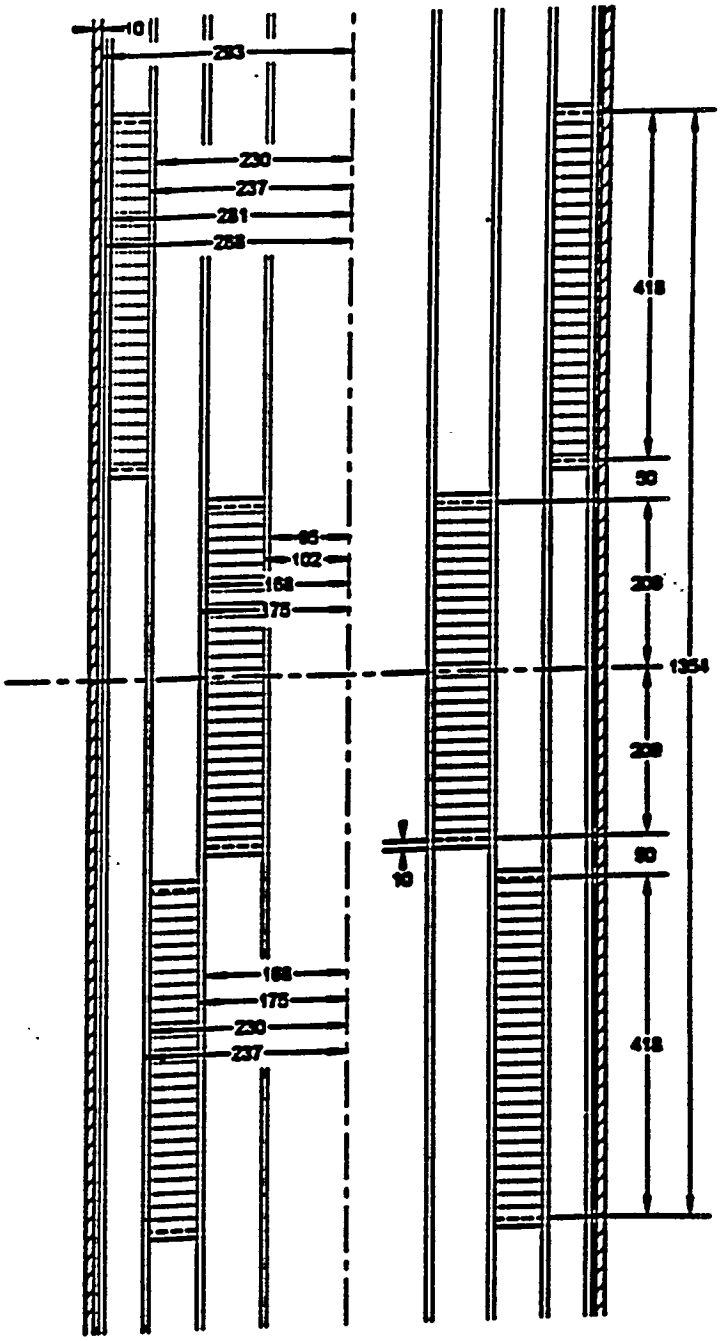

Fig. 2.4. Three-element ST core configuration.

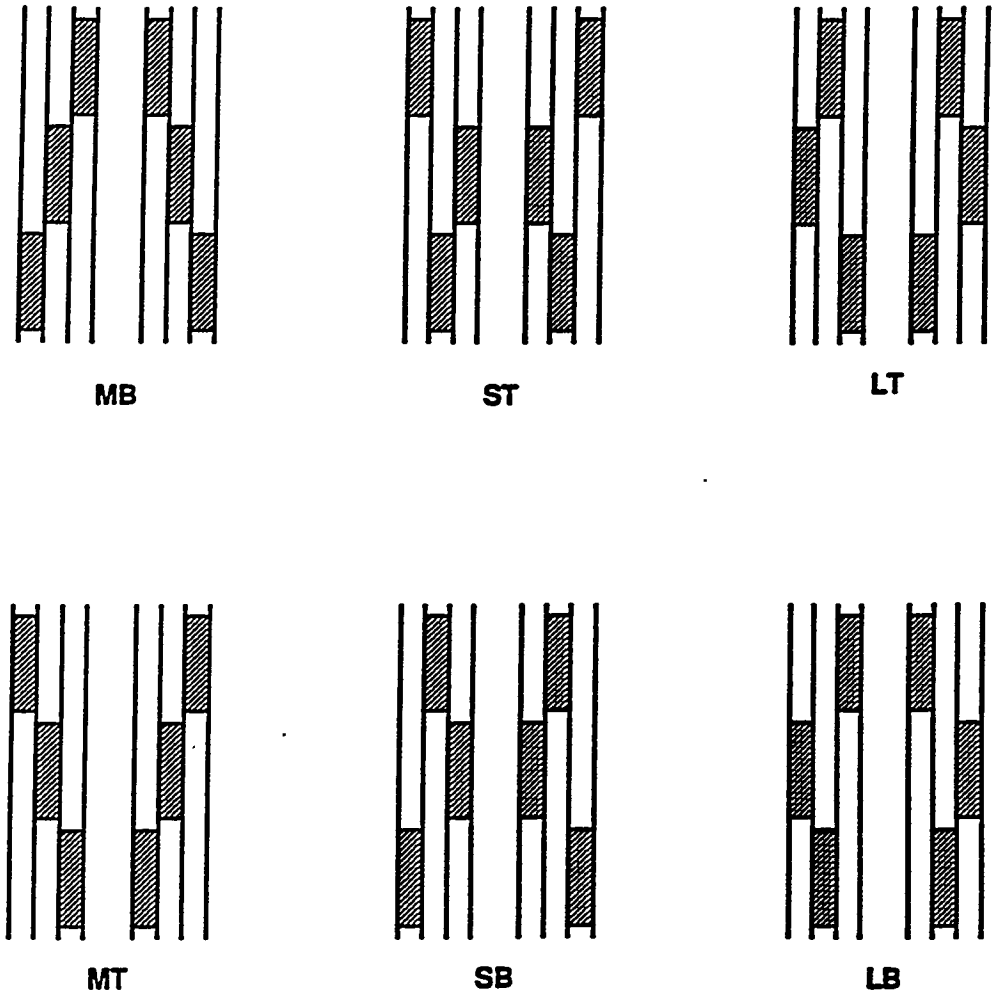

Fig. 2.5. Diagram showing the different three-element core configurations.

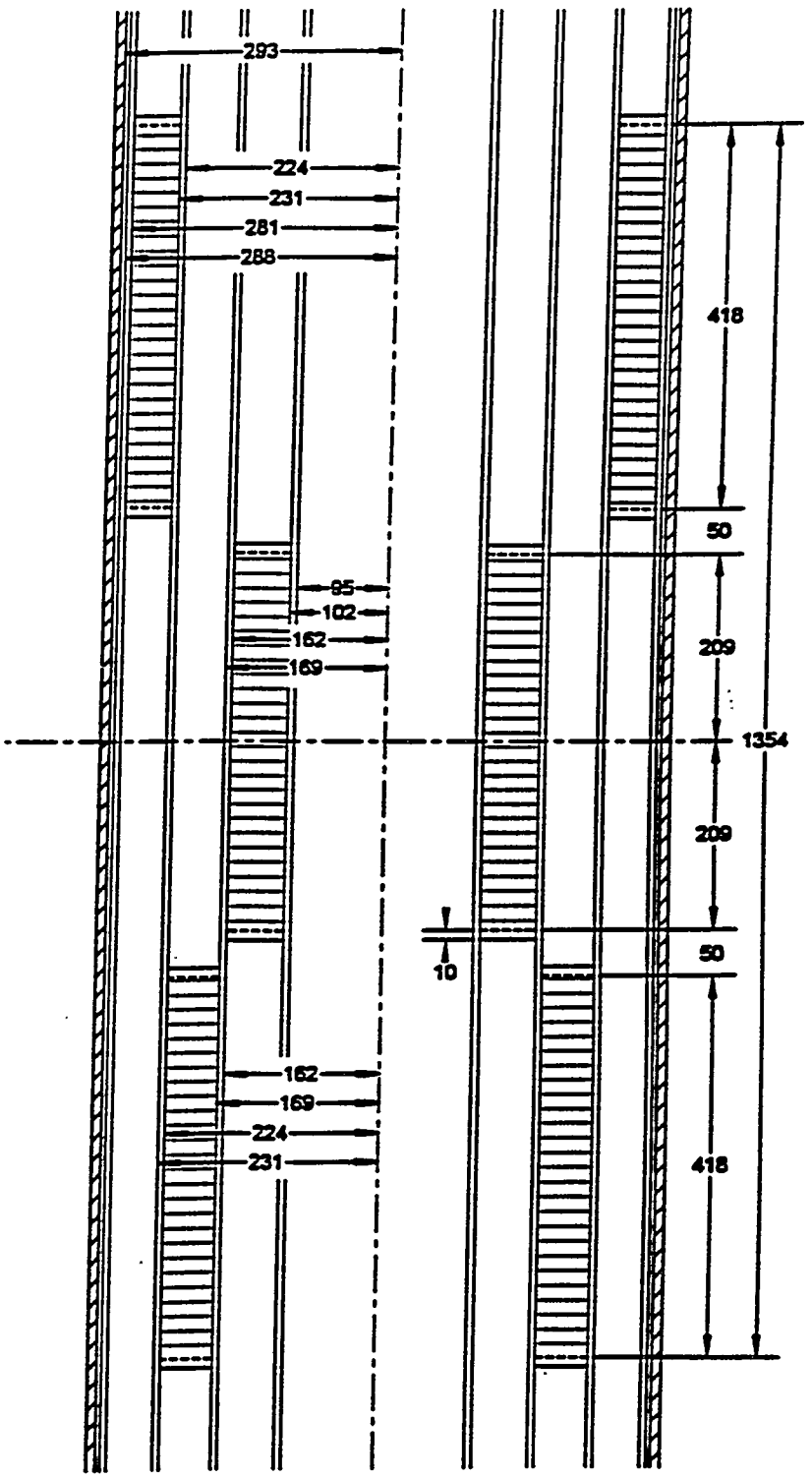

Fig. 2.6. Three-element modified core configuration (ST-MOD).

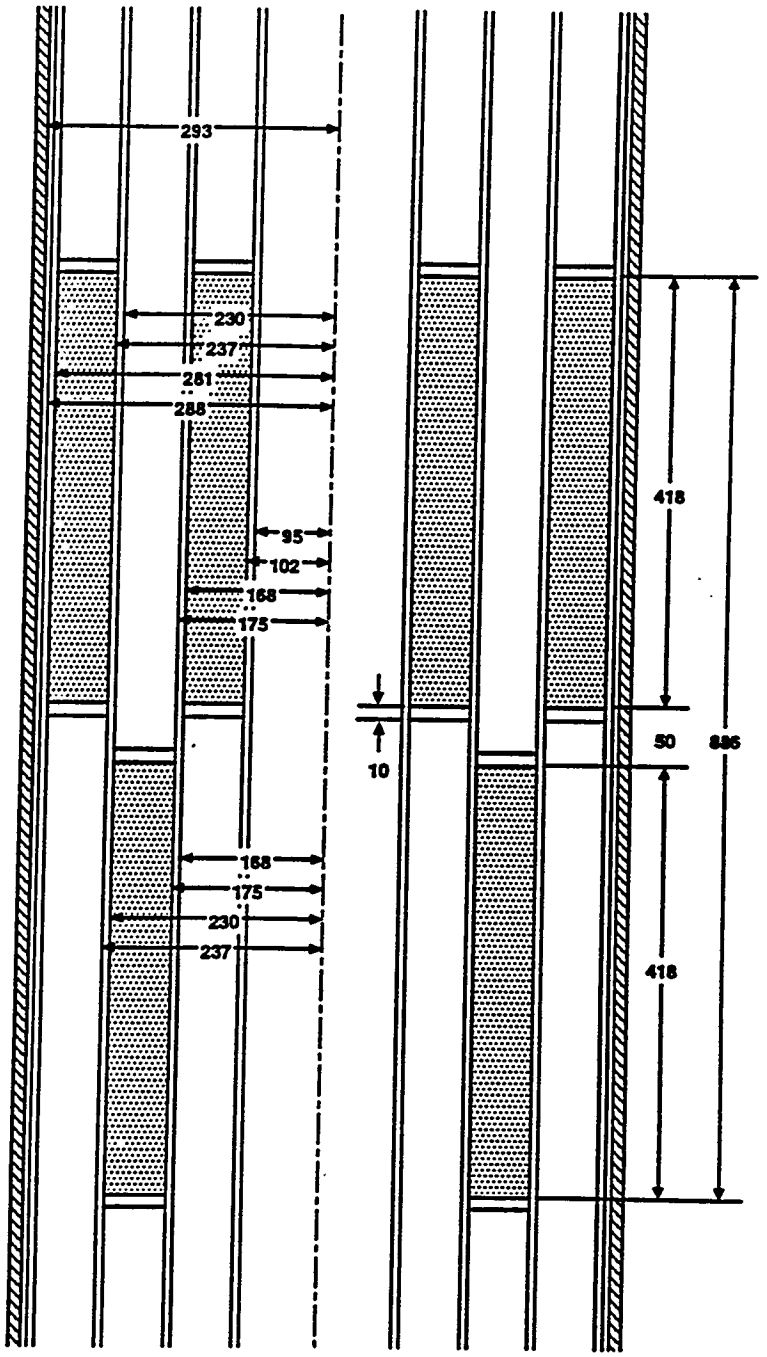

Fig. 2.7. Three-element full overlap core configuration (ST-OL2).

3. CALCULATIONAL MODEL DESCRIPTION

3.1 INTRODUCTION

Several different core geometries were considered in this study: the conceptual two-element design having a volume of 67.6 L, six basic three-element configurations having volumes of 82.6 L, two alternate three-element configurations with volumes of 82.8 L (this insignificant difference is the result of repositioning the fuel sideplates by an exact integral number of millimeters for drafting and calculational convenience), and two overlapping three-element configurations with volumes of 82.6 L. Geometrical descriptions of these configurations were presented in Chap. 2. This chapter contains a description of the fuel-cycle models of these reactors and the methods used in the analysis.

In previous studies the fuel-cycle analysis for the two-element conceptual core design had been performed with four-group finite-difference diffusion theory in r-z geometry using the VENTURE code system.[6] This model did not include the reflector components, which resulted in an underestimation of the required fuel loading. That was not a concern because any increase in the fuel density required to offset the presence of reflector components was not expected to reach unacceptable values. In addition, the design of the reflector components is under constant development from other design considerations. In this study, however, the impact of reflector components was determined to be important because of different effects on the various three-element configurations and because efforts to reduce enrichment were limited by the practical, safe fuel density, so an attempt was made to account for the reflector components in the fuel-cycle analysis model.

3.2 GENERATION OF COLLAPSED CROSS SECTIONS

The VENTURE finite-difference diffusion theory code[6] requires, as input, weighted neutron group cross sections for the fuel cycle cases. In this study, the weighted cross sections with a four-neutron group structure were created using the AMPX[7] and SCALE[8] systems and the ANSL-V 99-group master cross-section library.[9] Starting with the master cross-section library, the unresolved resonance region is processed with the BONAMI[7] module, which is followed by the resolved resonance processing in the NITAWL-II[7] module. The material temperatures required for resonance broadening are representative of the ANS operational conditions. The thermal scattering calculations of the D_2O coolant, moderator, and reflector were performed with the WORKER[7] module. The neutron group weighting and collapse is performed using the spectrum from one-dimensional discrete-ordinates calculations with the XSDRNPM[7] module. Radial cross-section collapses are performed for each element of the reference design with and without the central control rods inserted.

3.3 EQUIVALENT CONTROL ROD MODEL

The current ANS control rod design consists of three hafnium rods in the central hole of the core, as shown in Fig. 3.1. This geometry cannot be modeled in two-dimensional r-z geometry, so an equivalent two-ring control rod model is used. Calculations of the two-element ANS core were also performed with the MCNP Monte-Carlo code[10] using an explicit three-rod model and the equivalent two-ring model. The D_2O gaps between the materials were adjusted until the equivalent model matched the results obtained with the explicit model. Two rings are used to provide more degrees of freedom in matching the explicit rods. The hafnium number densities and thicknesses are not modified when this model is adjusted. The

dimensions of the equivalent two-ring model are presented in Fig. 3.2. Table 3.1 contains a comparison of the multiplication factor for the MCNP explicit and two-ring models, along with VENTURE calculations in which the control rods were at several rod positions for the two-element core configuration. This equivalent control rod model was also used in all three-element core calculations.

3.4 REFLECTOR COMPONENT MODEL

To determine the correct amount of fuel required for the entire fuel cycle, it is important to consider the reflector components, which constitute a substantial reactivity penalty to the system. The aluminum structure not only absorbs neutrons but also, along with large voids in the components, displaces D_2O. Figure 2.3 provides a horizontal plan view showing the reflector components. In the 2-D fuel-cycle models, the reflector components are represented with the components smeared radially and axially inside the reflector. Five radial zones and several axial zones—one corresponding to each axial fuel zone—are used. The shut-down rods and in-core irradiation facilities, however, are not modeled.

3.5 FUEL-GRADING MODEL

The two-element core analyzed in this study used the G693 fuel grading, which is shown in Fig 3.3. This grading is modeled with 299 (13 × 23) zones in each element. For the three-element designs, a uniform fuel grading was used because of the effort required to determine an optimized fuel grading for each configuration. However, the same volume of fuel lost to fuel grading in the two-element core was also removed from the three-element cores to account for the fuel that might be displaced if a grading had been used. The use of a uniform grading vs an optimized grading has only a small effect on the core reactivity and neutron fluxes in the reflector.

3.6 DEPLETION MODEL

The same depletion model used for previous ANS analyses was also used in this study. Depletion steps for the 17-d cycle are at 1, 4.25, 8.5, 12.75, and 17 d. An equilibrium model is used at 1 d to bring in the xenon to avoid an excessive number of depletion steps. At each step in the cycle, the axial position of the control rods is adjusted to obtain a unity multiplication factor using the CTRLPOS[11] module of the VENTURE system. Each of the 299 zones in each element, used to represent the fuel grading, is used as a depletion zone. The xenon and samarium fission product chains, along with approximately 25 additional fission products, are represented explicitly. The remaining fission products are represented by two lumped materials.

3.7 SUMMARY

In this chapter a brief description of methods and models used in the analysis of the different reactor configurations was presented. The cross-section generation, central control rod, reflector component, fuel grading, and depletion models were discussed.

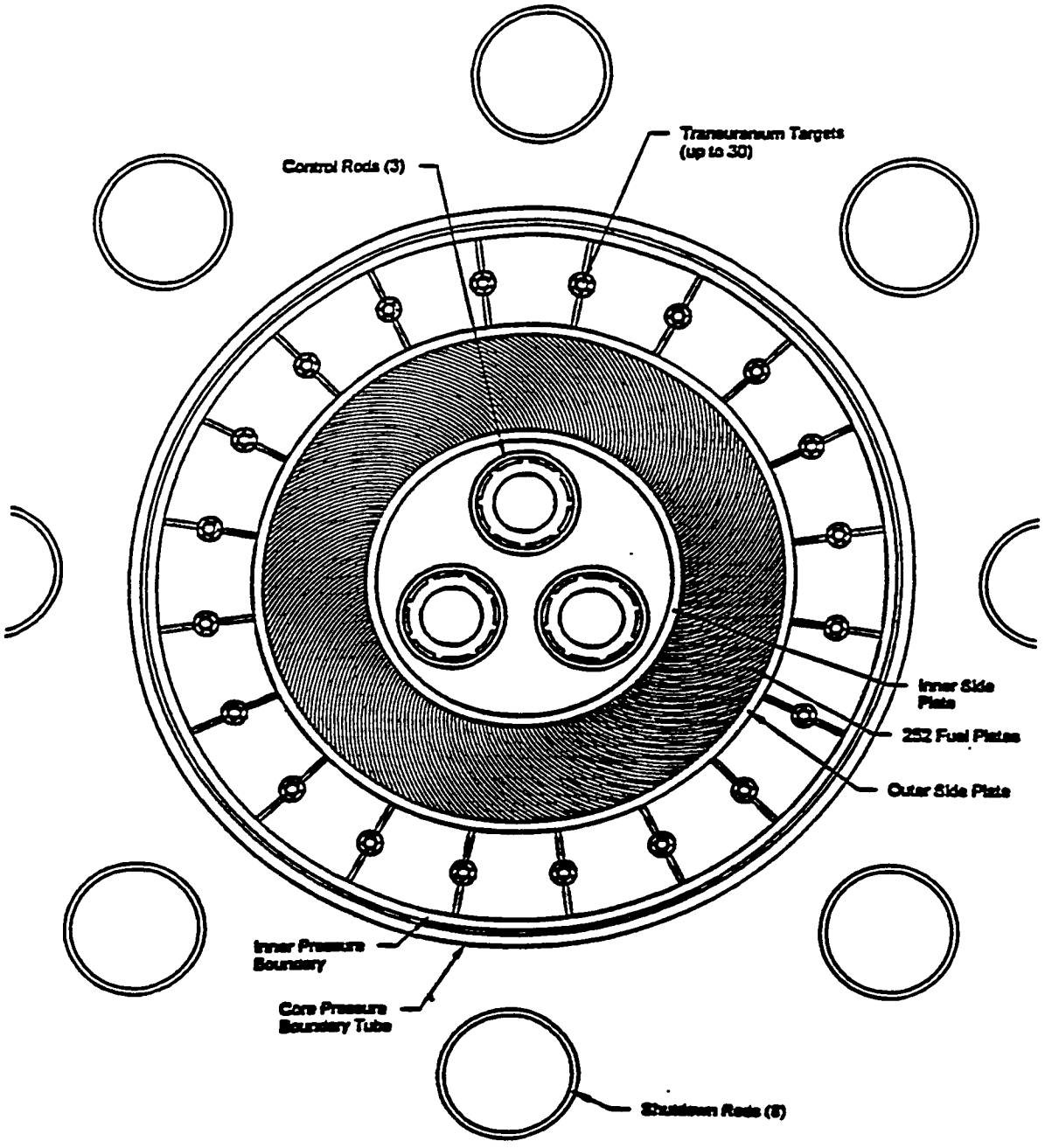

Fig. 3.1. Horizontal view of the ANS central control rods.

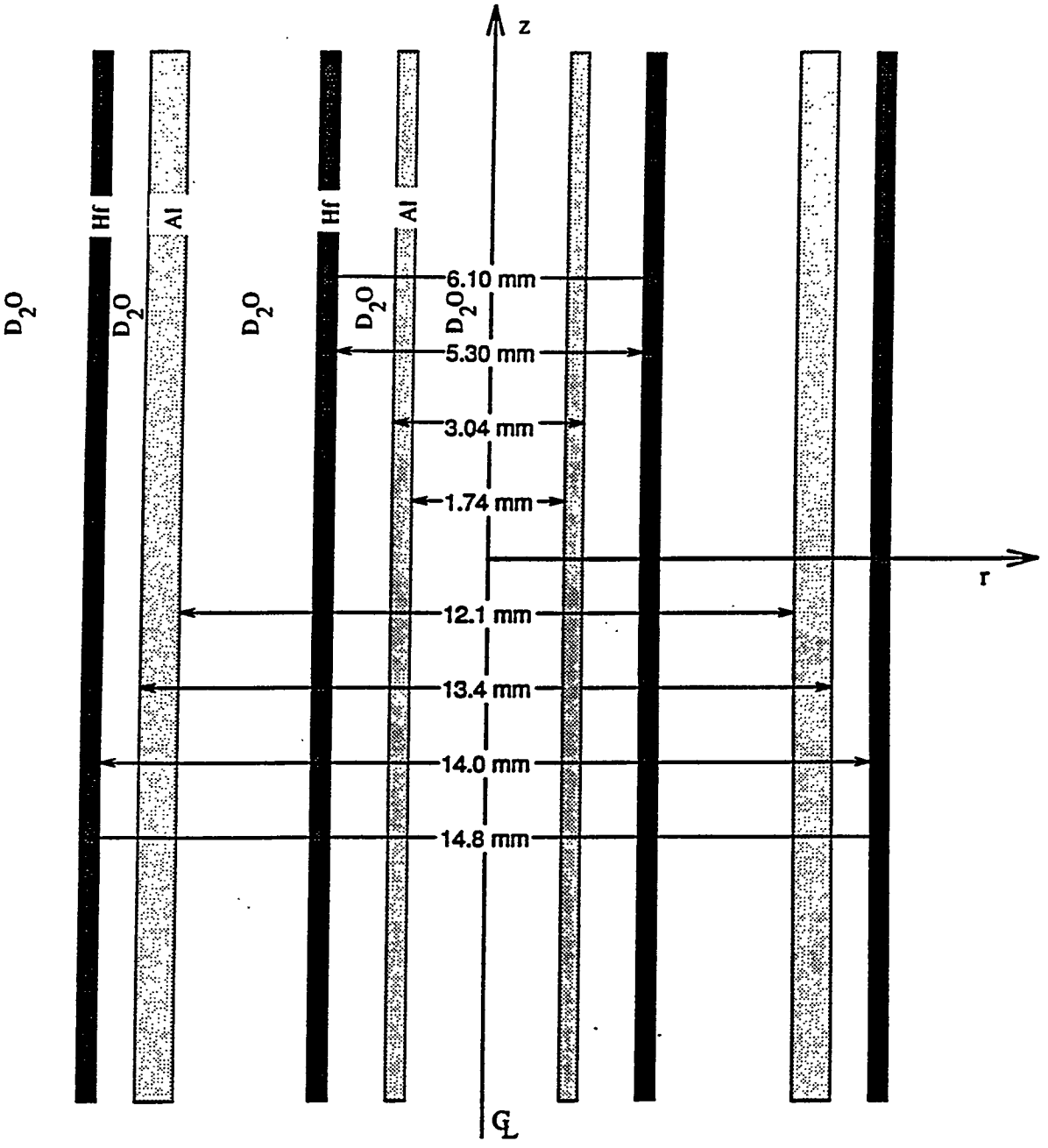

Fig. 3.2. R-Z equivalent control rod model.

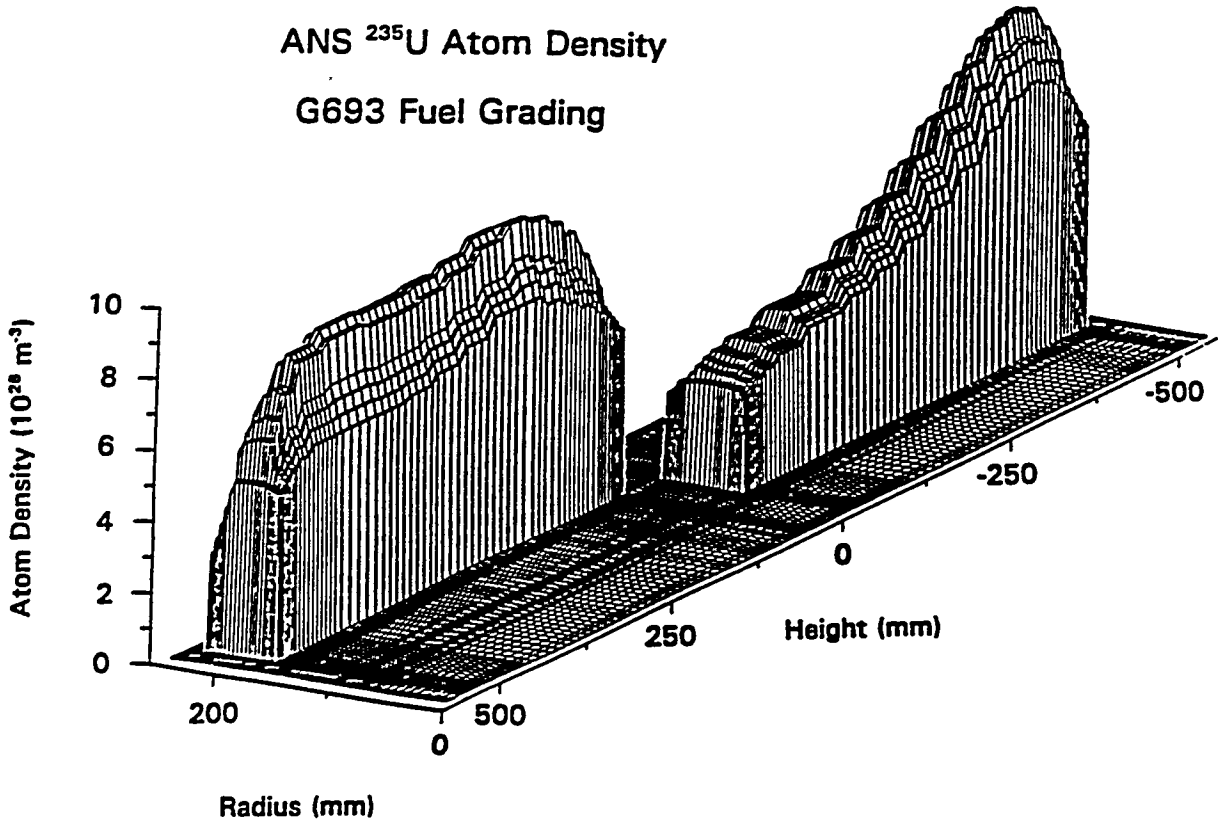

Fig. 3.3. Two-element core G693 fuel grading.

Table 3.1. Comparison of two-ring and explicit control rod models for two-element conceptual core

Rod position (mm from MP)	MCNP explicit	MCNP two-ring	VENTURE two-ring
−300	0.9904±0.0013[a]	0.9854±0.0014	0.9793
+100	1.0610±0.0010	1.0649±0.0011	1.0532
+300	1.1091±0.0090	1.1138±0.0011	1.0990

[a]Statistical uncertainties are one standard deviation.

4. CALCULATIONAL RESULTS

4.1 INTRODUCTION

This chapter contains results of the calculations for the different core configurations. The fuel-cycle results, neutron flux results, control rod worth curves, and other information are presented for all of the core configurations discussed in Chap. 2. The impact of the smaller element dimensions on fuel element criticality is also discussed.

All of the calculations presented in this chapter were performed with the four-energy group finite-difference model briefly discussed in Chap. 3. Previous comparisons of the beginning of cycle (BOC) VENTURE calculations indicate that the bias in the multiplication factors is approximately +1.5 to +2% and the peak thermal flux in the reflector is approximately -6%. The results presented are intended to provide an intercomparison of the different core configurations. Therefore, all of the numbers that are presented here are those obtained directly from the VENTURE calculations and have not been multiplied by a VENTURE/MCNP bias factor, as was done in previous studies.

4.2 FUEL-CYCLE RESULTS

For each configuration, fuel-cycle calculations were performed with the VENTURE model previously discussed. Each case consisted of a 17-d cycle at a power level of 330 MW_t. The control rods were adjusted to maintain a critical system throughout the cycle. Also, the boron loading in the fuel-element endcaps was adjusted so that nearly all of the ^{10}B has been depleted at the end of the cycle (EOC). Table 4.1 presents a summary of the results. This table contains the required fuel density, critical control rod position, the ^{10}B loading, component reactivity worth, and key neutron flux parameters throughout the cycle. The beam tube, cold source, and hot source locations in this table are those of the two-element core.

With highly enriched (93% ^{235}U) fuel, all of the three-element configurations except ST-OL2 required essentially the same fuel density, 0.95 gU/mL, to maintain a 17-d cycle. The fully overlapping configuration ST-OL2, however, requires a slightly lower density of 0.91 gU/mL. These density values are much lower than those of the conceptual two-element design, 1.7 gU/mL, because the larger total surface area of the three elements exposes more fuel to the moderator.

As part of the fuel-cycle calculations, the fuel-element power densities were computed. In an ideal configuration, each one of the fuel elements would have the same power density as the others throughout the fuel cycle. Fuel grading can improve the power density splits by moving fuel from one element to another, although large movements of fuel would leave little room for localized power shaping. Plots of the element power density throughout the fuel cycle for each of the core configurations are in Fig. 4.1. The ST and MT configurations have the best fuel-element power densities; each element has comparable power densities, which remain relatively constant over the fuel cycle. All of the configurations with the large element on the bottom (SB, MB, LB) have a large disparity in the power density between each fuel element and large power density changes over the fuel cycle. The examination of the power density distribution within the fuel elements is not particularly meaningful because of the nonoptimal uniform fuel grading.

4.3 NEUTRON FLUX RESULTS

In this section all of the neutron flux results at the peak location as well as at various experiment system facility locations are presented. All of the fluxes presented are unperturbed values. These unperturbed values are computed by using all of the isotope concentrations obtained in the fuel-cycle calculations in separate calculations at each time step in the cycle but with all of the reflector components and experimental facilities replaced by heavy water. Because the multiplication factor of such a system is not equal to unity, the flux values are multiplied by the multiplication factor to adjust the neutron source to that of a precisely critical system.

4.3.1 Peak Thermal Flux

One of the key measures of performance of a given core configuration is the peak thermal flux in the reflector. The values for each configuration at BOC, middle of cycle (MOC), and EOC are in Table 4.1. This table shows that the nonoverlapping three-element core configuration results in a 15 to 20% loss in peak thermal flux in comparison with the two-element core. Of the six basic three-element designs, the best peak thermal fluxes occur in the configurations with the largest element in the bottom location (SB, MB, LB), and configuration MB gives the largest peak thermal flux. The peak flux differences between the regular and modified configurations (ST, SB and ST-MOD, SB-MOD) are relatively small. The overlapping configurations, however, result in a substantial increase in the peak thermal flux. The half-overlap configuration (ST-OL1) shows a 7.7% increase, and the full overlap configuration (ST-OL2) shows a 13.5% increase over the ST configuration.

The location of the peak thermal flux throughout the fuel cycle is shown in Fig. 4.2 for each configuration. The peak fluxes for the ST and SB configurations appear to be well centered about the core midplane as the cycle progresses. The MT and LT configurations have peak flux locations that are generally above the core midplane, whereas the MB and LB tend to have peak flux locations below the midplane.

4.3.2 Fluxes at Reflector Experimental Facilities

The flux parameters at several important reflector experimental facility locations are in Table 4.1. These parameters include the thermal flux at the beam tube tips, the thermal-to-fast flux ratio at the beam tube tip, the thermal flux at the cold source, and the thermal flux at the hot source. These fluxes are given at the conceptual-design locations, which may not be the best location for each core configuration, as demonstrated by the differing location of the peak thermal flux. The thermal flux at the beam tube tips is generally the most sensitive to the location because of the close proximity to the core.

To determine the best location of the beam tube tips for each configuration, thermal flux and thermal-to-fast flux ratio contours were determined and are presented in Figs. 4.3 through 4.13. In these plots the fluxes and ratios for each configuration are given at BOC, MOC, and EOC along with the cycle-averaged values. In all cases the peak thermal flux moves upward throughout the cycle, whereas the thermal-to-fast flux ratios remain relatively constant. The thermal flux peak tends to be very broad, but the fast flux drops off very quickly in the radial direction, which leads to a rapid increase in the thermal-to-fast flux ratio with increasing radius. Because of the larger elements, the thermal flux peak occurs farther out in the reflector than it does for the two-element core. Therefore, although the peak flux may be substantially lower in the three-element design, the peak may occur closer to the beam tube tips.

The flux contours were used to determine the best beam tube locations. The best location is defined to be the location that has the largest cycle-averaged thermal neutron flux and a thermal-to-fast ratio greater than 120, which was chosen as a conservative value exceeding the design requirement of 80. The minimum radius for the beam tube tip is 430 mm to allow room for the beam tubes and to provide enough

distance from the core to give acceptable heat loads on the beam tubes. Table 4.2 presents the parameters for the best beam tube location for each configuration and the parameters at a radius of 430 mm and midplane for comparison. The best beam tube positions are also indicated by a square marker on the thermal-to-fast flux ratio contours.

4.3.3 Neutron Fluxes in the Irradiation Positions

For each configuration the material irradiation and transuranic production locations have been identified. Figure 4.14 shows these locations for the six basic three-element core configurations (ST, SB, MT, MB, LT, LB) and the two-element design. The irradiation positions are inside the upper two elements in the overlapping configurations. All of the locations in the three-element configuration have been located in an exit stream to reduce the chance of a flow blockage by debris from these facilities or capsules. The parameters of interest in the materials irradiation location are the fast flux and the fast-to-thermal flux ratio, whereas the parameters of interest in the transuranic production location are the epithermal flux and epithermal-to-thermal flux ratio. Plots of these parameters for each core configuration are presented in Figs. 4.15 through 4.25.

4.4 CENTRAL CONTROL ROD WORTH CURVES

The control rod worth curves for each core configuration were computed at BOC, MOC, and EOC with 14 different rod positions. The integral control rod worth (in pcm) and the differential rod worth (in pcm/mm) as a function of the control rod position are presented in Figs. 4.26 through 4.36. These figures also indicate the critical rod positions. A comparison of the curves for the ST and SB configurations with the modified cores ST-MOD and SB-MOD indicates only a small change in the control rod behavior. A decrease in the differential worth occurs as the control rod tips pass the endcap regions with burnable absorber at BOC and, to a lesser extent, at MOC. This effect does not occur at EOC since the boron is nearly burned out by then. In general, the insertion rates for a given rod position increase throughout the cycle. The curves for several of the configurations, including the conceptual two-element core, show that a small withdrawal of the control rod from the fully inserted position results in a negative reactivity insertion. While this small effect may be the result of the control rod modeling, it is believed to occur because the control rod has a larger worth at the top of the core than at the bottom. As the control rod is withdrawn from full insertion, the top of the hafnium absorbs neutrons that would otherwise be available for the upper element.

From these control rod worth curves, reactivity insertion rates (in pcm/mm) for the rods in the critical positions at BOC, MOC, and EOC were determined and are presented in Table 4.3. For each configuration the minimum reactivity insertion rate occurs at EOC since the control rods are fully withdrawn and not next to a fueled region. The two-element configuration has larger reactivity insertion rates than all of the three-element configurations. The control rod insertion (from the critical control rod position) required for a dollar of negative reactivity is in Table 4.4 for each configuration. The effective delayed neutron fraction for all configurations was assumed to be that of the baseline two-element core, 0.0077. These insertion distances were obtained from the integral control rod worth curves and are nearly identical to dividing –770 pcm (–$1) by the reactivity insertion rates in Table 4.4, indicating a near-linear behavior over the 50- to 100-mm distances. The required insertions follow the same trends as the insertion rates, with the largest insertion required at EOC and the two-element core requiring less insertion than the three-element configurations.

4.5 FUEL-ELEMENT CRITICALITY

During refueling operations the criticality of the fuel elements is important. The multiplication factor of the fuel elements for the ST, ST-MOD, and the two-element core were computed. Each clean BOC fuel element was surrounded by an effectively infinite amount of heavy water (3 m on all sides). Although this situation never occurs in the refueling process, it represents the worst possible situation in terms of fuel-element criticality. The results of the calculations are summarized in Table 4.5. Note that all of the elements contain highly enriched fuel (93% ^{235}U) with the BOC loadings and no fission products. The largest multiplication factor occurs in the largest elements for each configuration and is the result of the increased amount of heavy water in the central region. The difference between the ST and the ST-MOD elements is small. The calculations show that the multiplication factor of the largest element in the three-element design is reduced by about 6.5% when compared with that of the two-element design.

4.6 SUMMARY

In this chapter the results of the calculations were presented for the different three-element configurations. These results include fuel-cycle parameters, neutron fluxes, control rod worth curves, and fuel-element criticality.

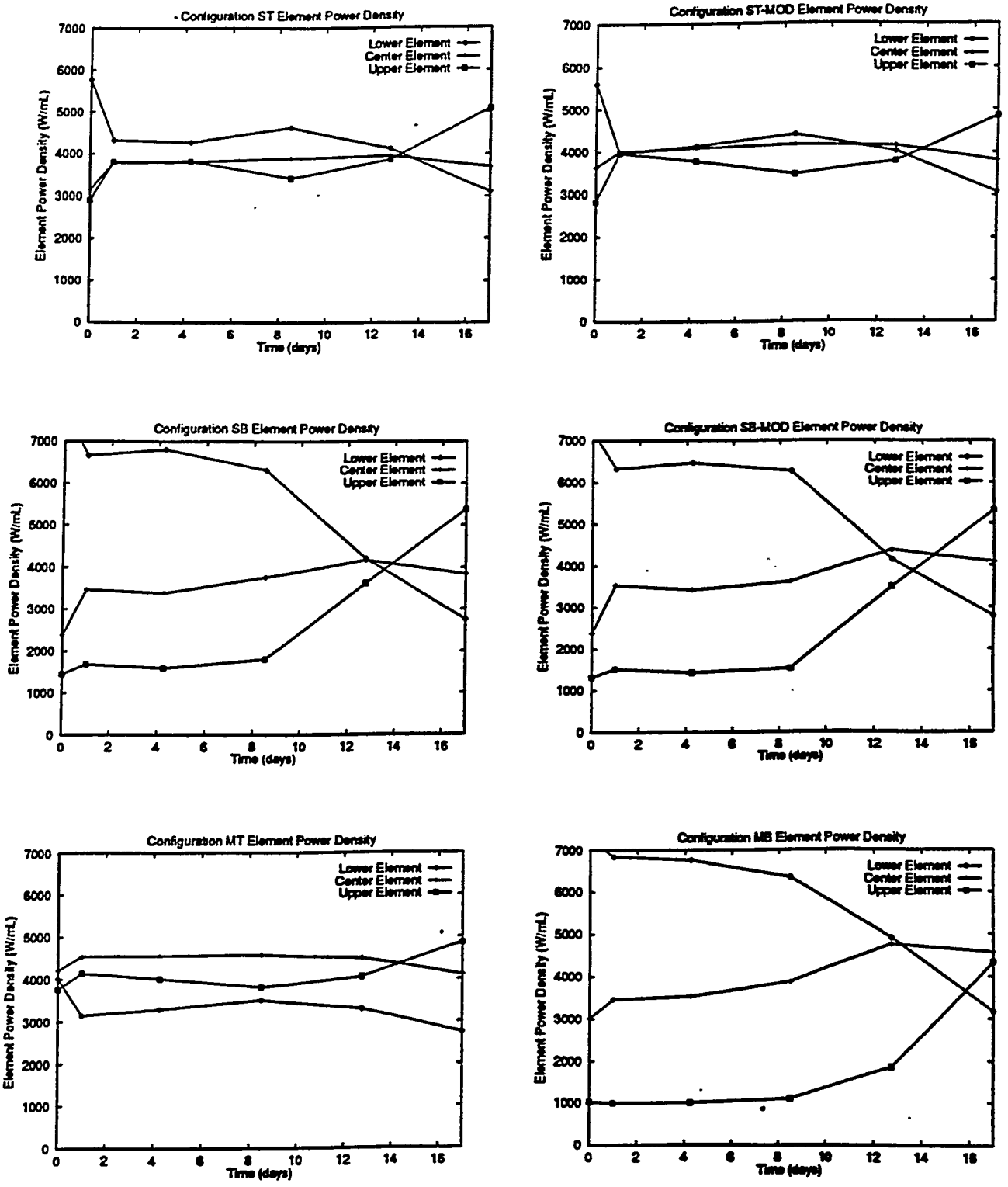

Fig. 4.1. Elemental power densities for the two-element and three-element core configurations.

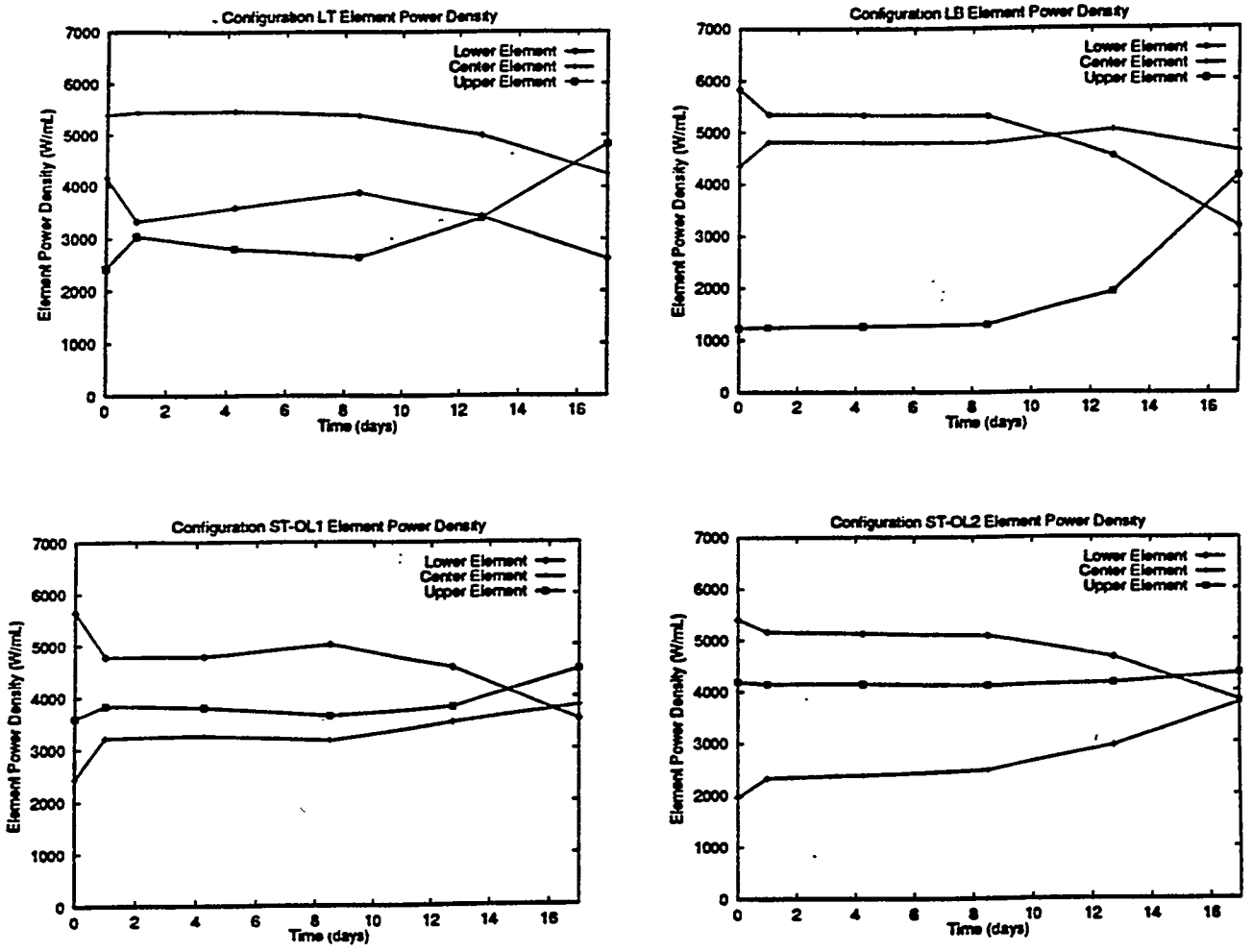

Fig. 4.1. Elemental power densities for the two-element and three-element core configurations (continued).

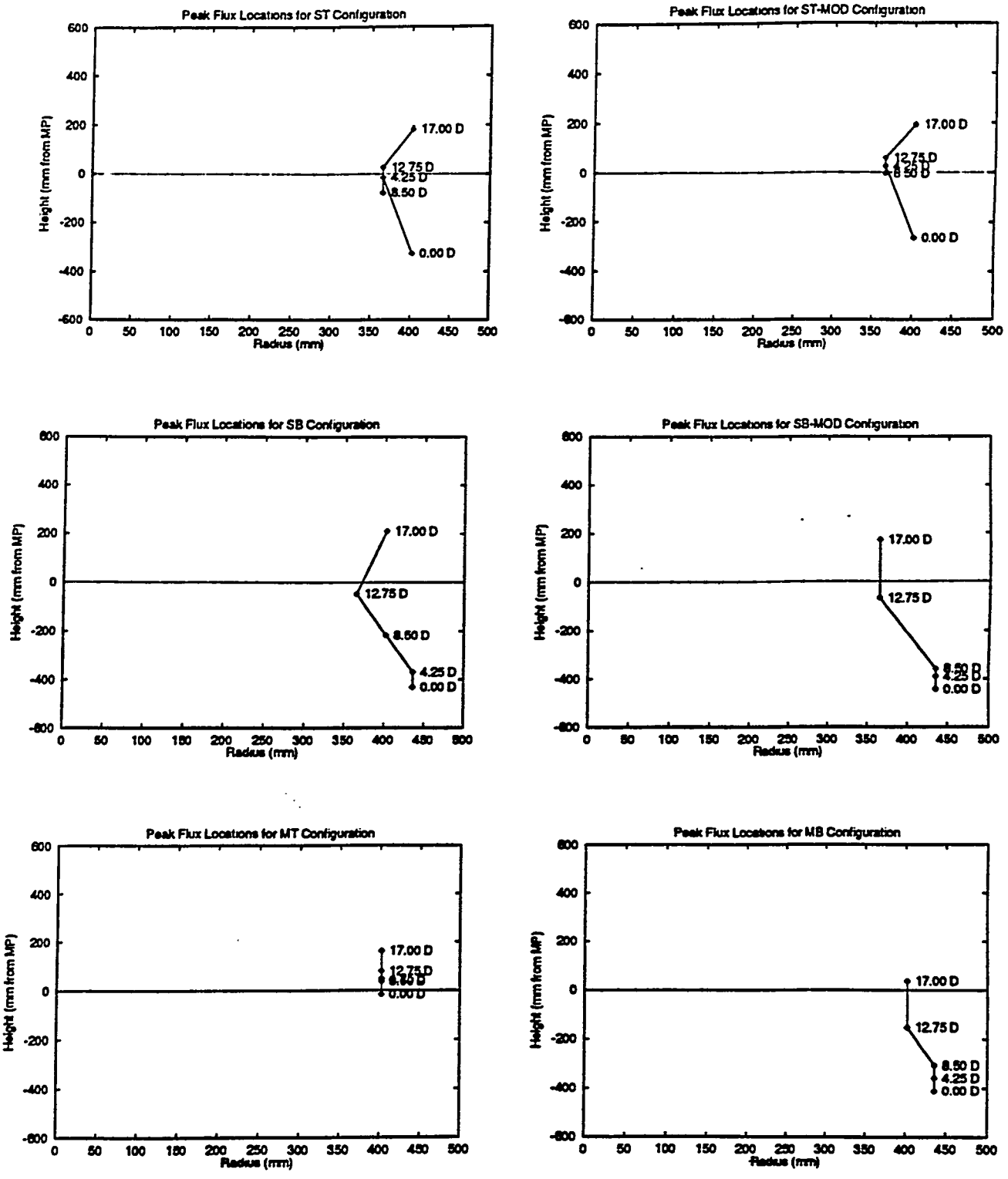

Fig. 4.2. Peak thermal flux location throughout the fuel cycle.

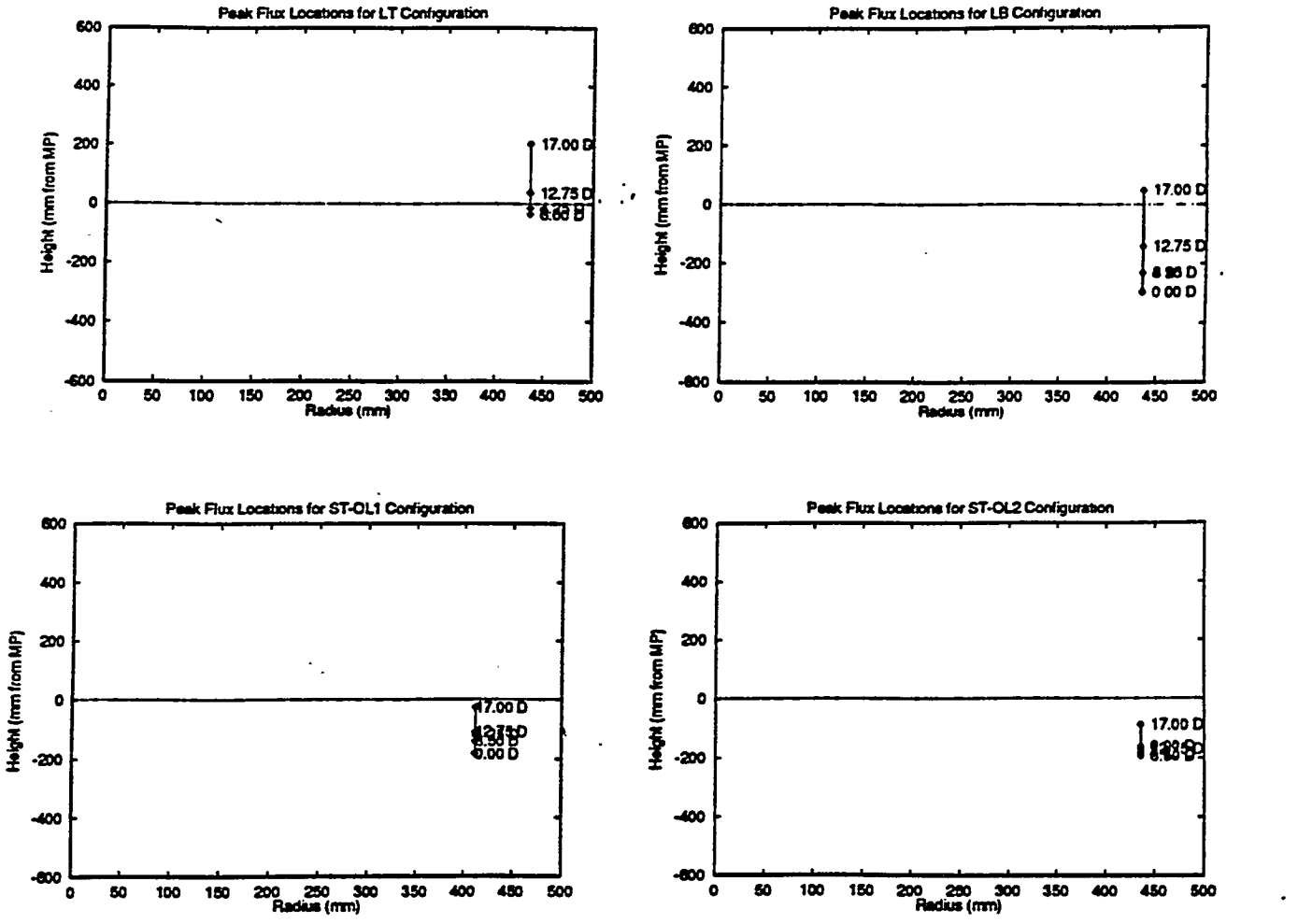

Fig. 4.2. Peak thermal flux location throughout the fuel cycle (continued).

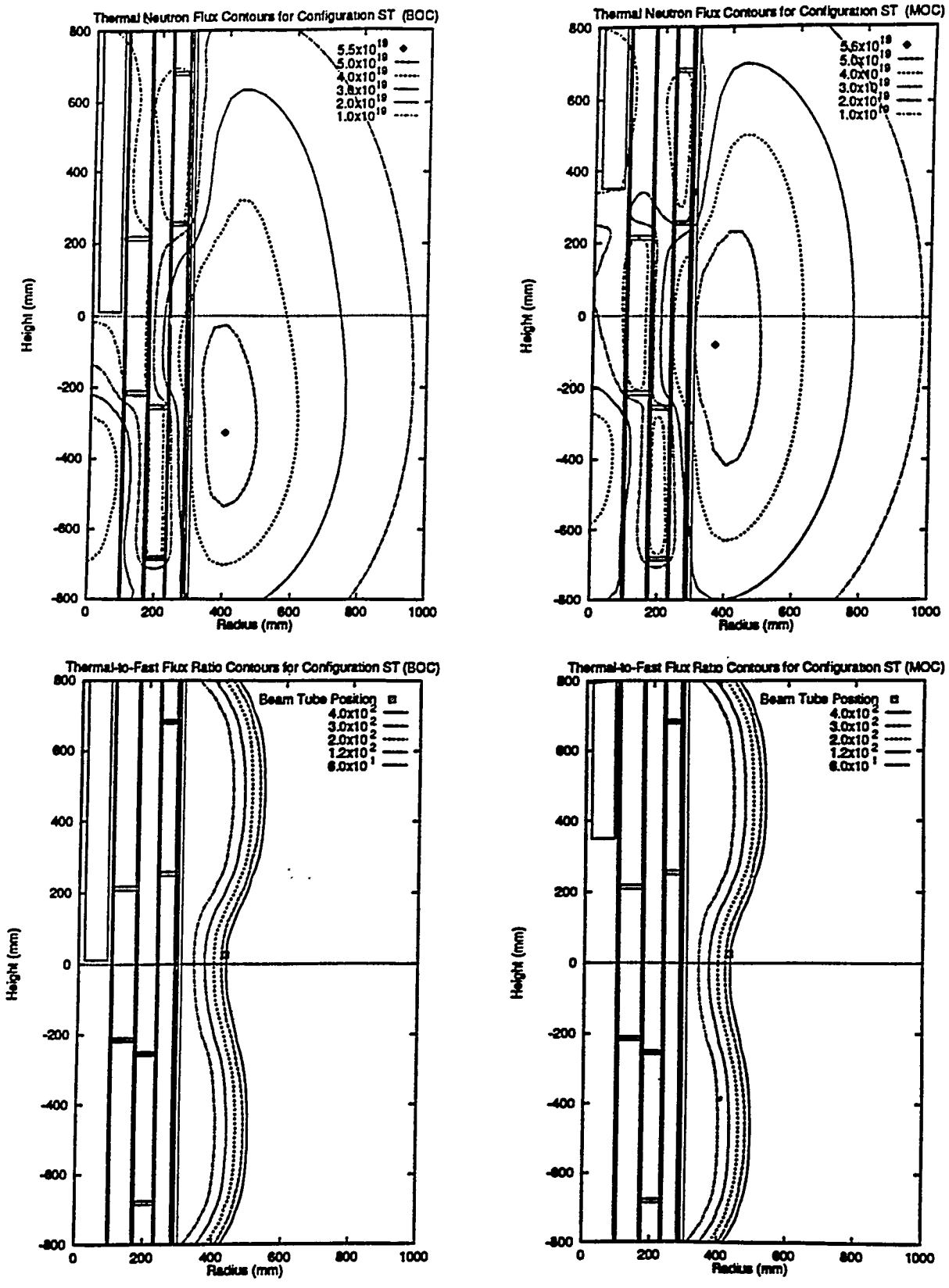

Fig. 4.3. Thermal neutron flux and thermal-to-fast flux ratio contours for configuration ST.

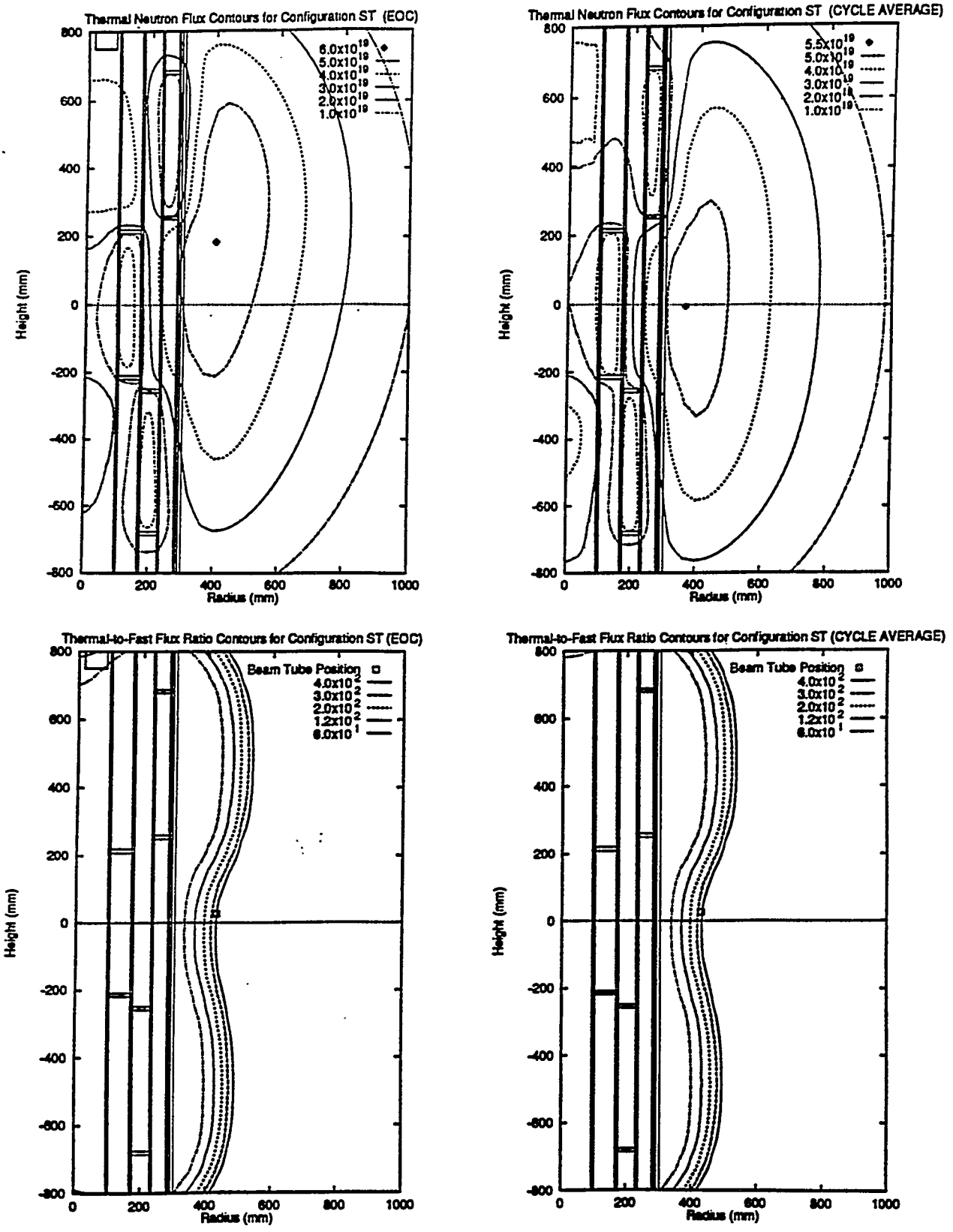

Fig. 4.3. Thermal neutron flux and thermal-to-fast flux ratio contours for configuration ST (continued).

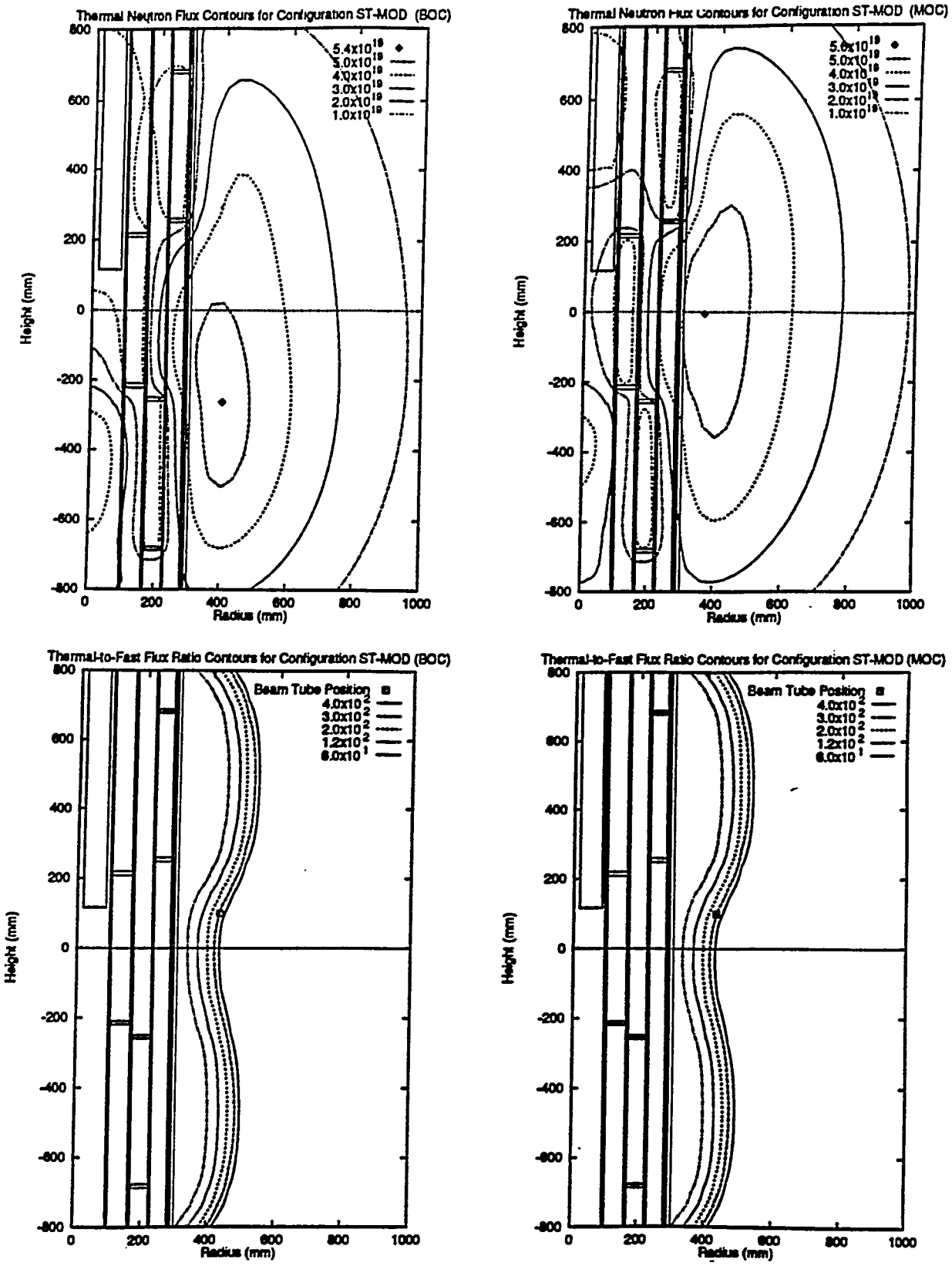

Fig. 4.4. Thermal neutron flux and thermal-to-fast flux ratio contours for configuration ST-MOD.

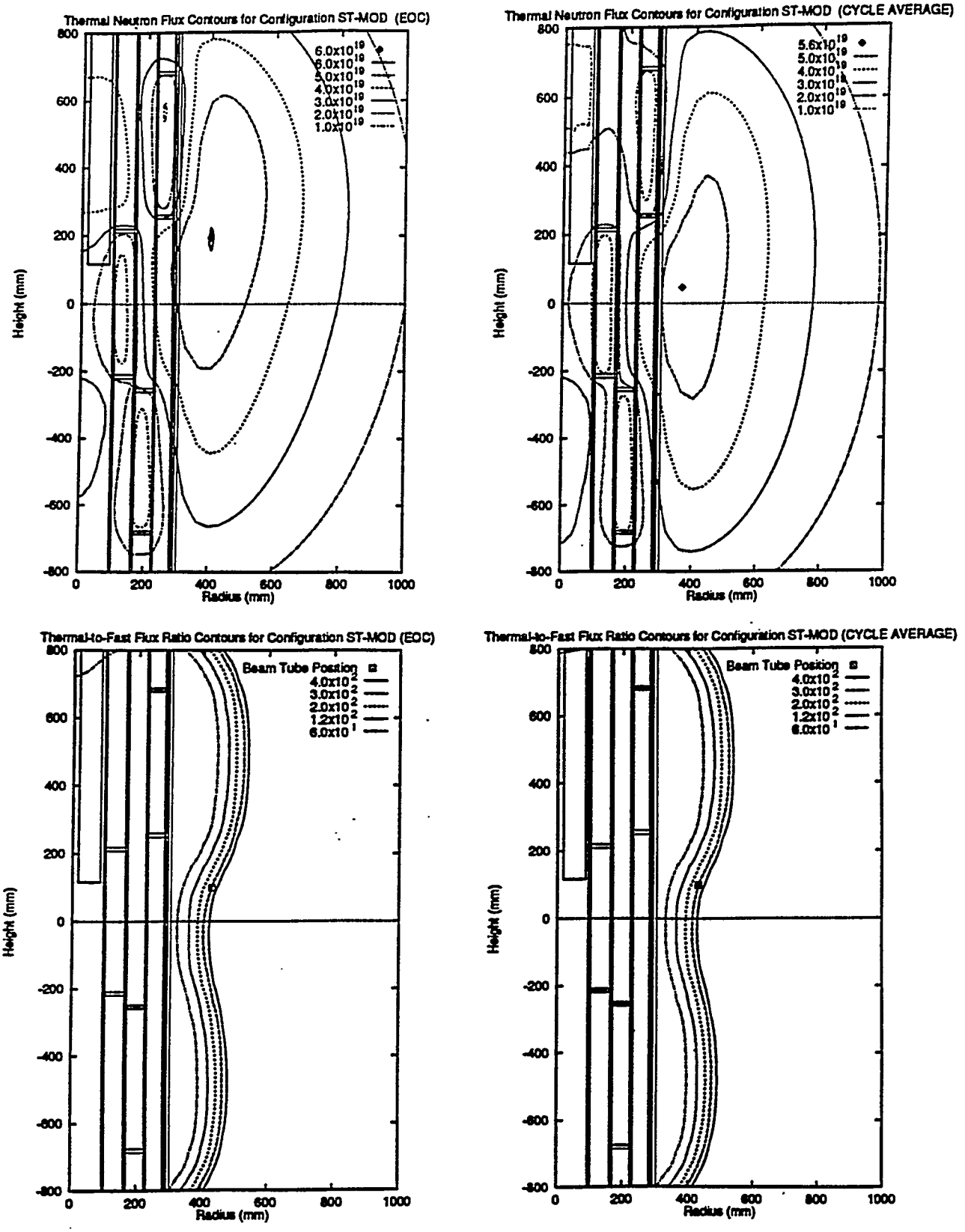

Fig. 4.4. Thermal neutron flux and thermal-to-fast flux ratio contours for configuration ST-MOD (continued).

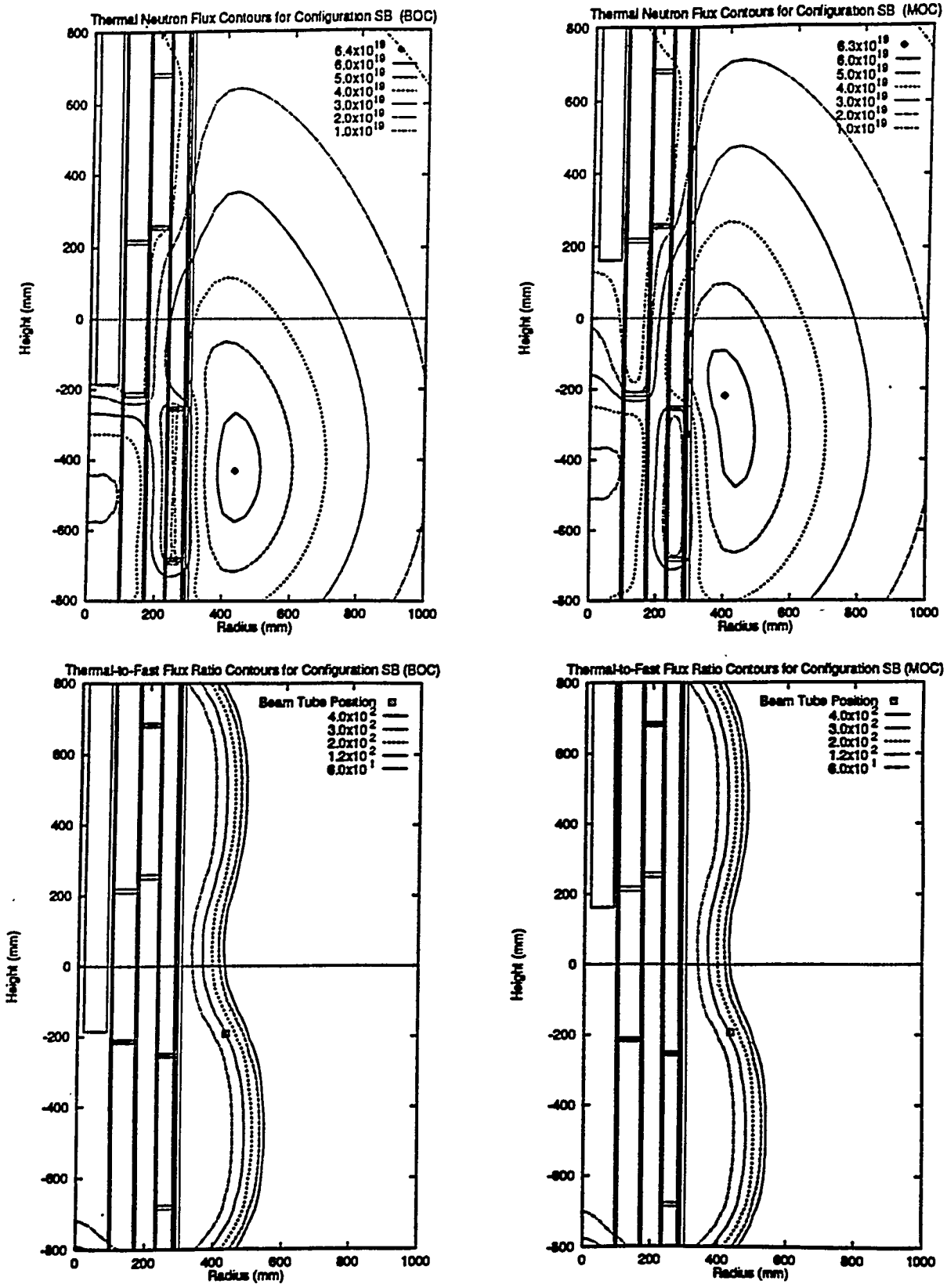

Fig. 4.5. Thermal neutron flux and thermal-to-fast flux ratio contours for configuration SB.

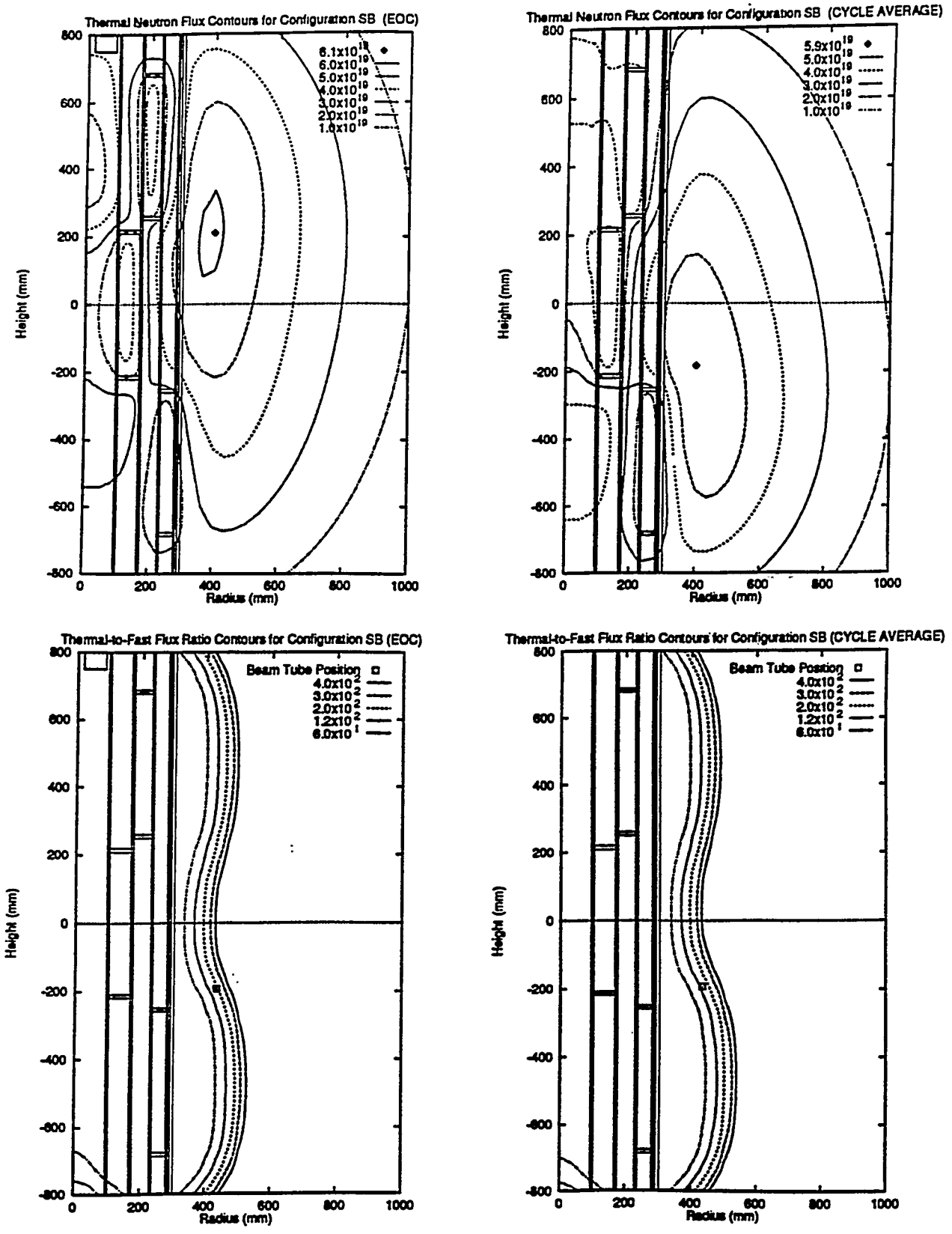

Fig. 4.5. Thermal neutron flux and thermal-to-fast flux ratio contours for configuration SB (continued).

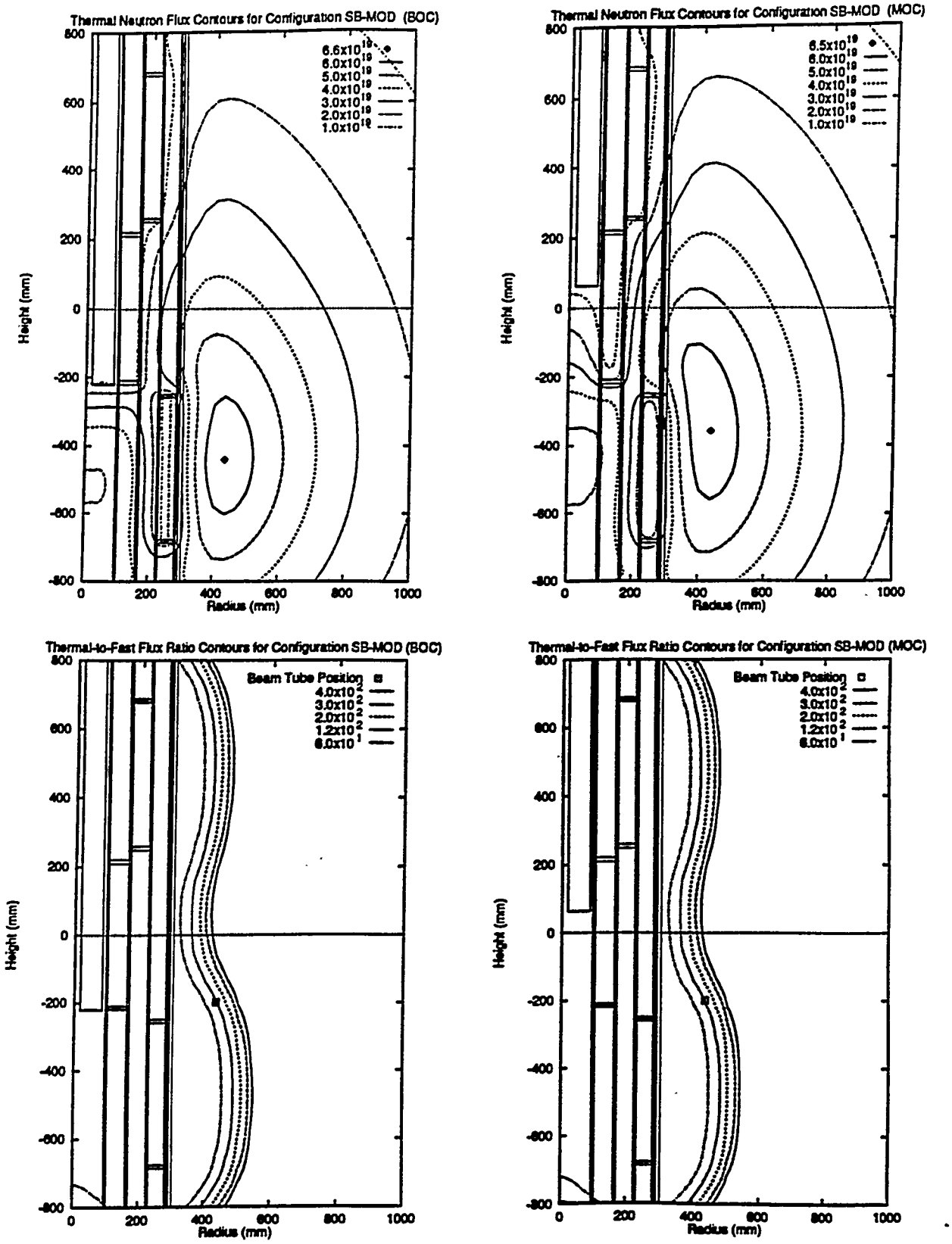

Fig. 4.6. Thermal neutron flux and thermal-to-fast flux ratio contours for configuration SB-MOD.

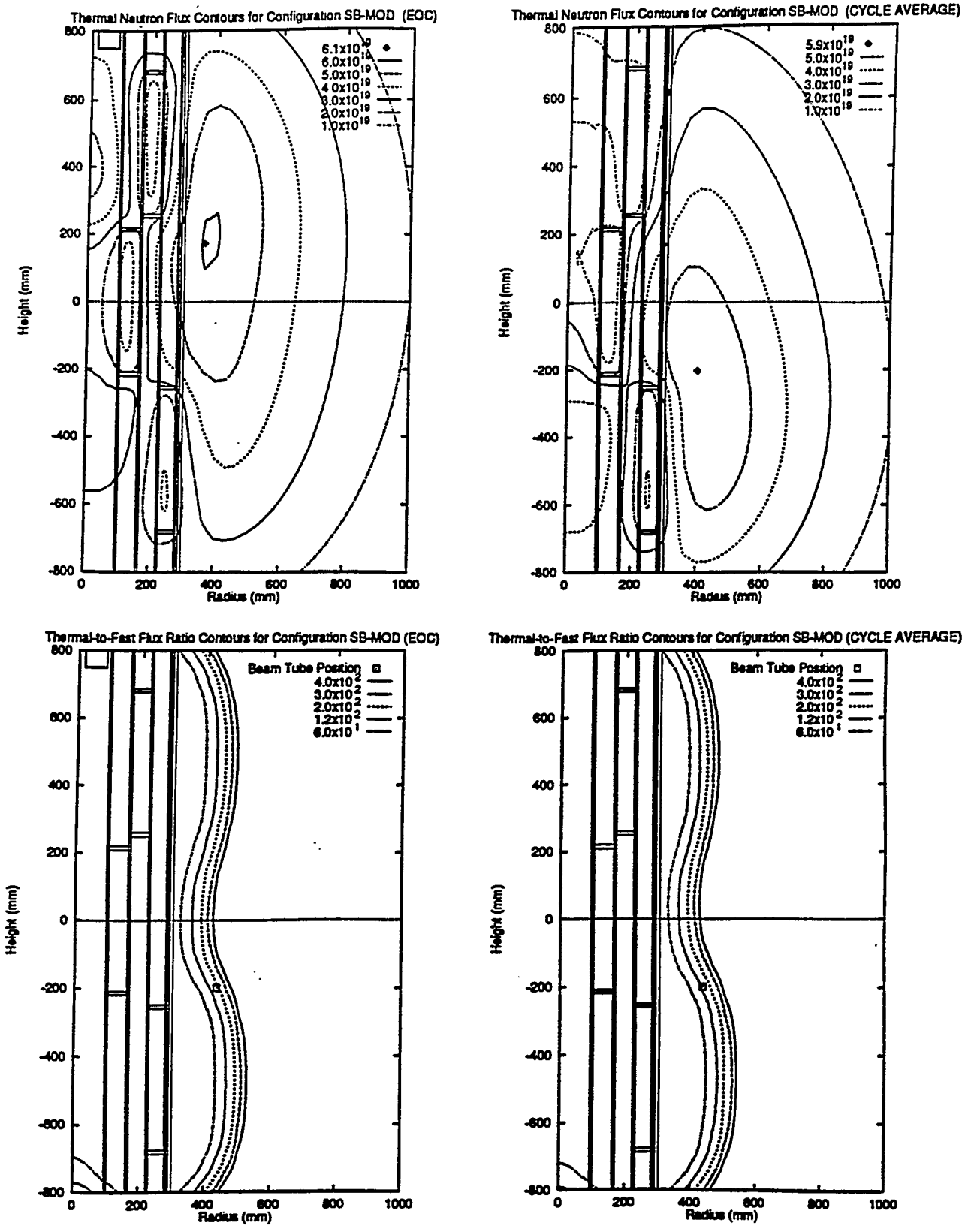

Fig. 4.6. Thermal neutron flux and thermal-to-fast flux ratio contours for configuration SB-MOD (continued).

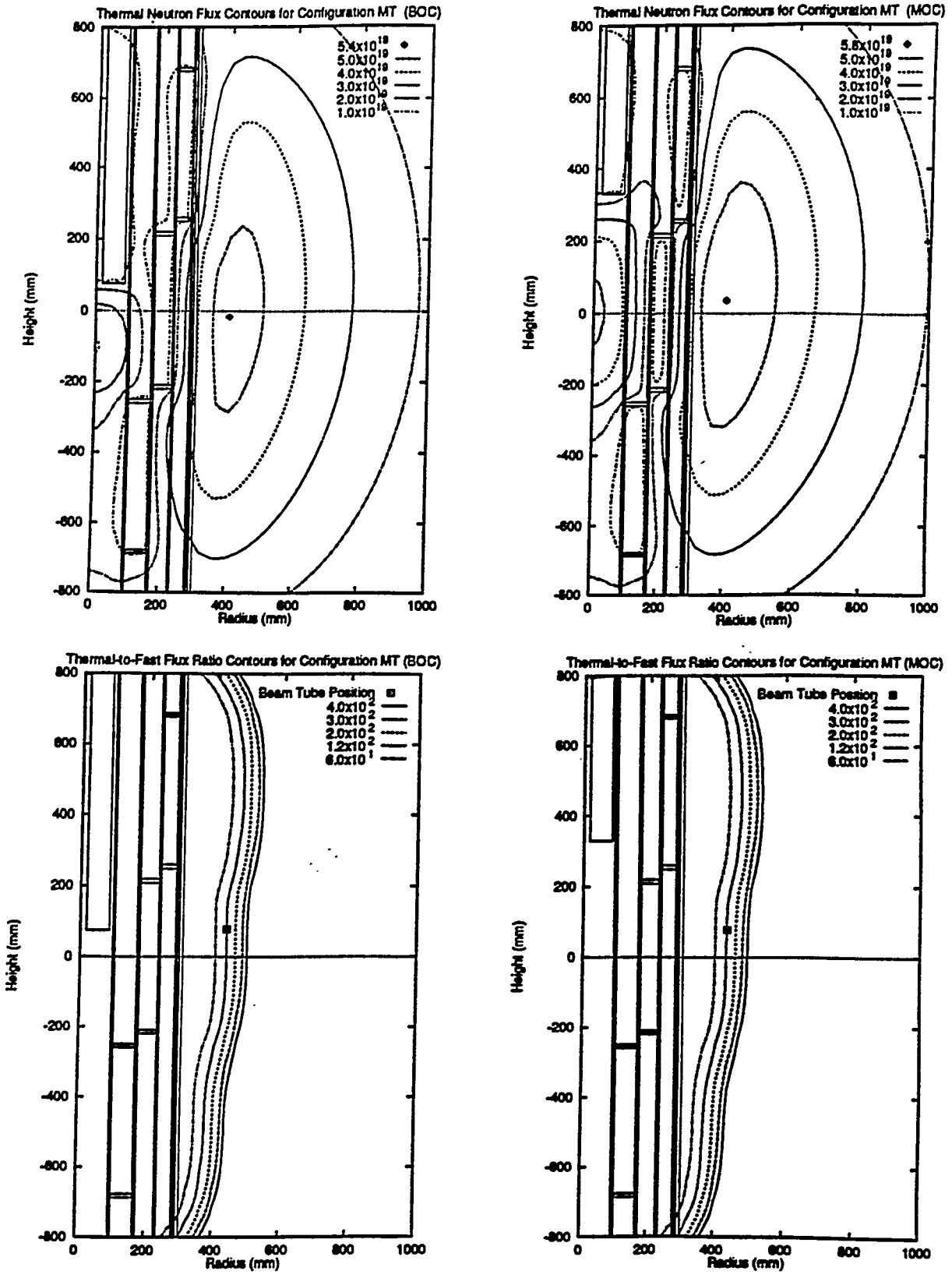

Fig. 4.7. Thermal neutron flux and thermal-to-fast flux ratio contours for configuration MT.

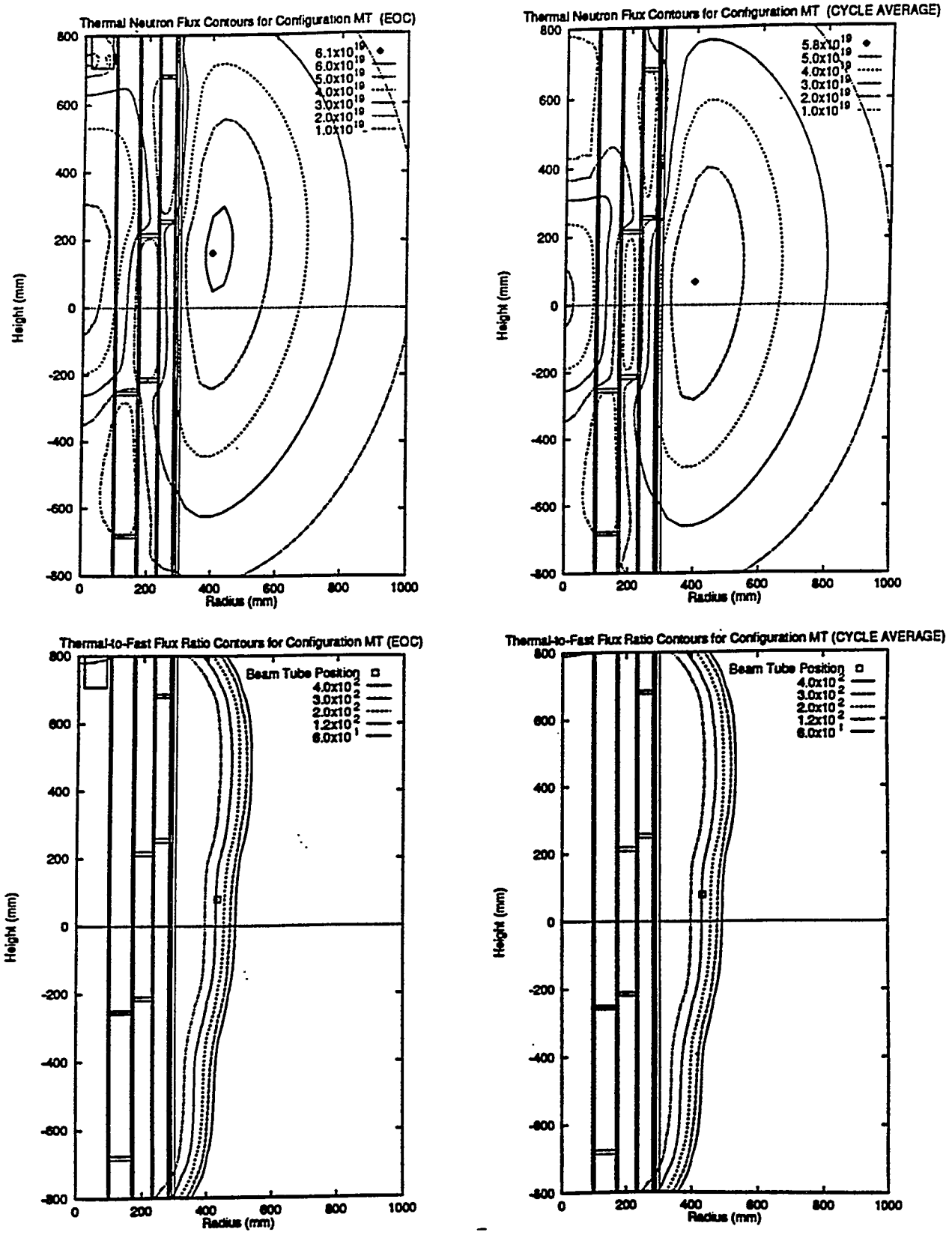

Fig. 4.7. Thermal neutron flux and thermal-to-fast flux ratio contours for configuration MT (continued).

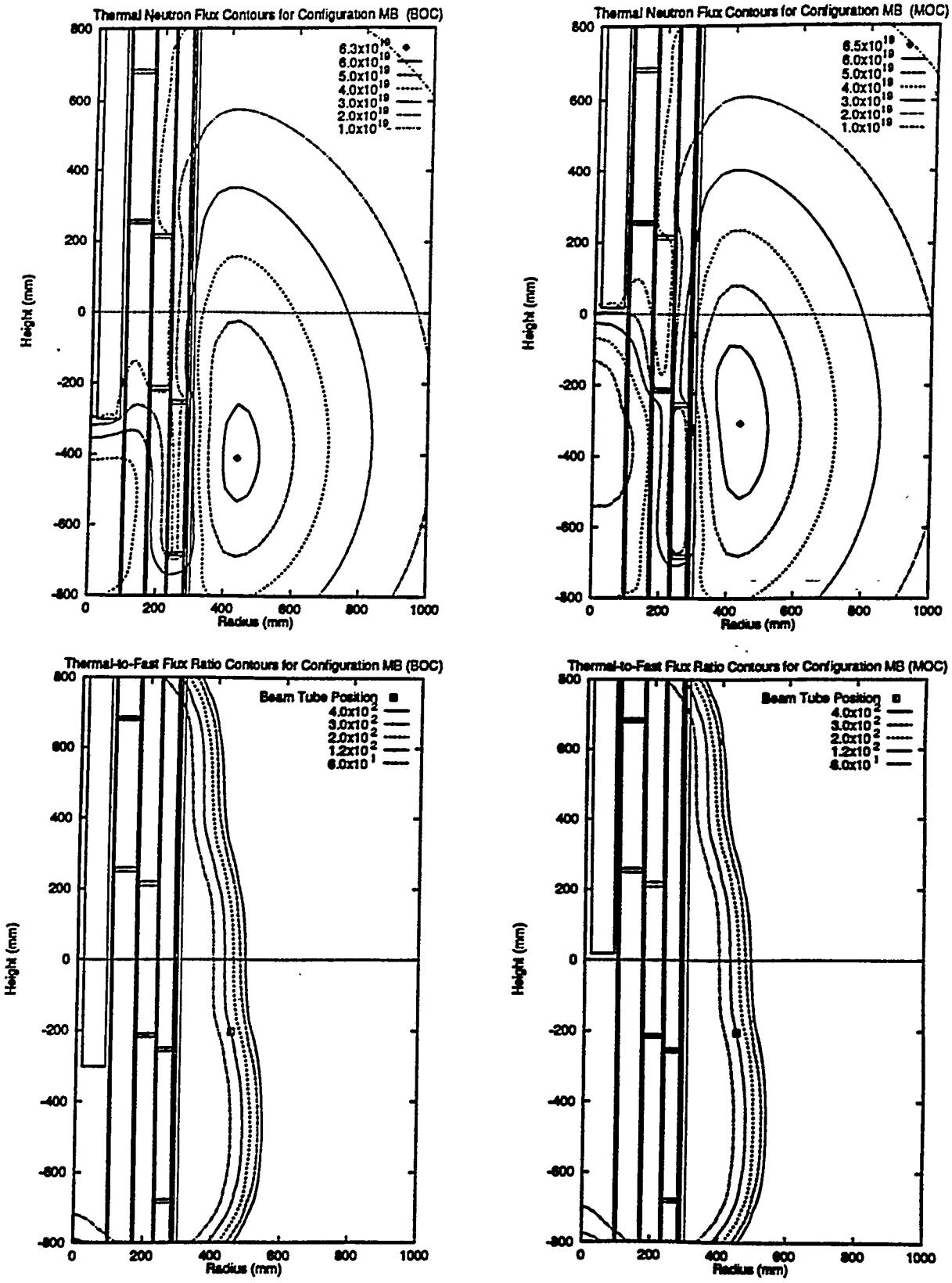

Fig. 4.8. Thermal neutron flux and thermal-to-fast flux ratio contours for configuration MB.

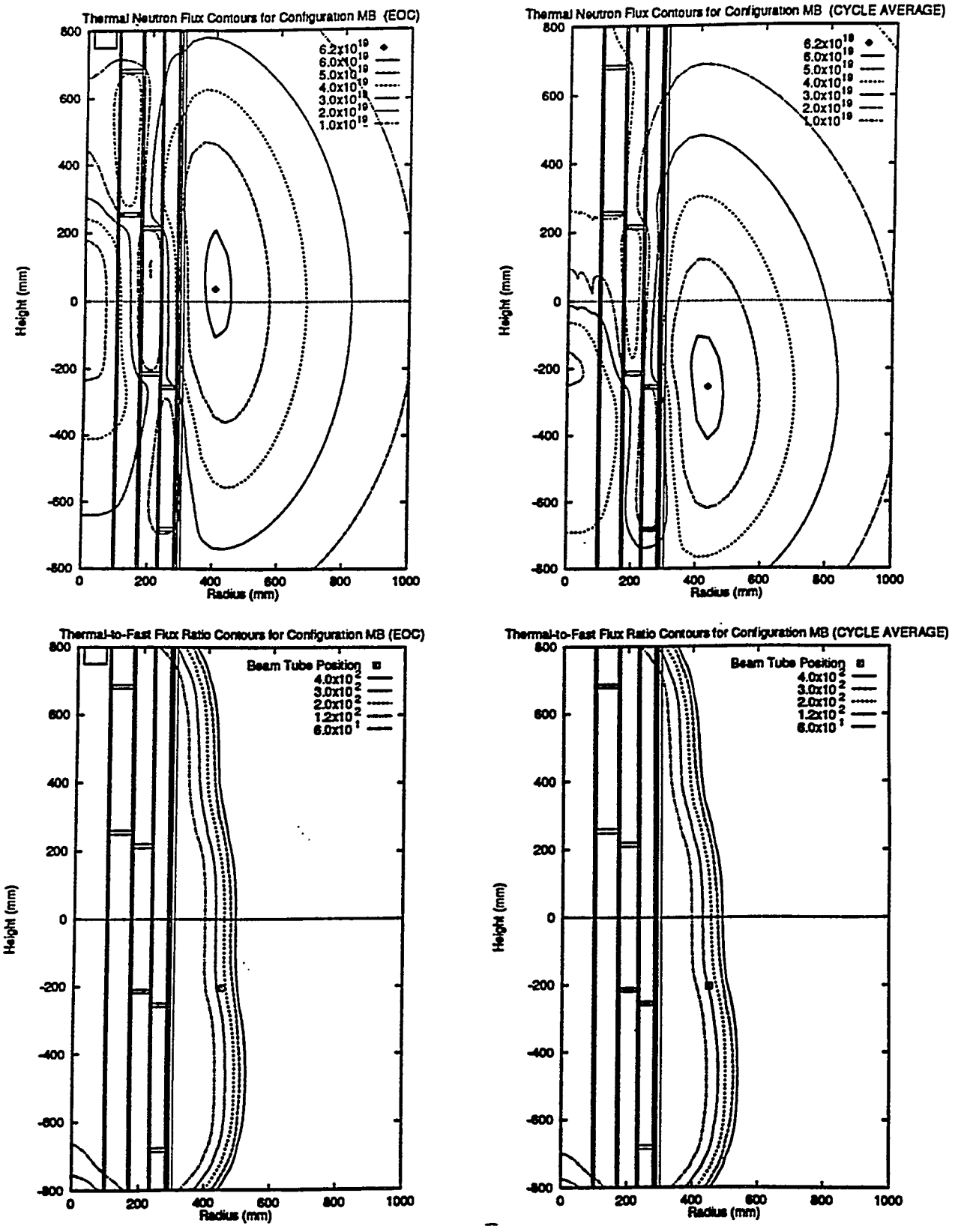

Fig. 4.8. Thermal neutron flux and thermal-to-fast flux ratio contours for configuration MB (continued).

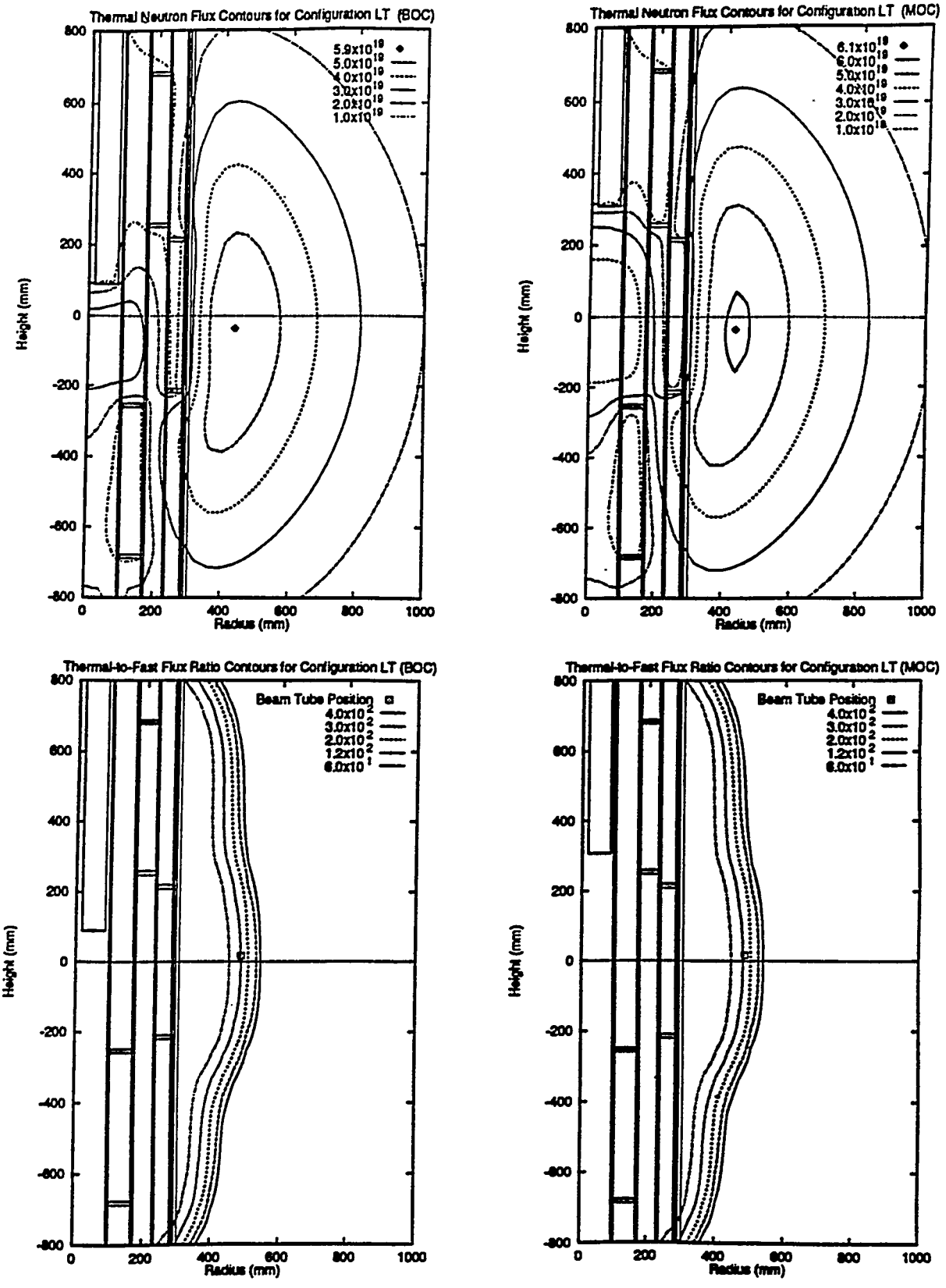

Fig. 4.9. Thermal neutron flux and thermal-to-fast flux ratio contours for configuration LT.

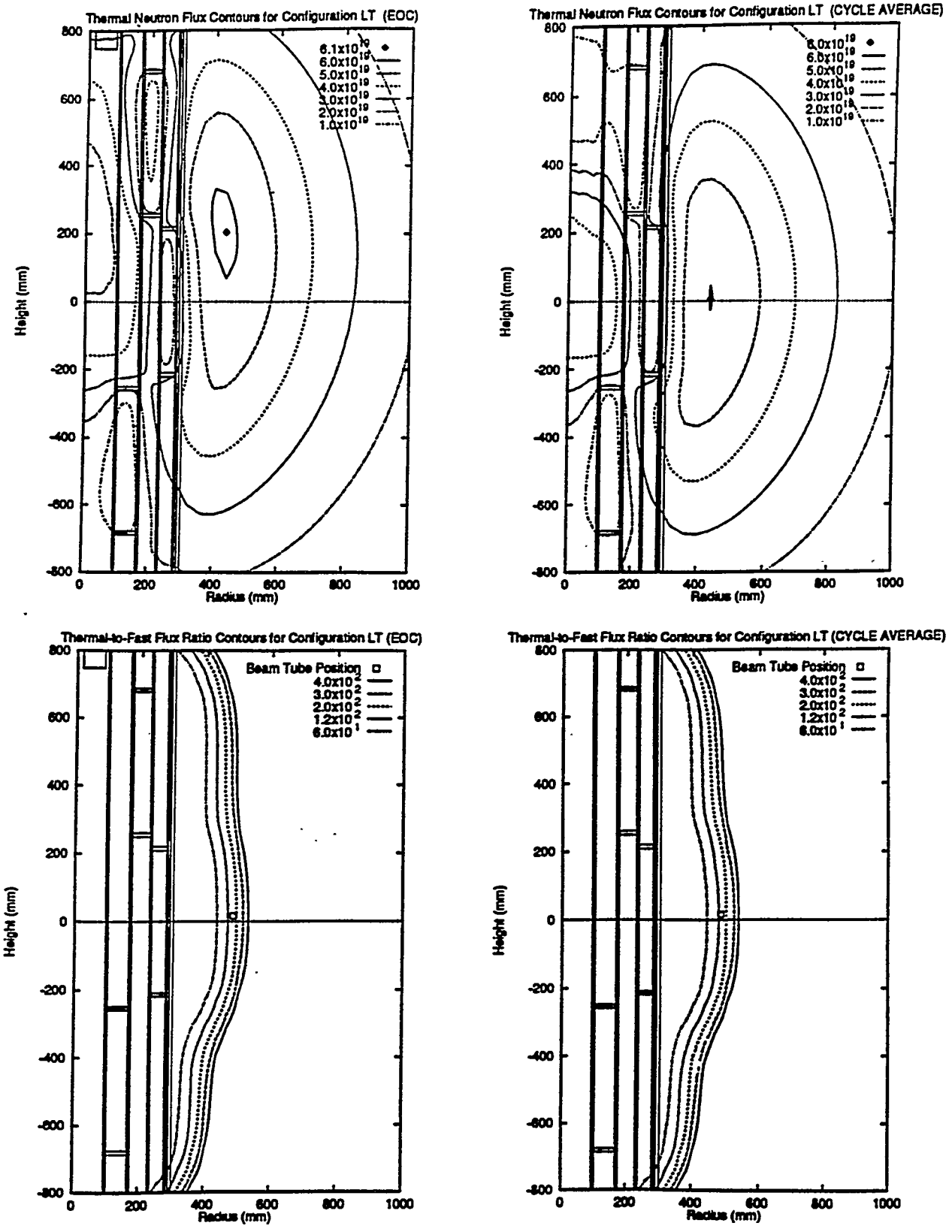

Fig. 4.9. Thermal neutron flux and thermal-to-fast flux ratio contours for configuration LT (continued).

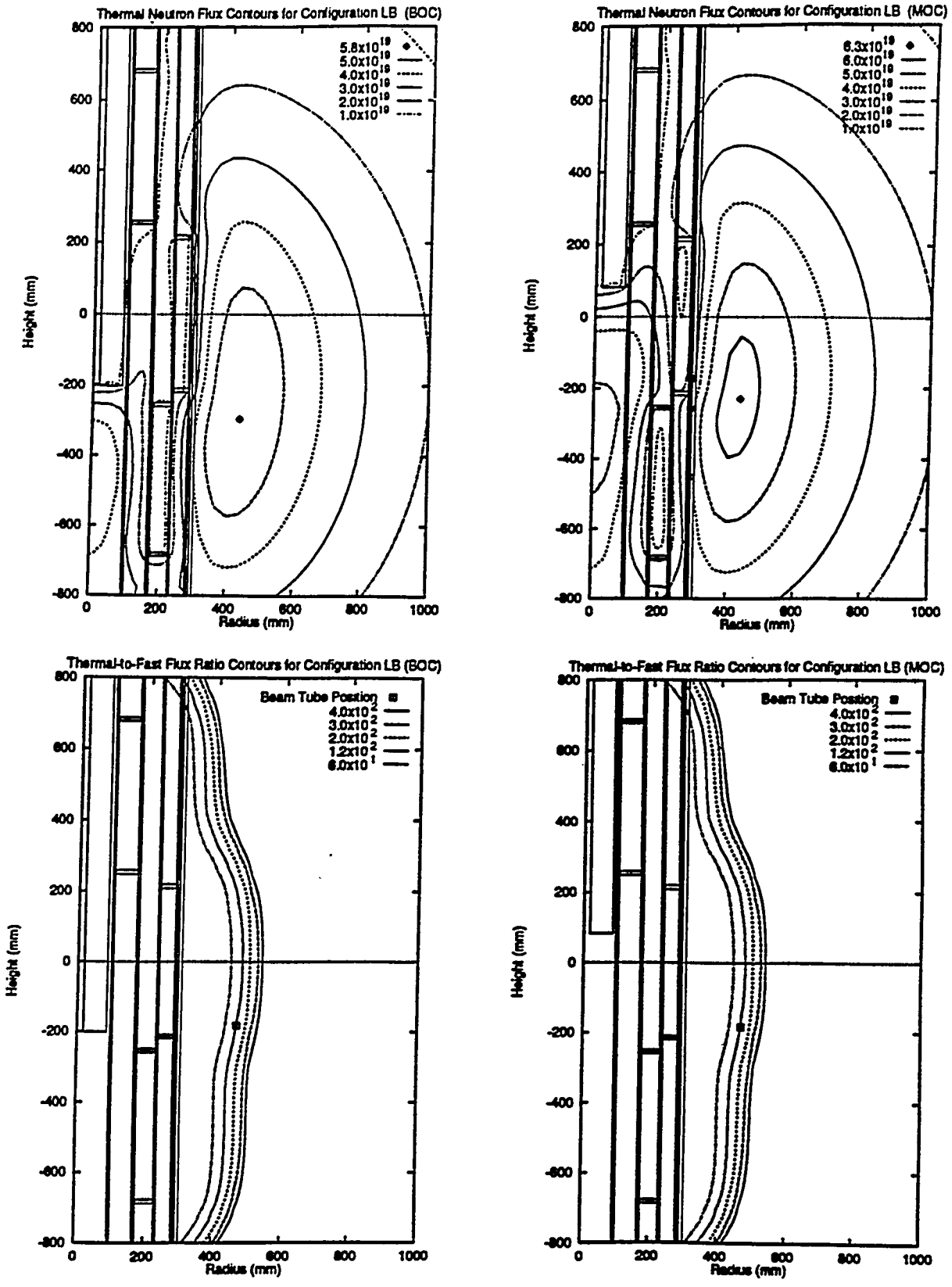

Fig. 4.10. Thermal neutron flux and thermal-to-fast flux ratio contours for configuration LB.

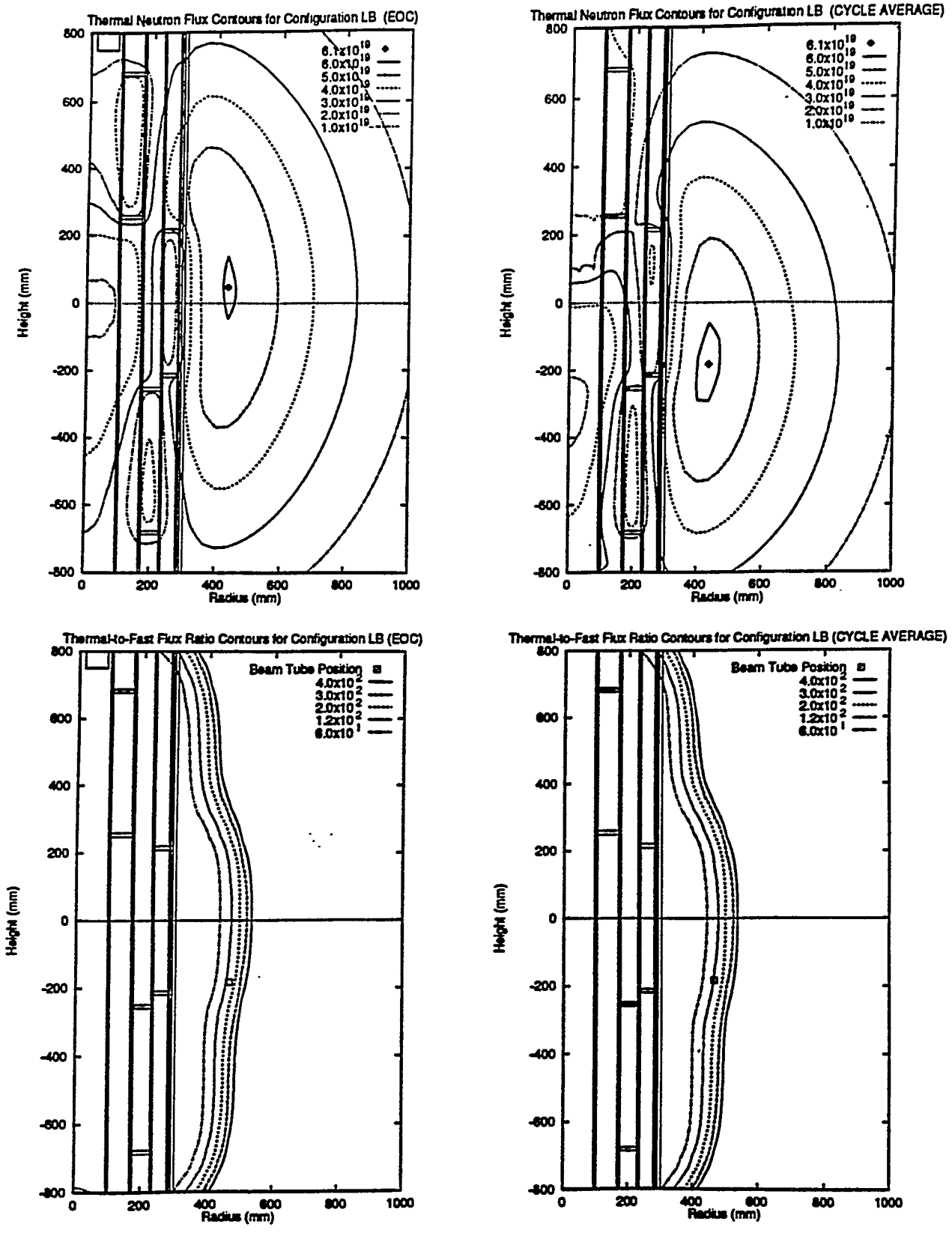

Fig. 4.10. Thermal neutron flux and thermal-to-fast flux ratio contours for configuration LB (continued).

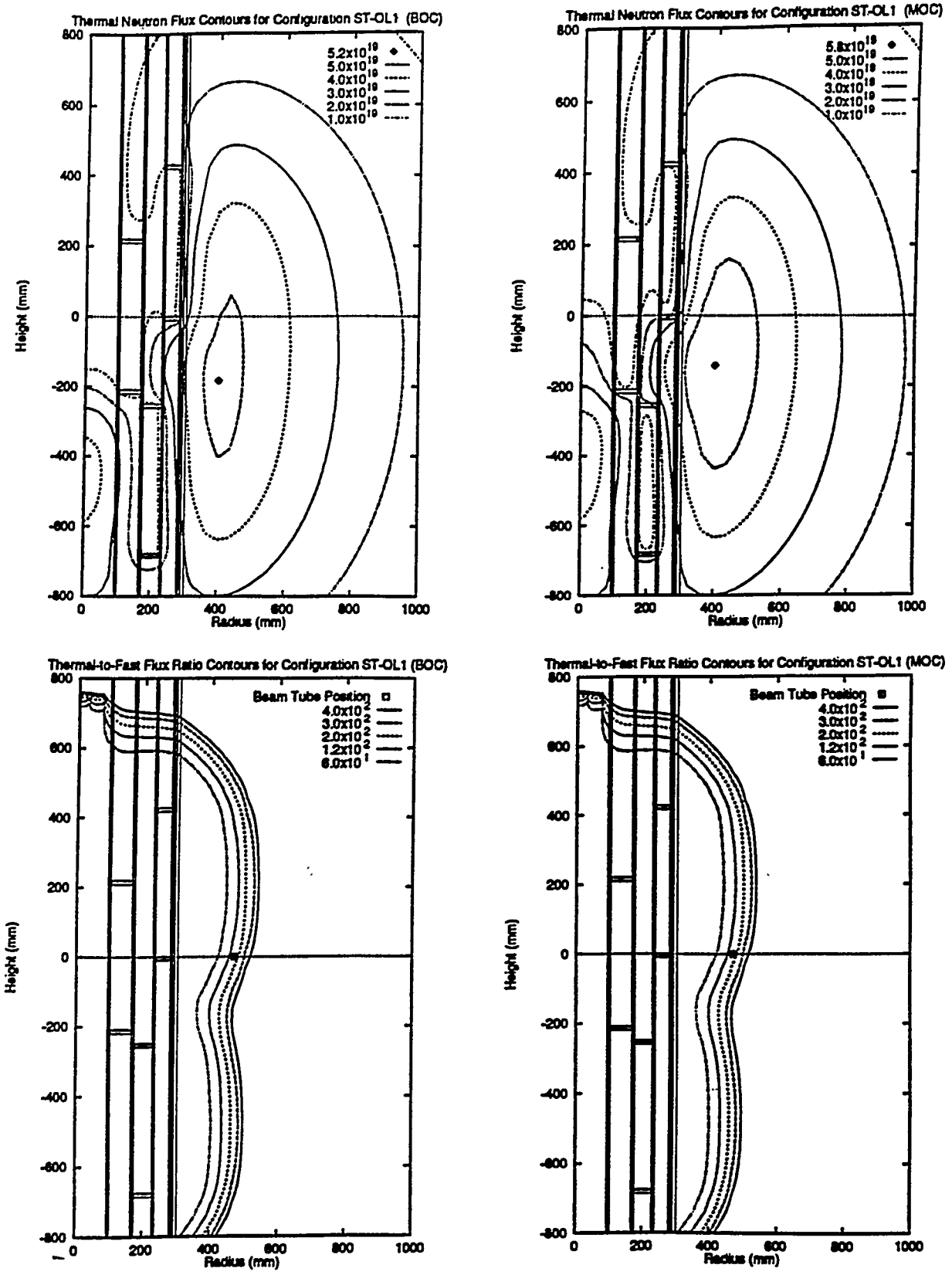

Fig. 4.11. Thermal neutron flux and thermal-to-fast flux ratio contours for half overlap ST-OL1 configuration.

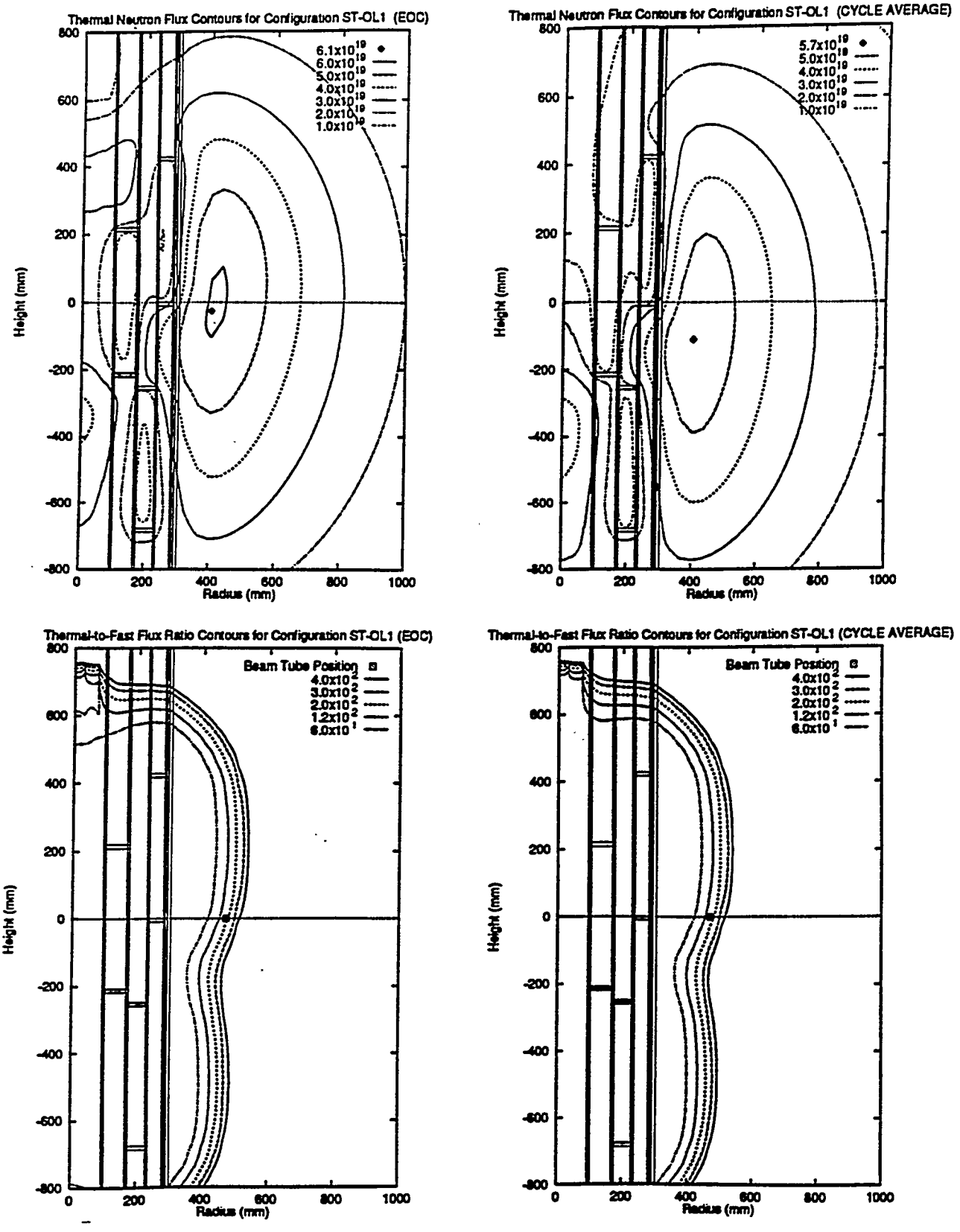

Fig. 4.11. Thermal neutron flux and thermal-to-fast flux ratio contours for half overlap ST-OL1 configuration (continued).

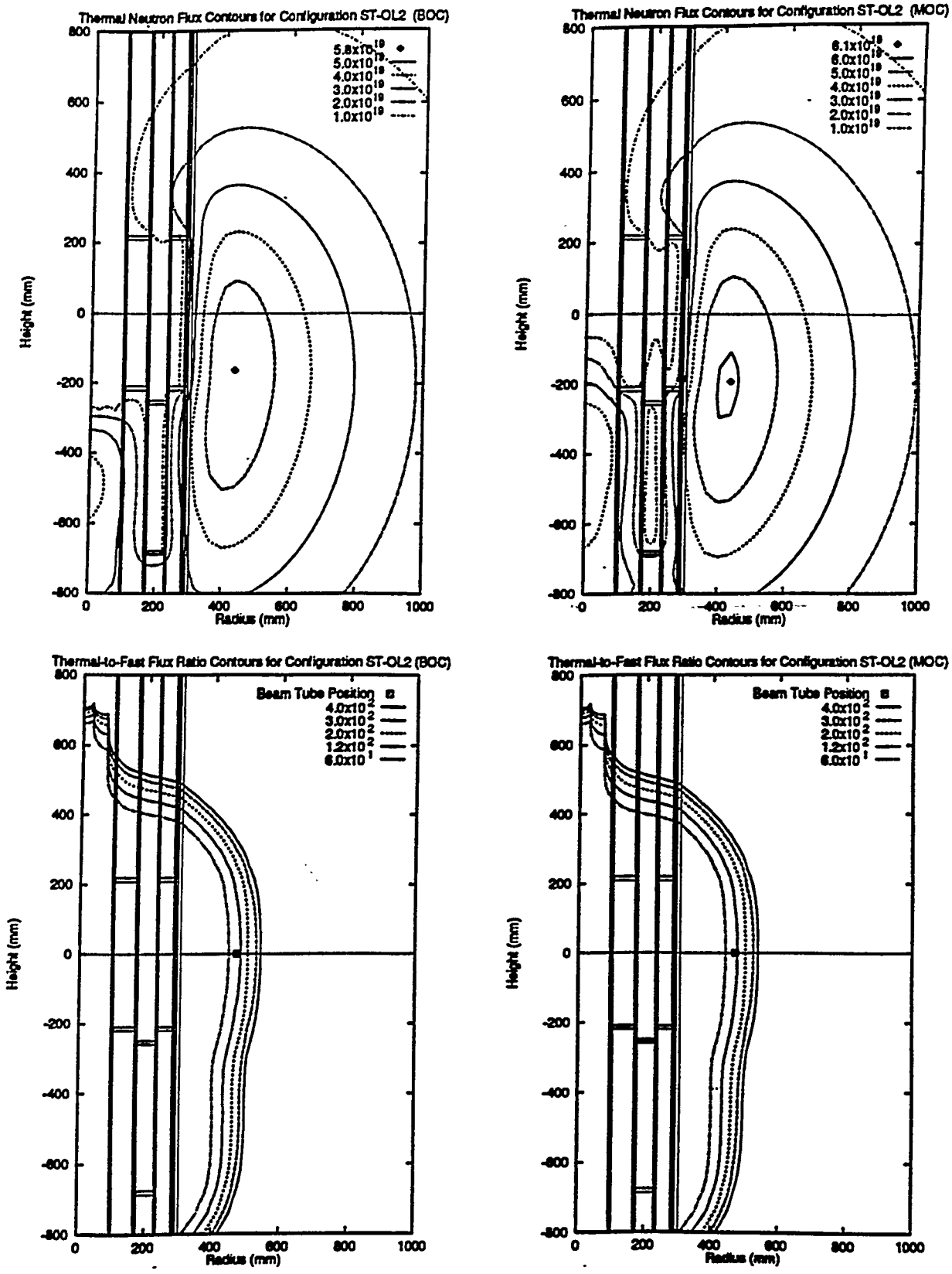

Fig. 4.12. Thermal neutron flux and thermal-to-fast flux ratio contours for full overlap ST-OL2 configuration.

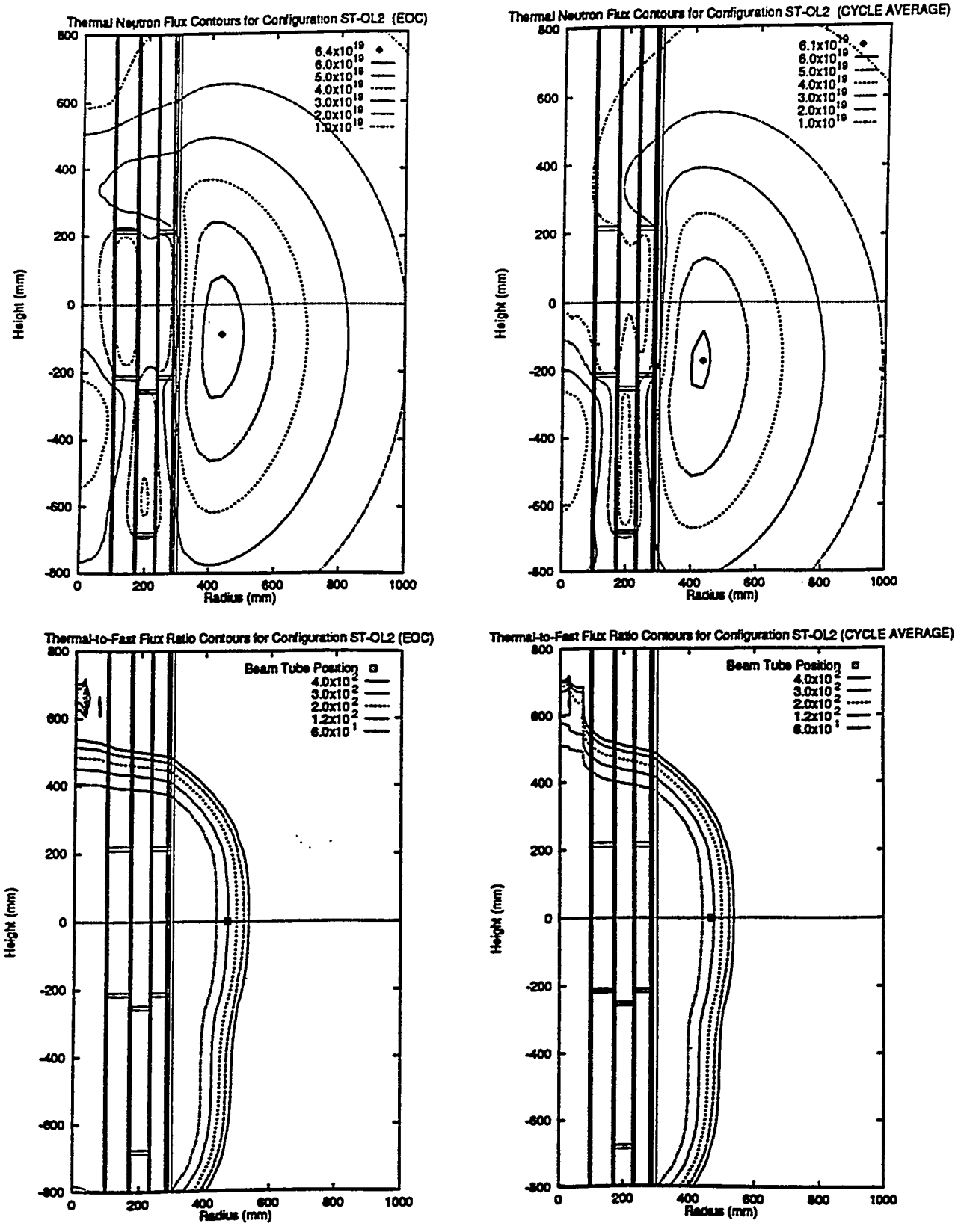

Fig. 4.12. Thermal neutron flux and thermal-to-fast flux ratio contours for full overlap ST-OL2 configuration (continued).

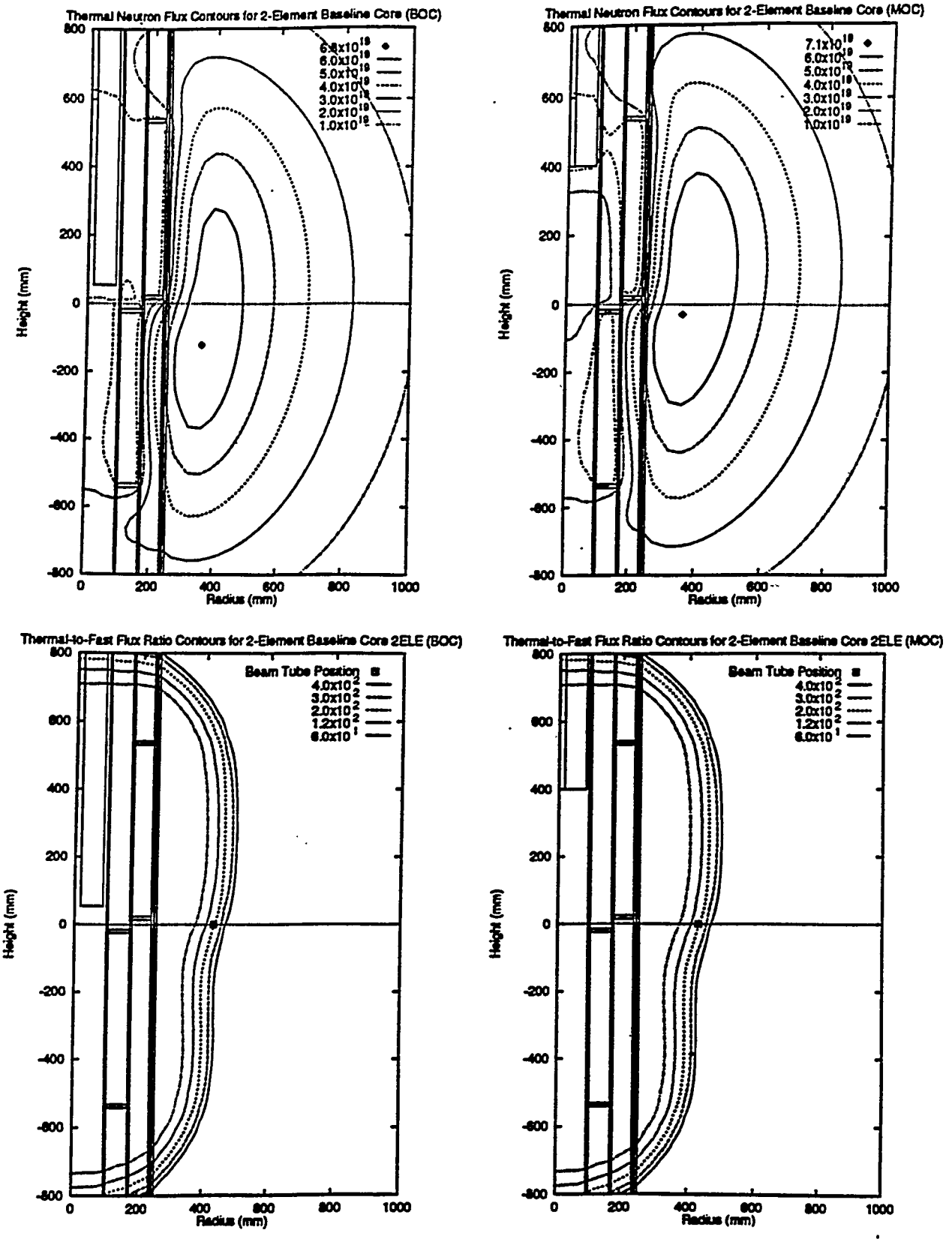

Fig. 4.13. Thermal neutron flux and thermal-to-fast flux ratio contours for two-element conceptual core configuration.

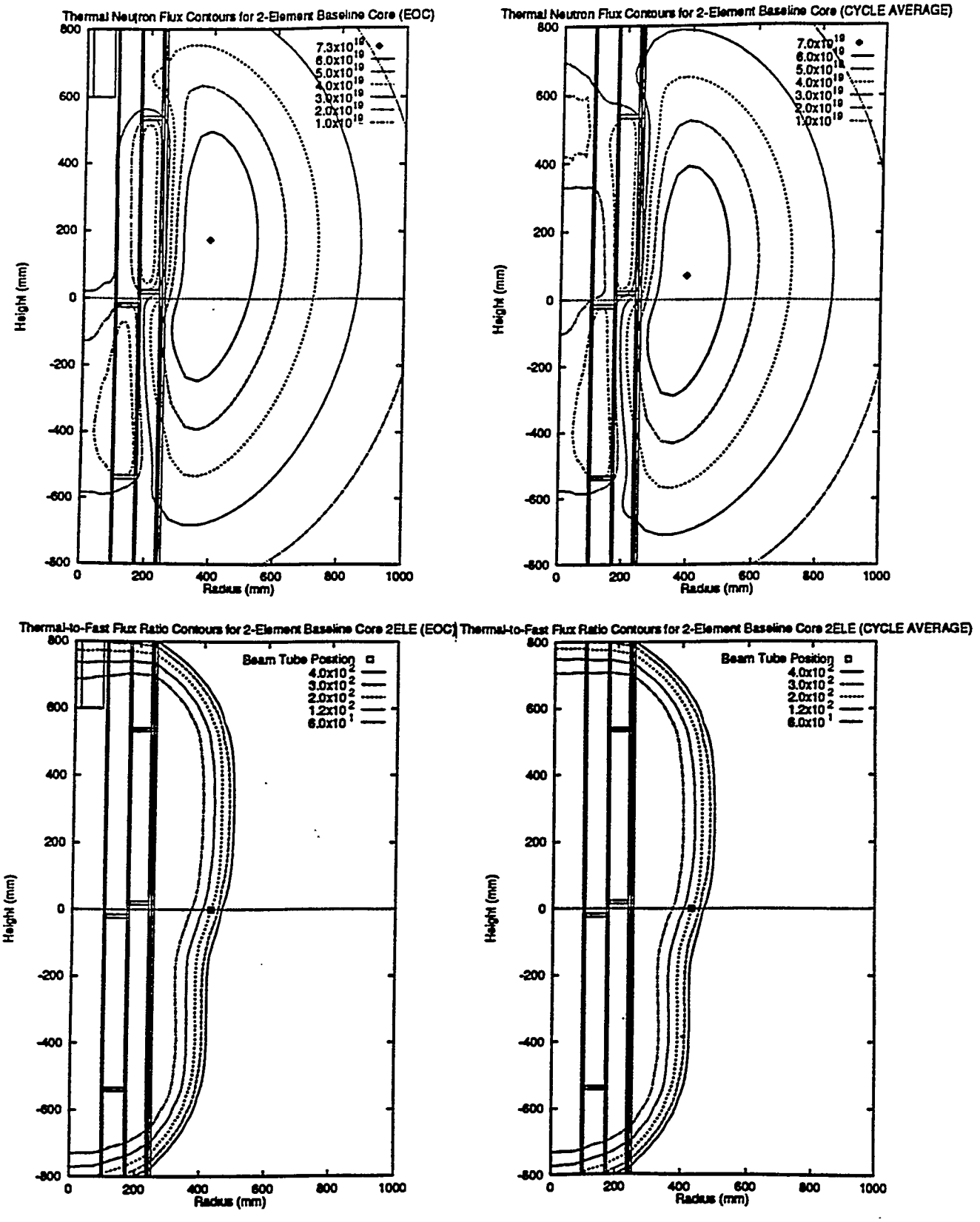

Fig. 4.13. Thermal neutron flux and thermal-to-fast flux ratio contours for two-element conceptual core configuration (continued).

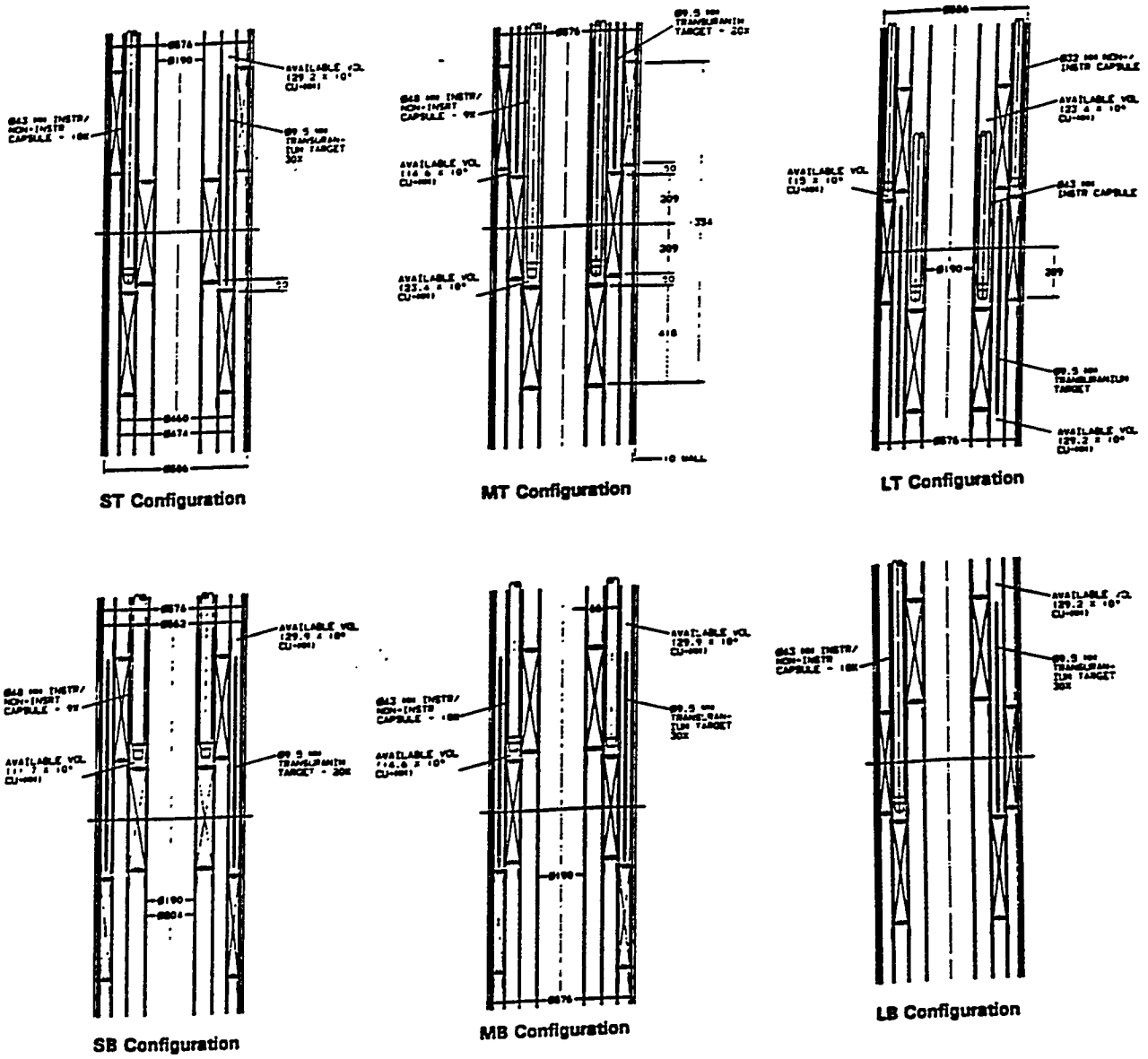

Fig. 4.14. Diagrams showing the locations of the irradiation and production regions for the basic three-element core configurations.

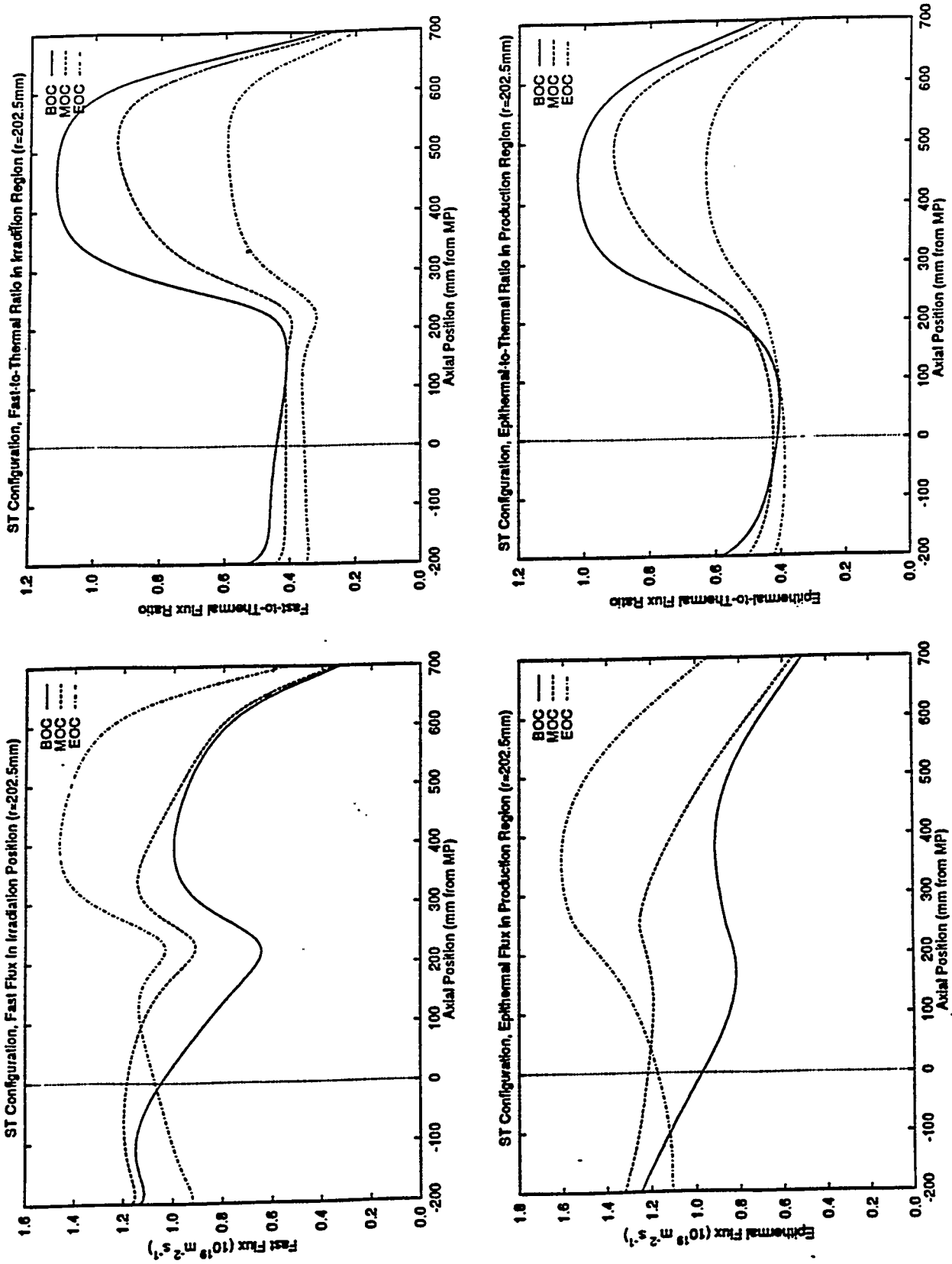

Fig. 4.15. Neutron fluxes and flux ratios in irradiation and production regions of three-element core configuration ST.

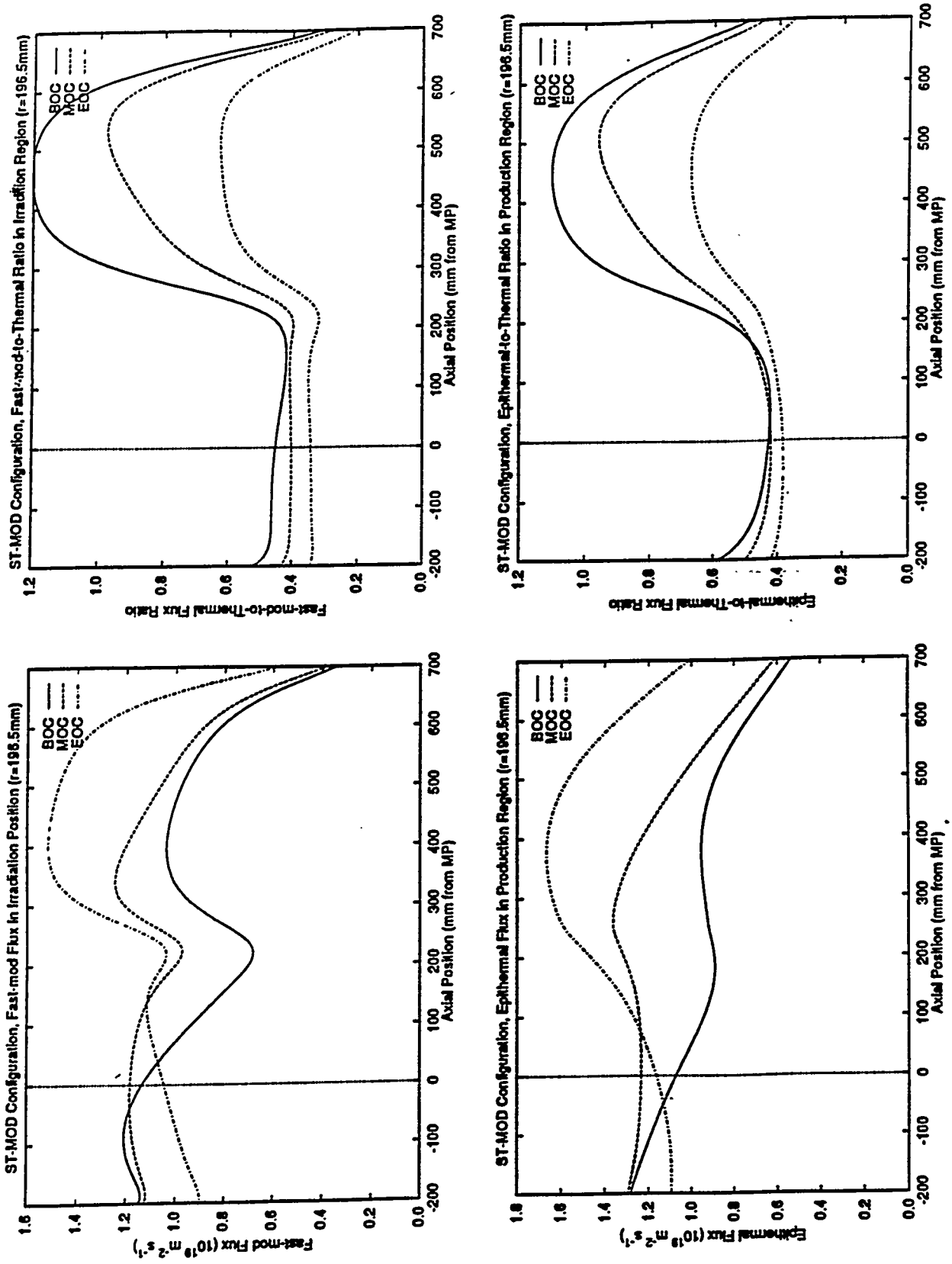

Fig. 4.16. Neutron fluxes and flux ratios in irradiation and production regions of three-element core configuration ST-MOD.

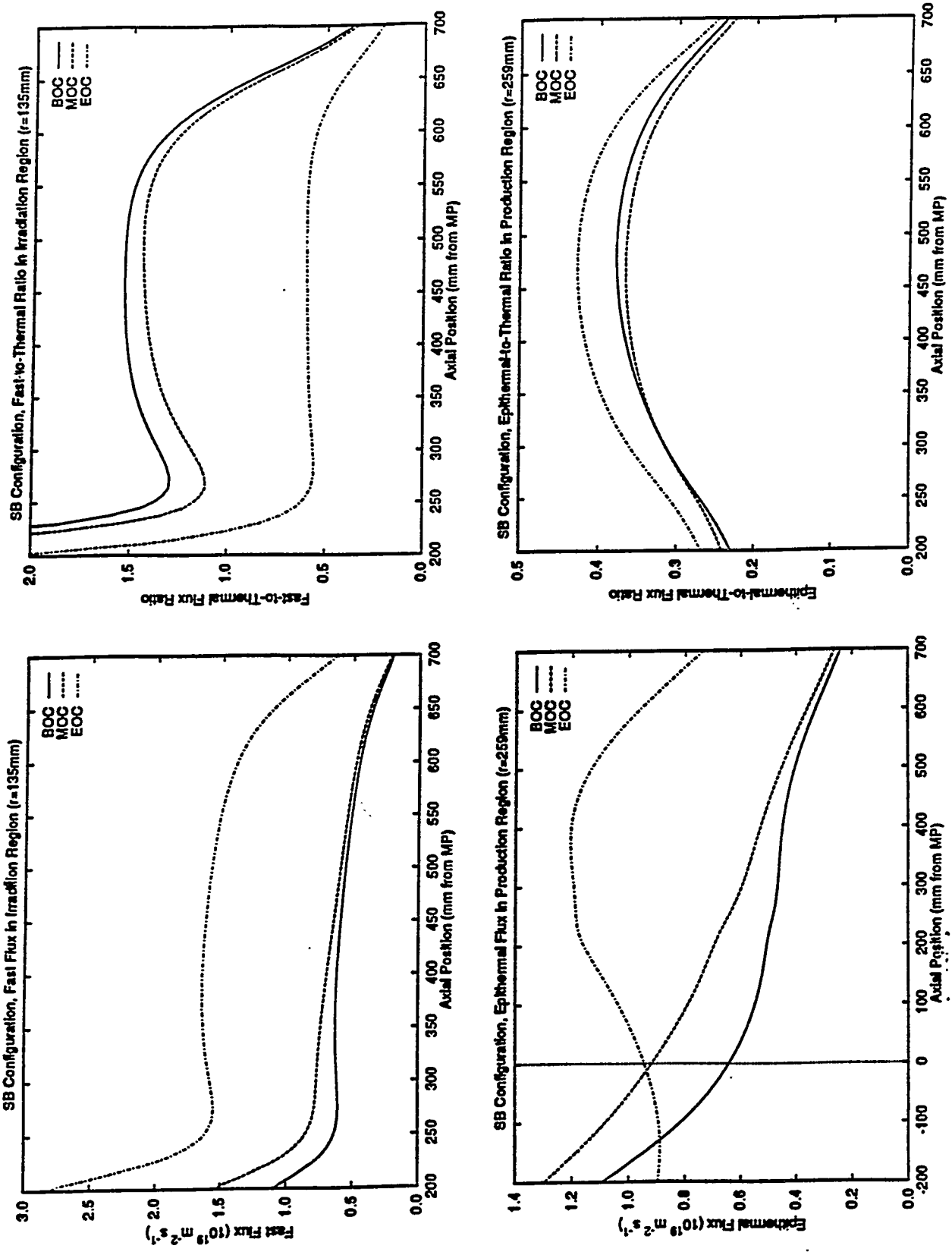

Fig. 4.17. Neutron fluxes and flux ratios in irradiation and production regions of three-element core configurations SB.

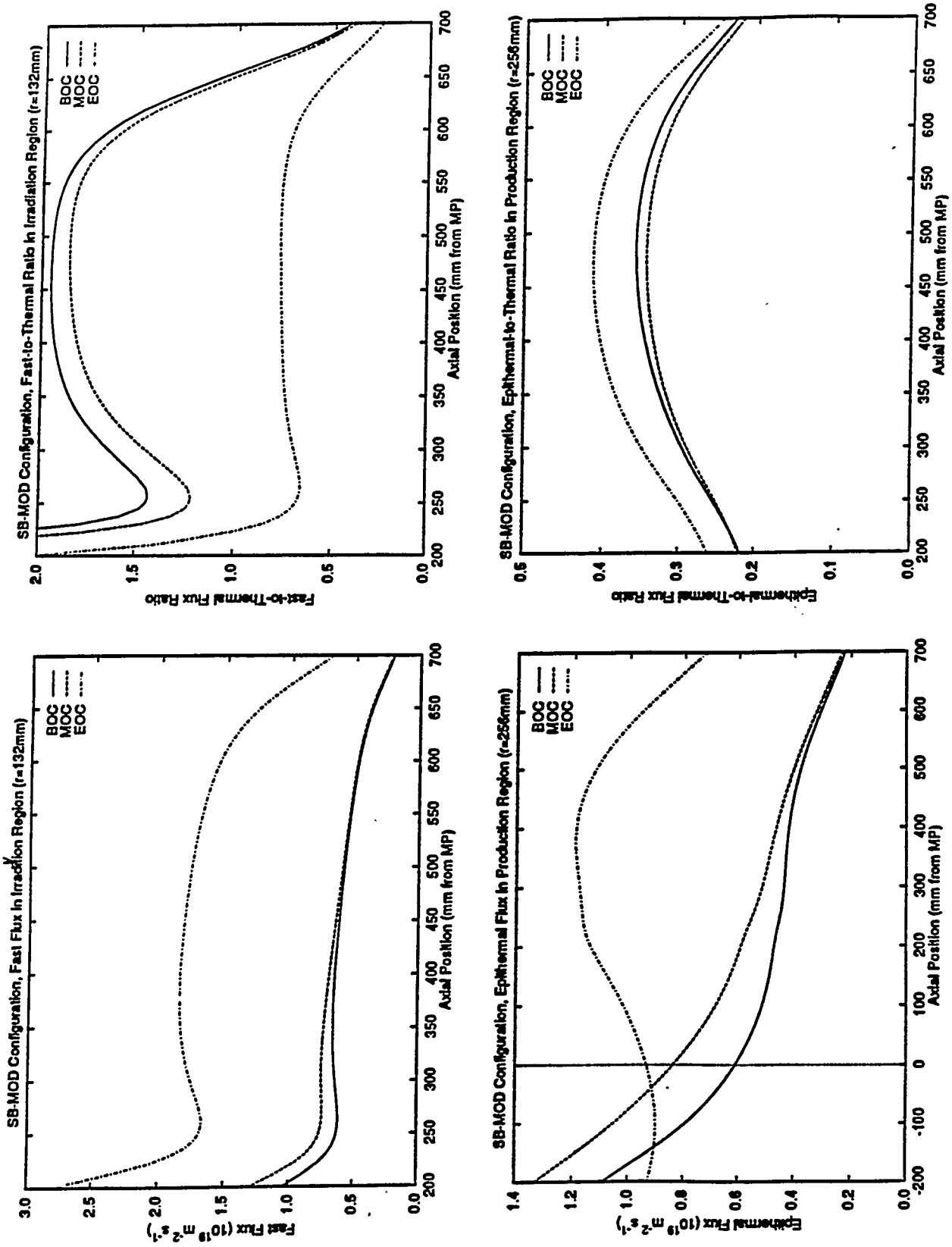

Fig. 4.18. Neutron fluxes and flux ratios in irradiation and production regions of three-element core configuration SB-MOD.

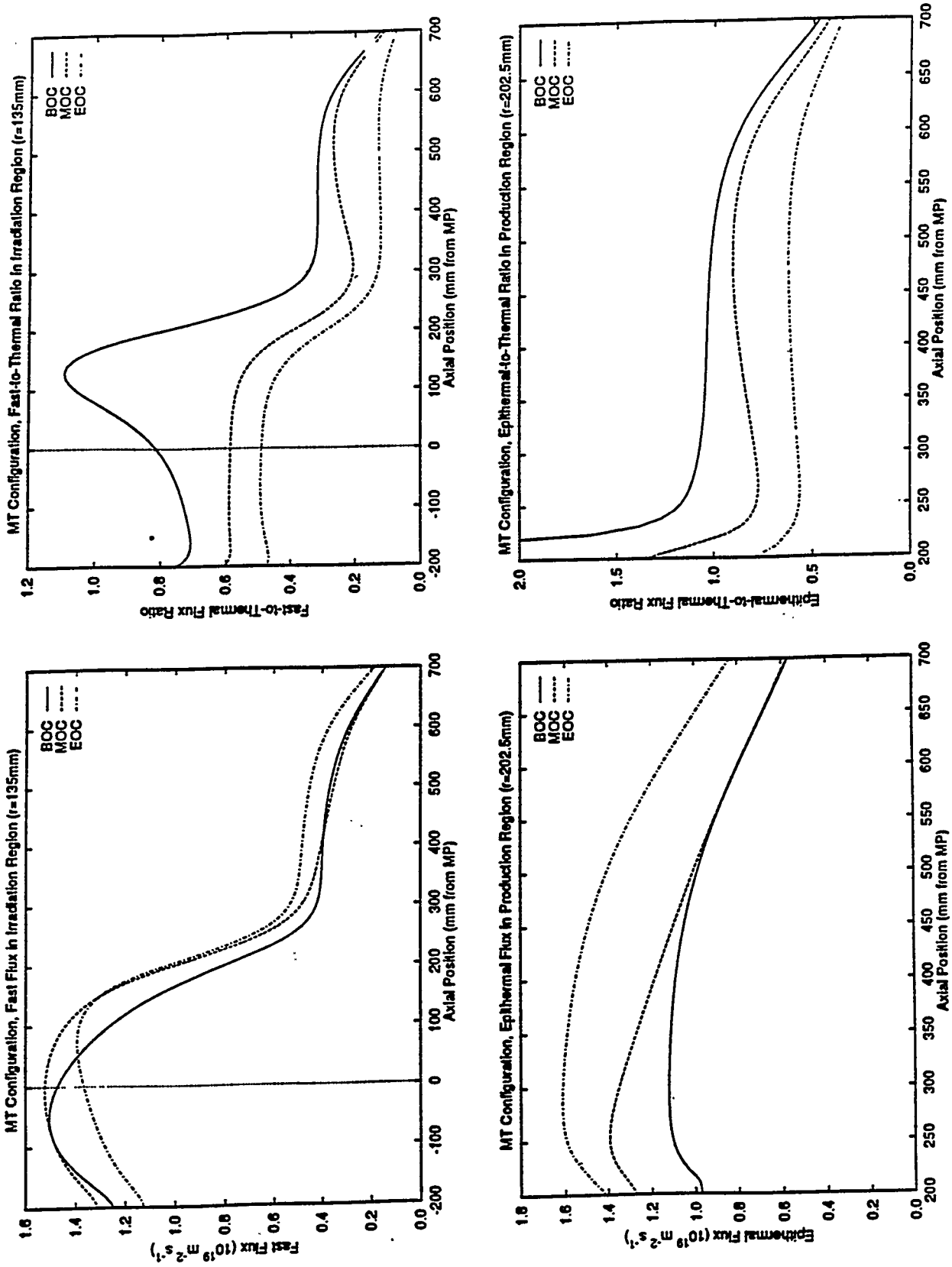

Fig. 4.19. Neutron fluxes and flux ratios in irradiation and production regions of three-element core configuration MT.

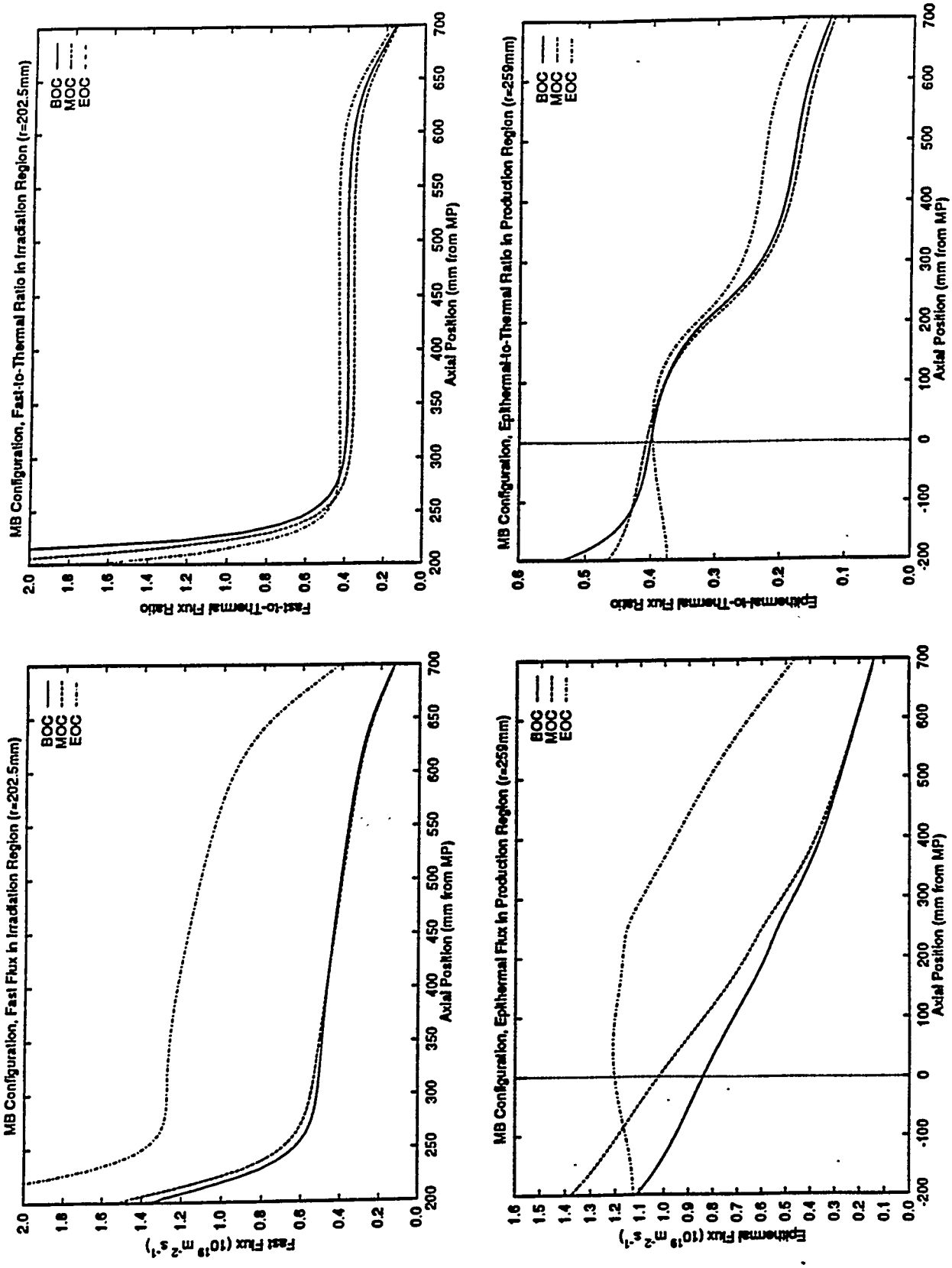

Fig. 4.20. Neutron fluxes and flux ratios in irradiation and production regions of three-element core configuration MB.

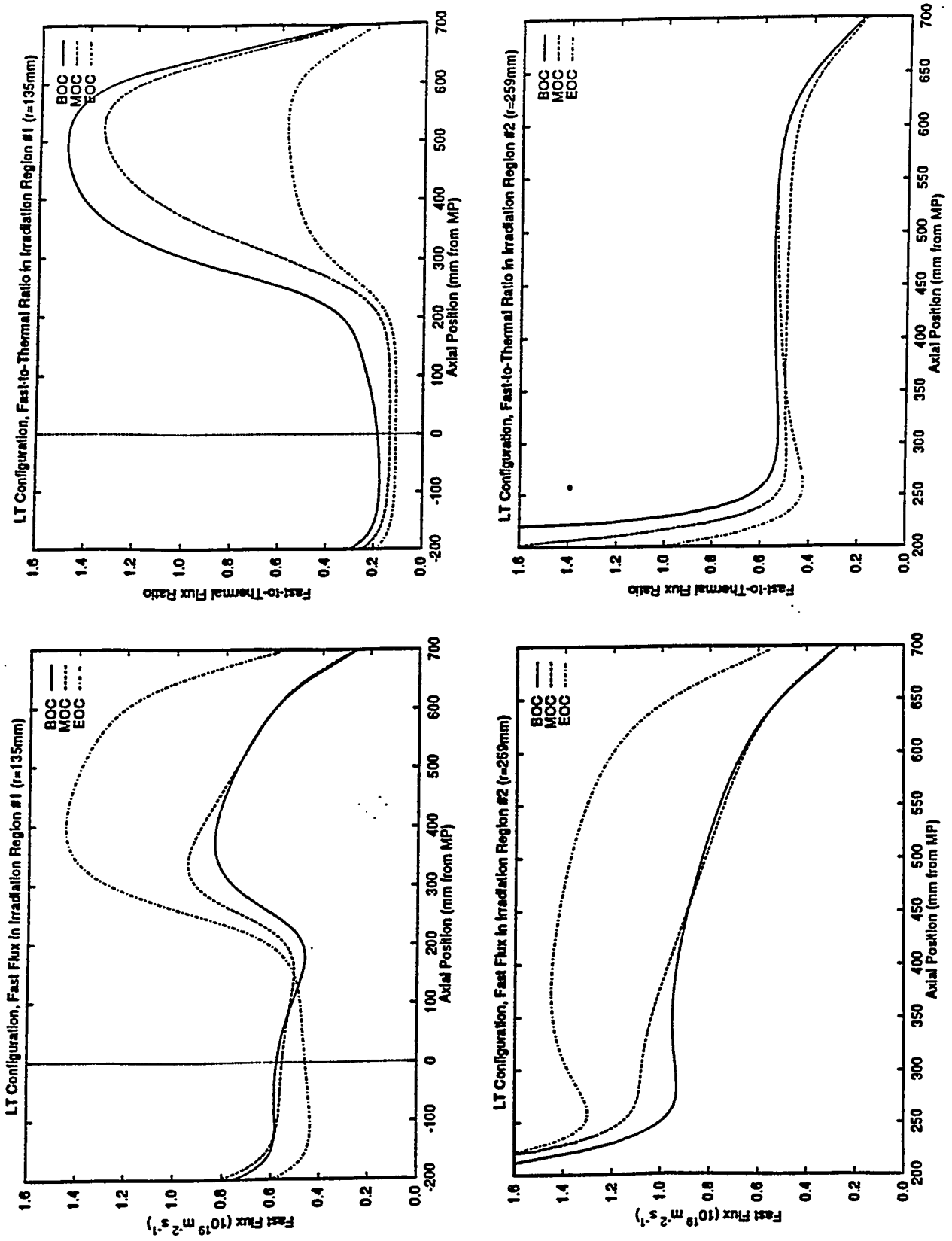

Fig. 4.21. Neutron fluxes and flux ratios in irradiation and production regions of three-element core configuration LT.

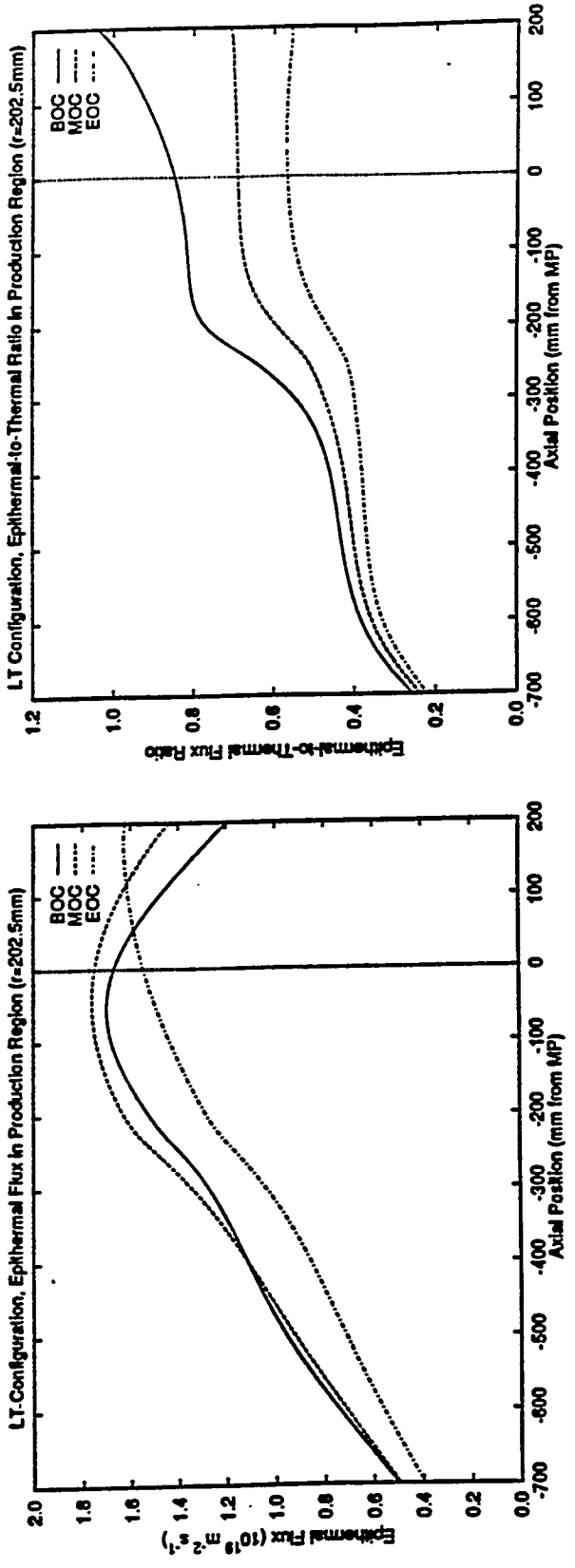

Fig. 4.21. Neutron fluxes and flux ratios in irradiation and production regions of three-element core configuration LT (continued).

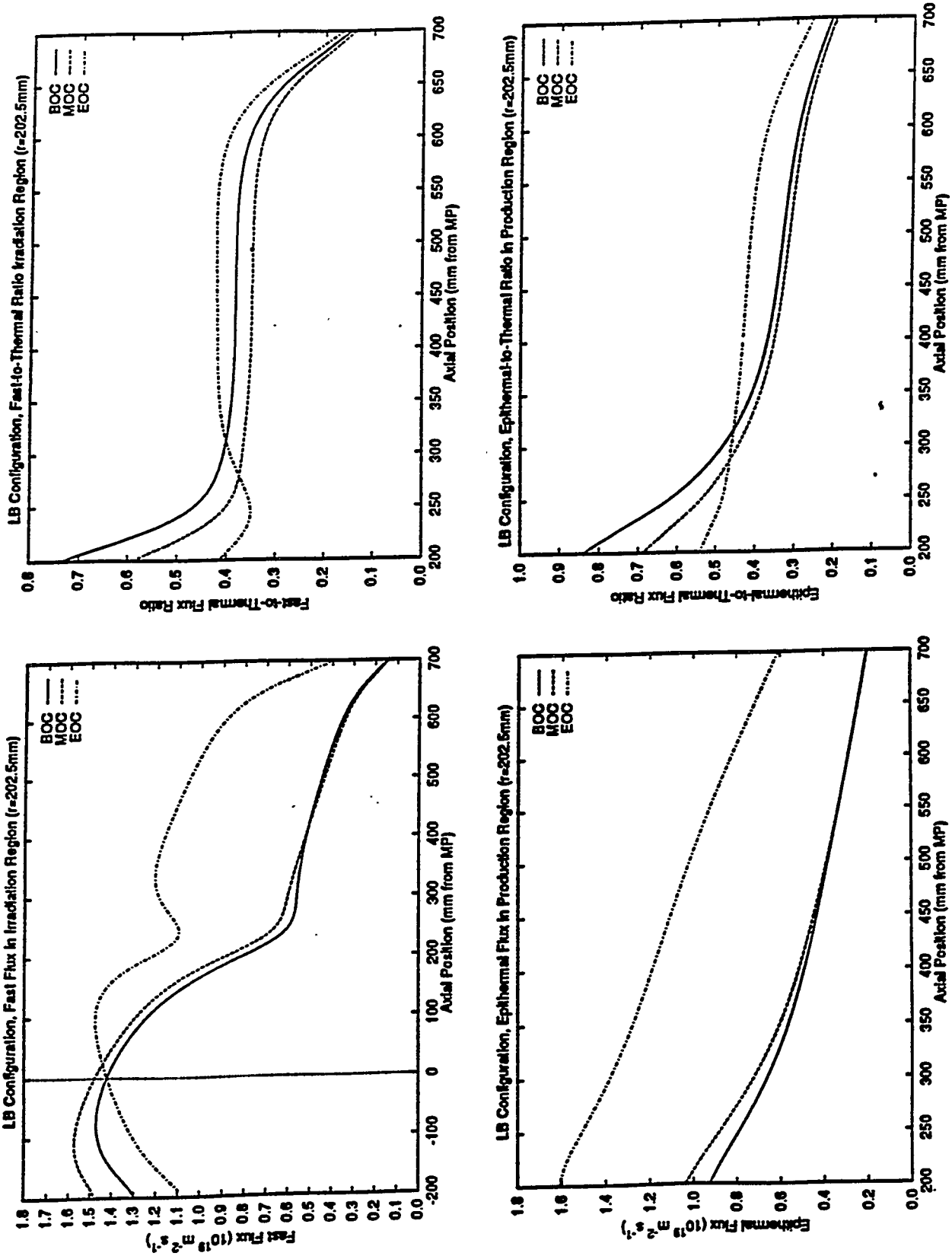

Fig. 4.22. Neutron fluxes and flux ratios in irradiation and production regions of three-element core configuration LB.

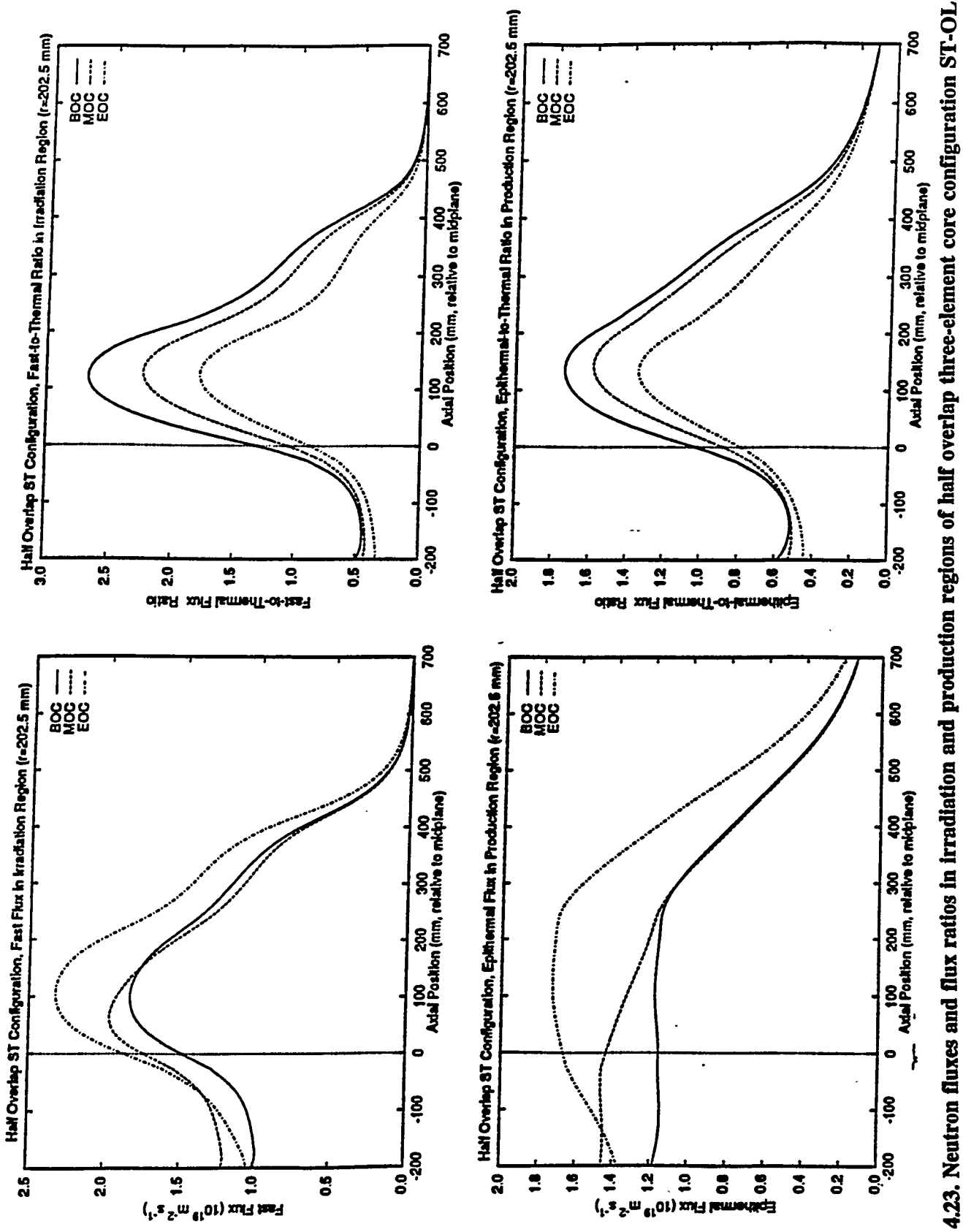

Fig. 4.23. Neutron fluxes and flux ratios in irradiation and production regions of half overlap three-element core configuration ST-OL1.

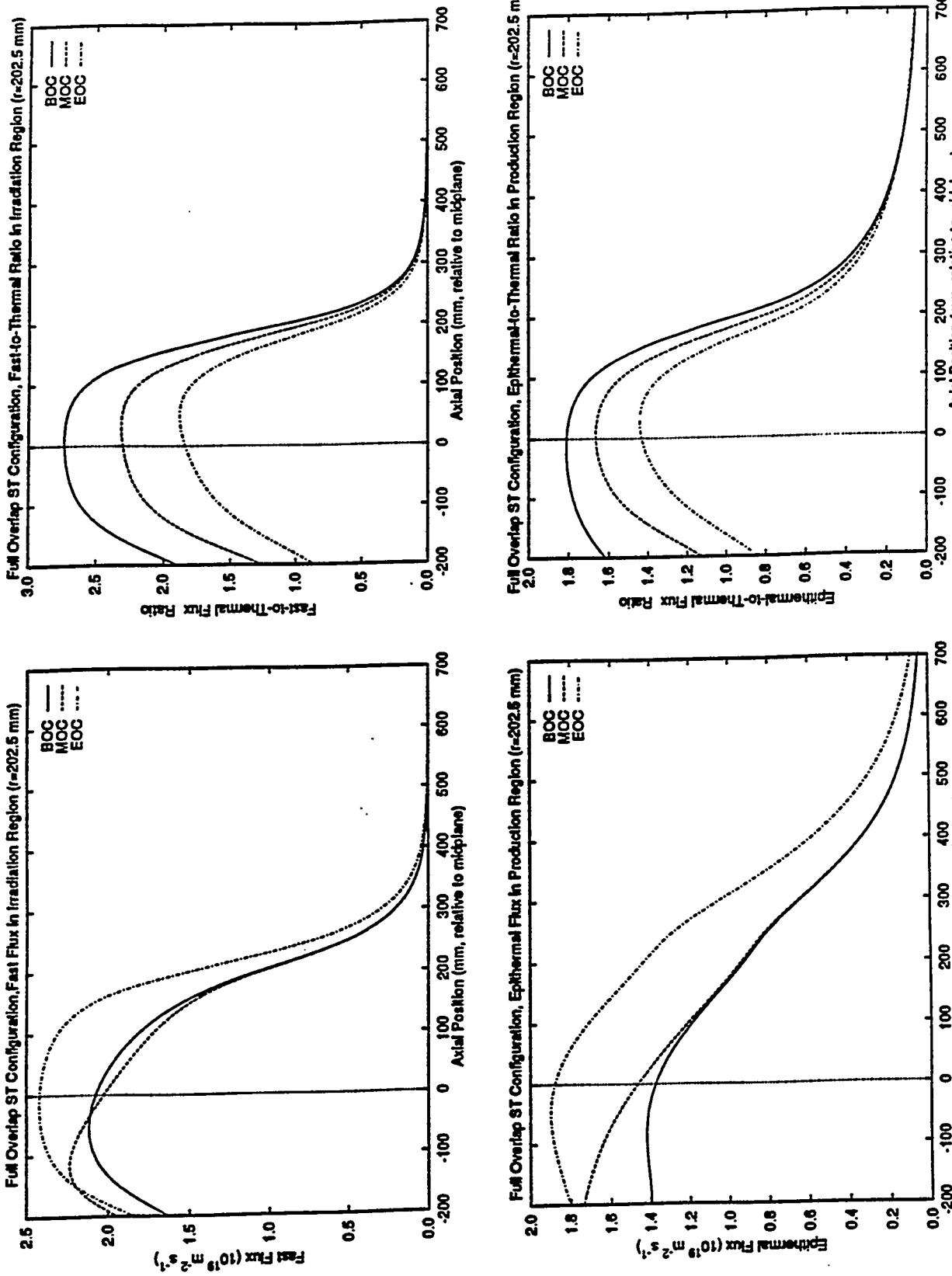

Fig. 4.24. Neutron fluxes and flux ratios in irradiation and production regions of full overlap three-element core configuration ST-OL2.

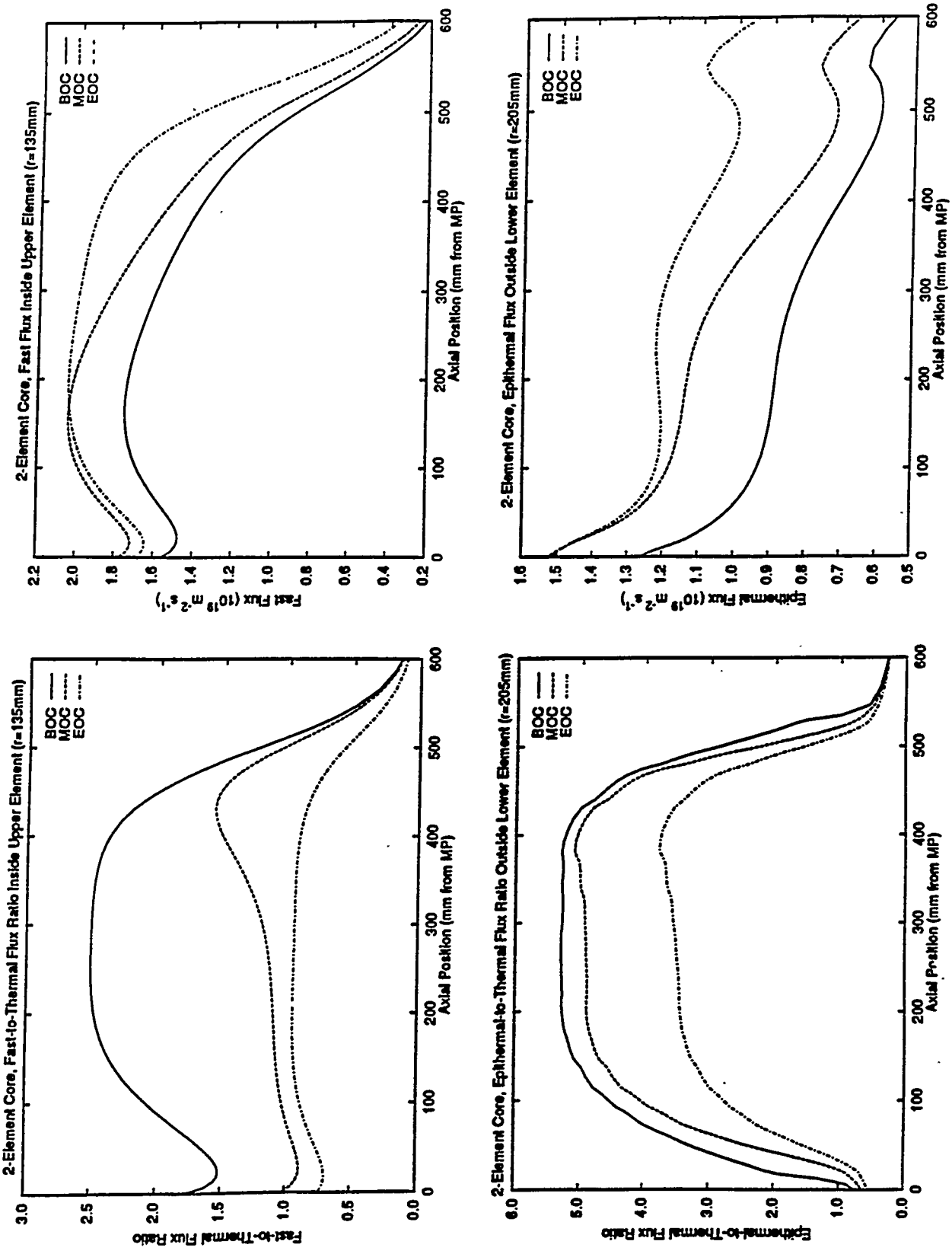

Fig. 4.25. Neutron fluxes and flux ratios in irradiation and production regions of two-element conceptual core configuration.

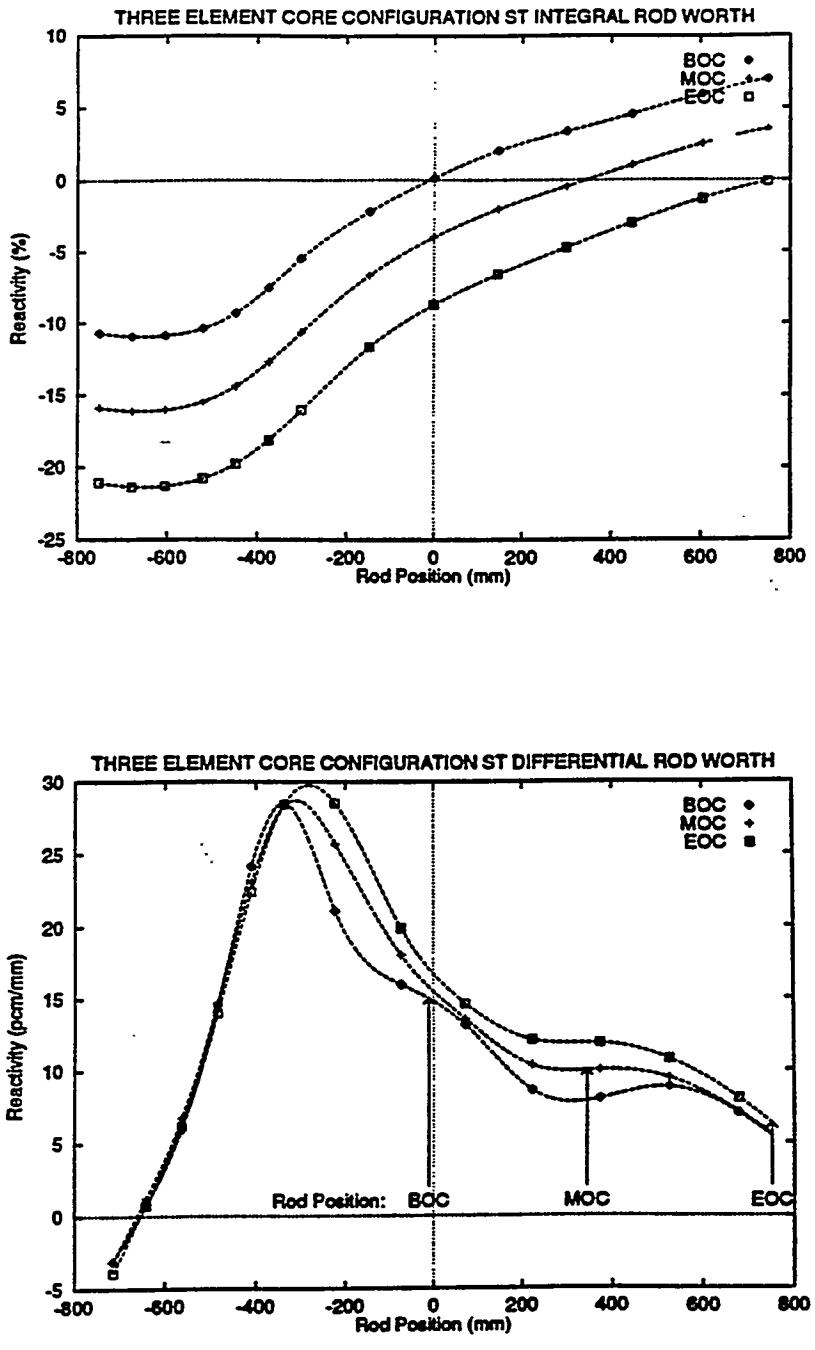

Fig. 4.26. Integral and differential control rod worth curves for three-element configuration ST.

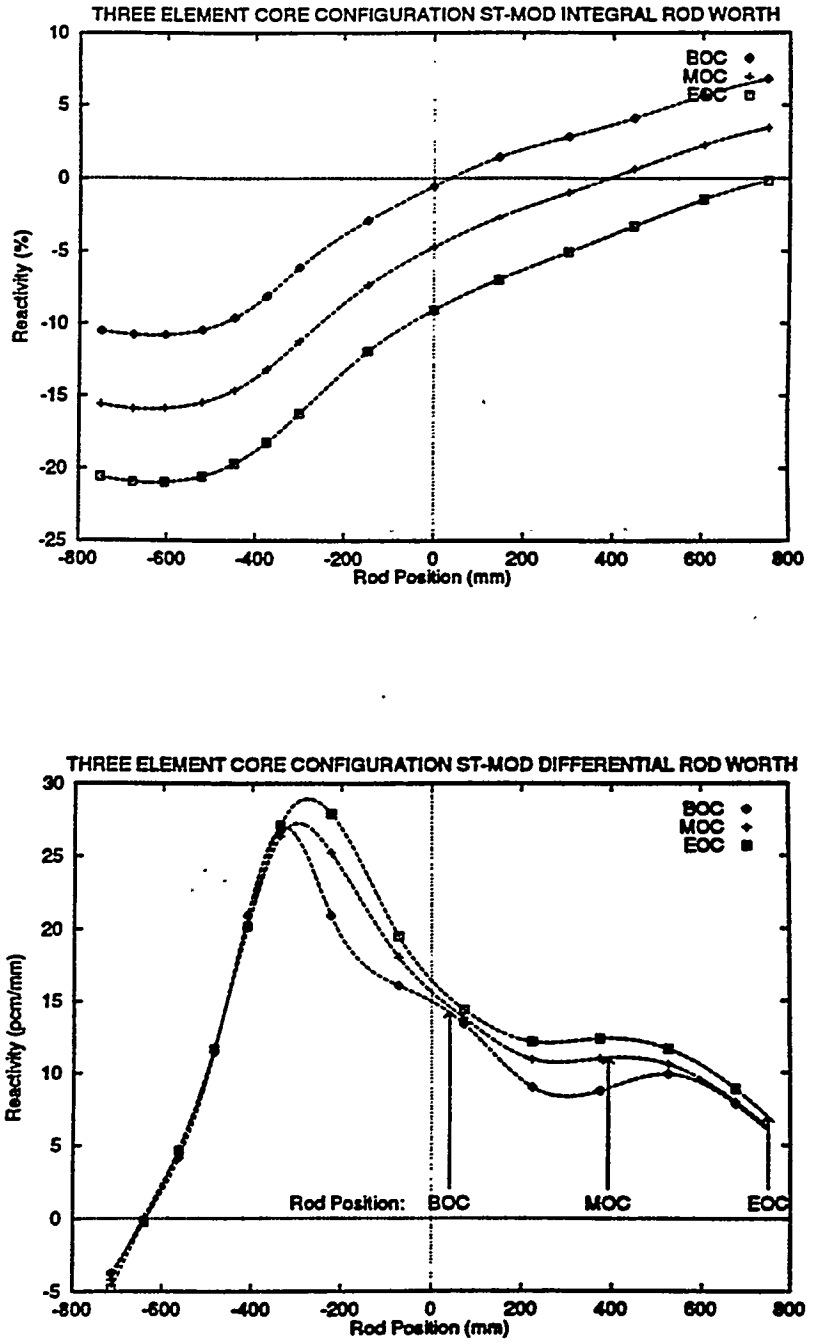

Fig. 4.27. Integral and differential control rod worth curves for three-element configuration ST-MOD.

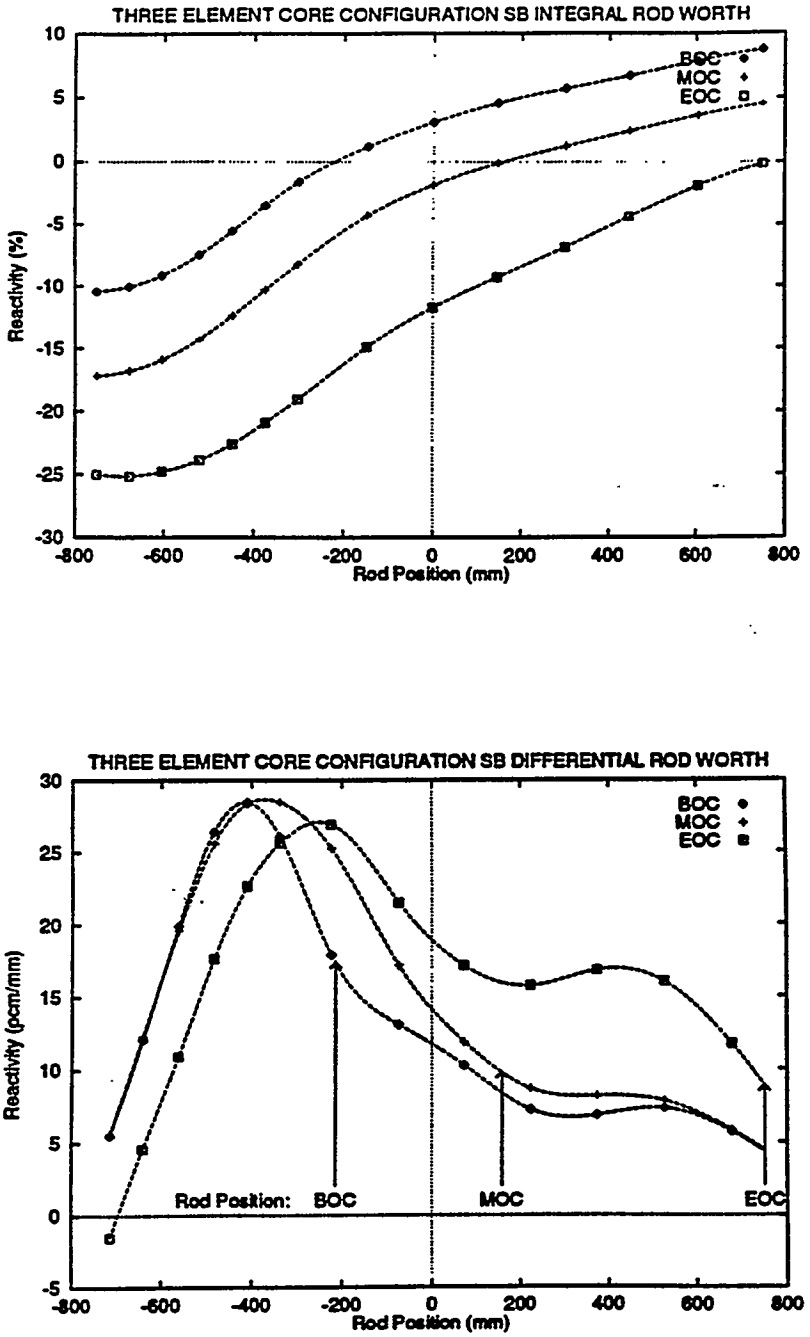

Fig. 4.28. Integral and differential control rod worth curves for three-element core configuration SB.

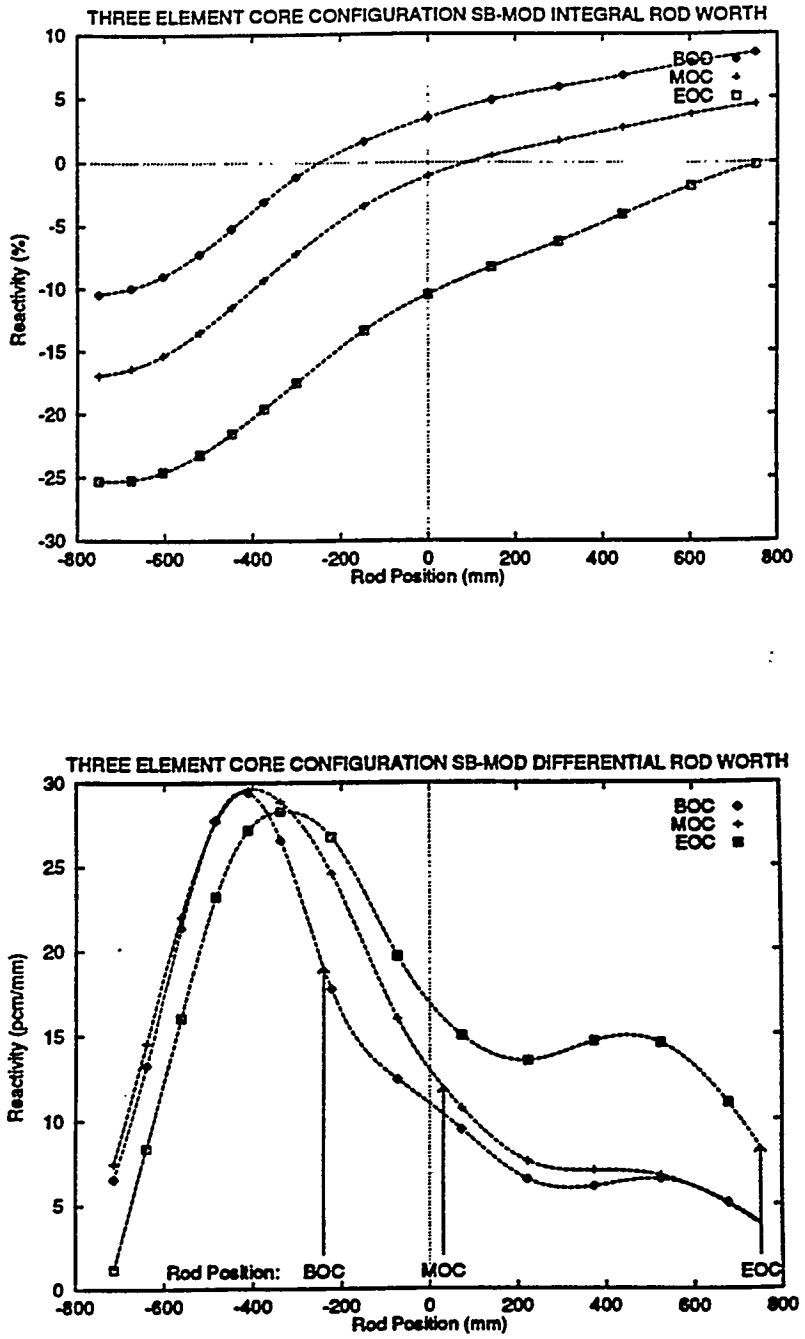

Fig. 4.29. Integral and differential control rod worth curves for three-element core configuration SB-MOD.

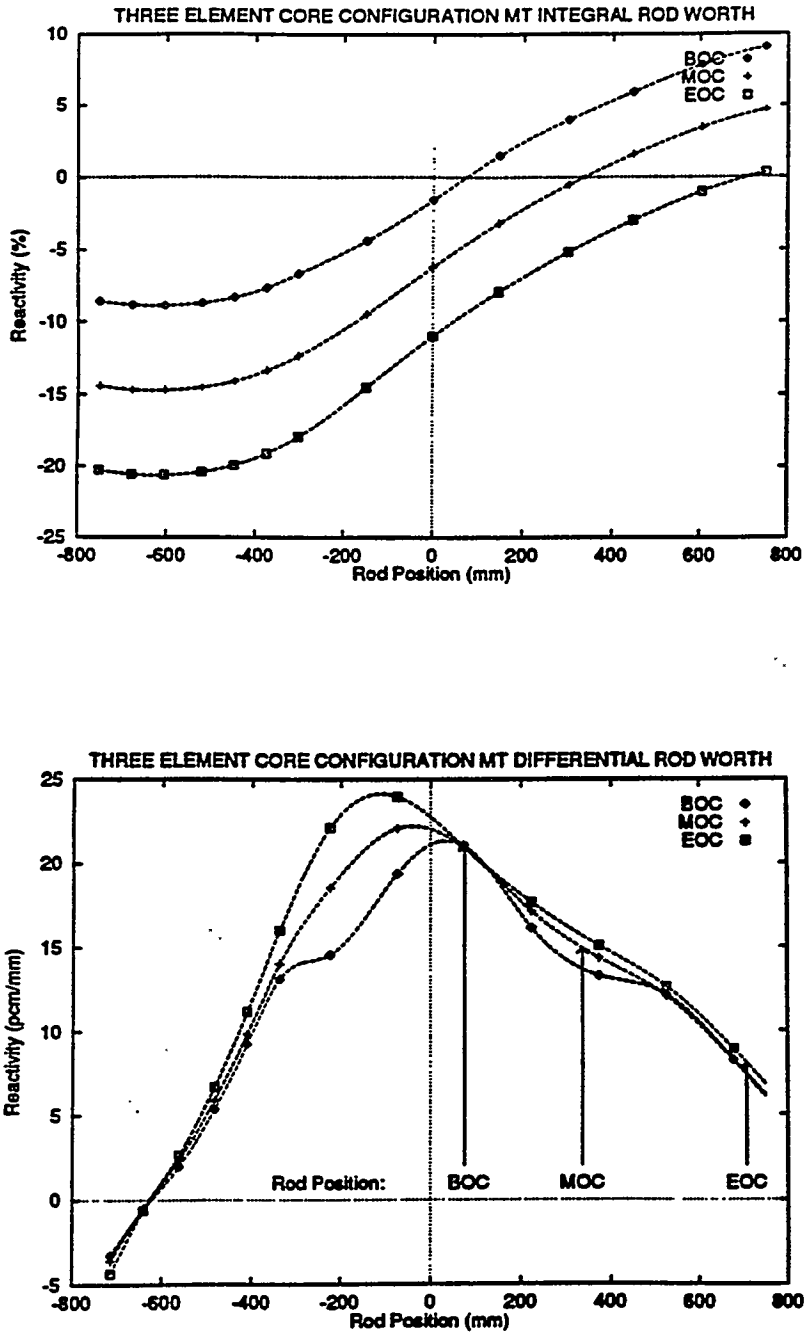

Fig. 4.30. Integral and differential control rod worth curves for three-element core configuration MT.

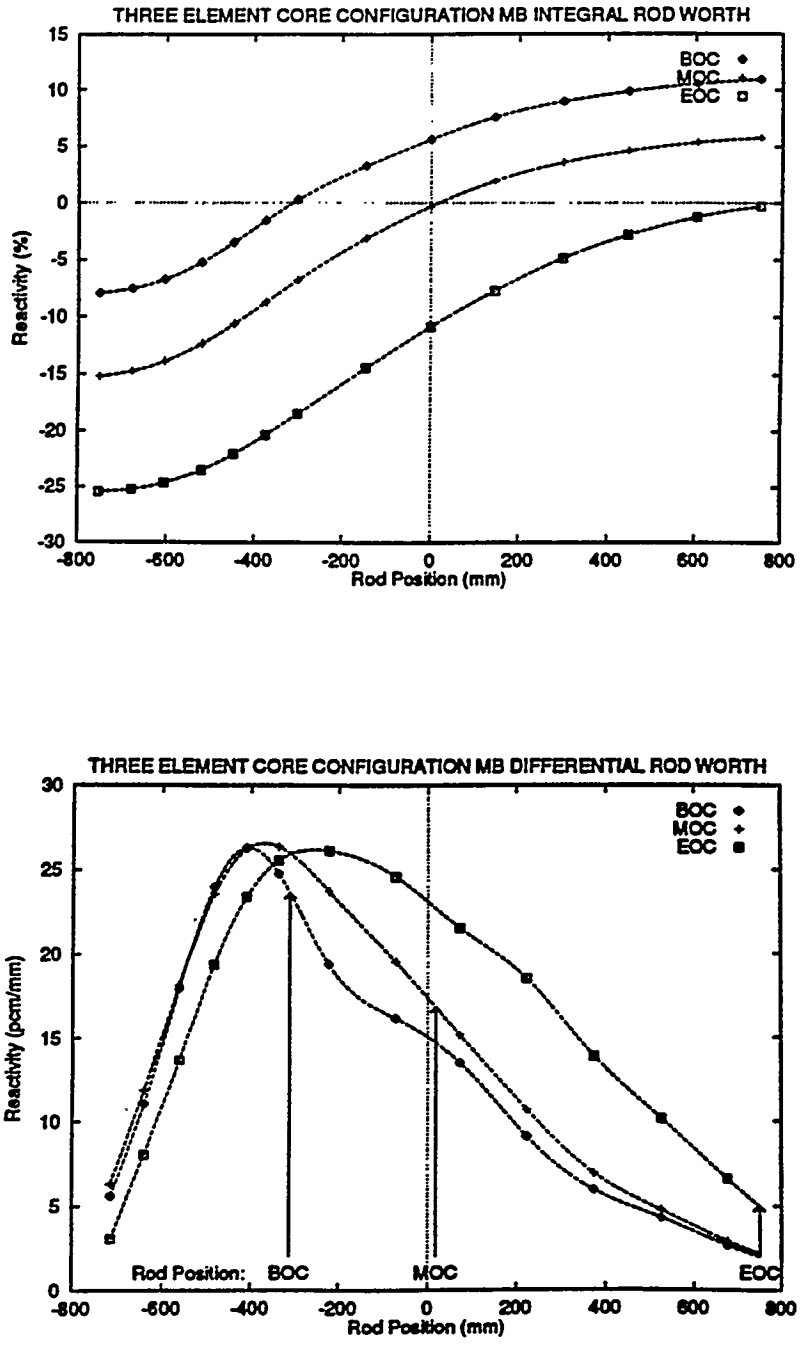

Fig. 4.31. Integral and differential control rod worth curves for three-element core configuration MB.

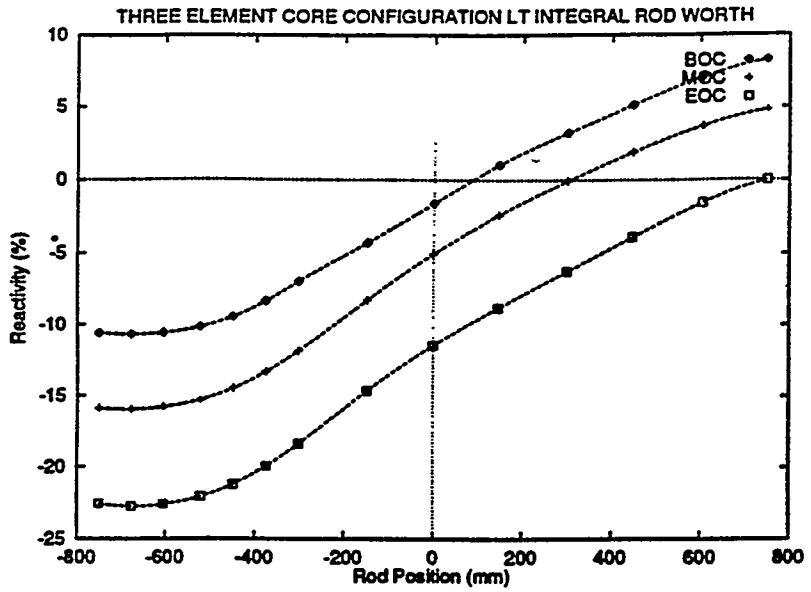

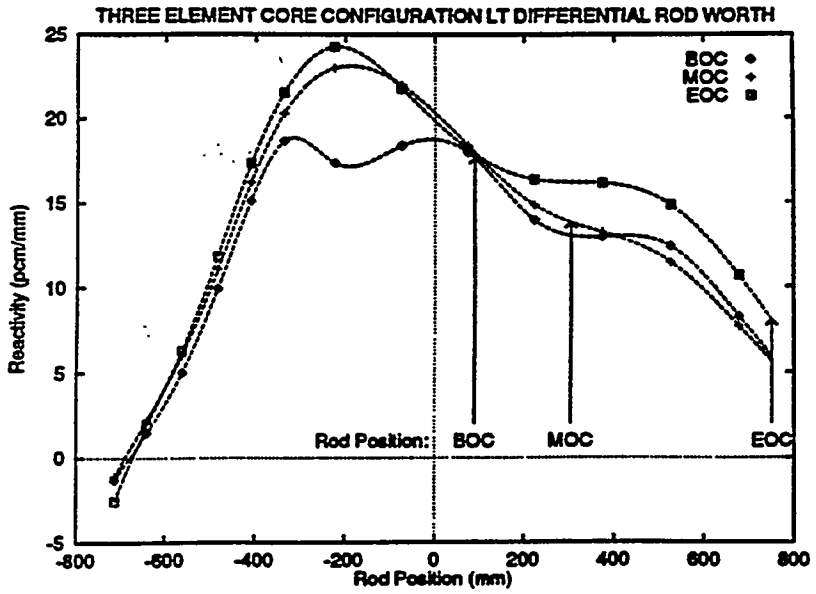

Fig. 4.32. Integral and differential control rod worth curves for three-element core configuration LT.

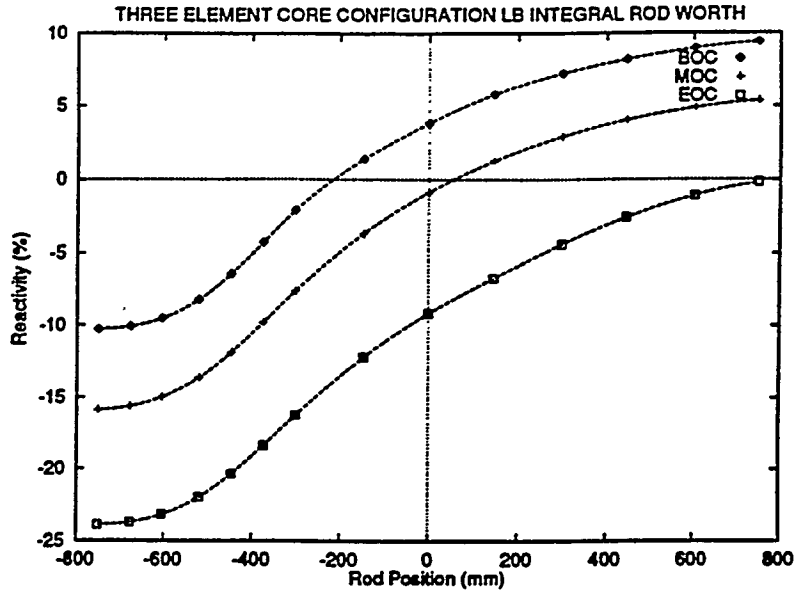

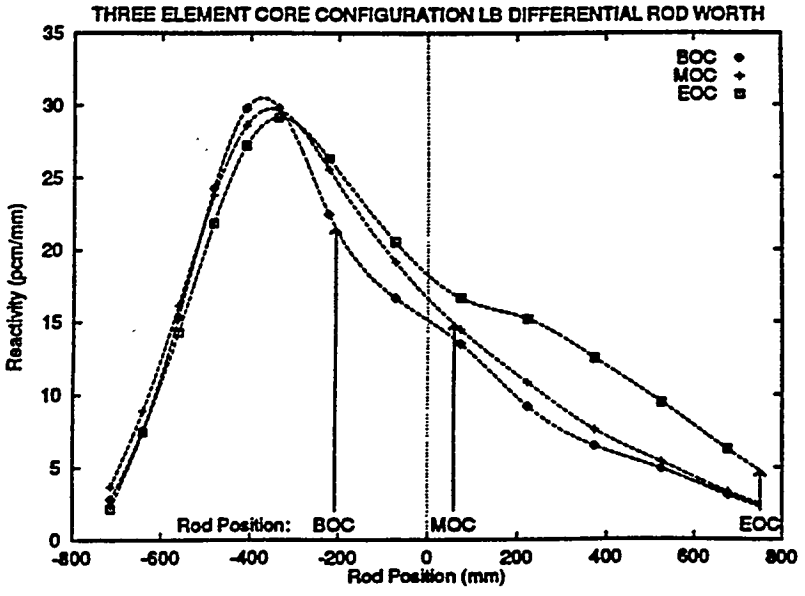

Fig. 4.33. Integral and differential control rod worth curves for three-element core configuration LB.

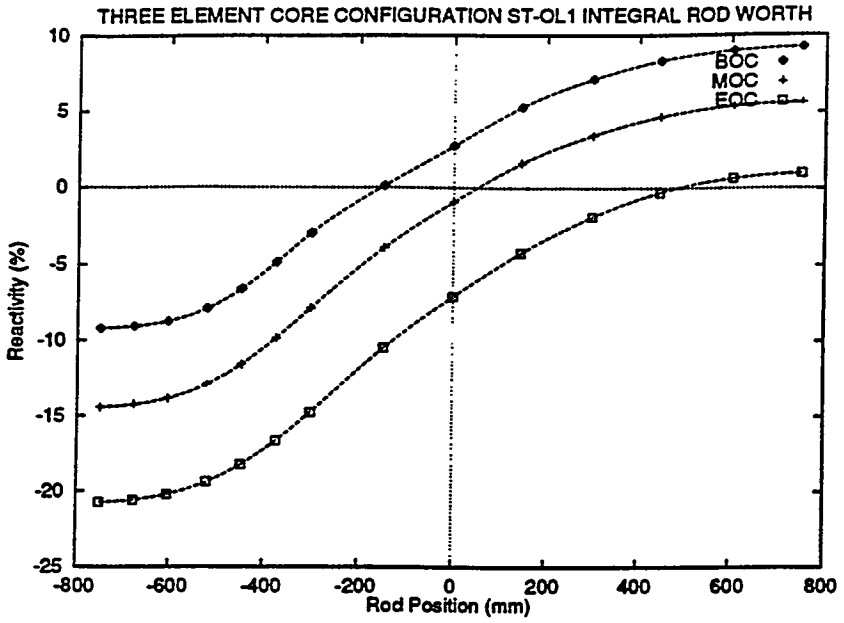

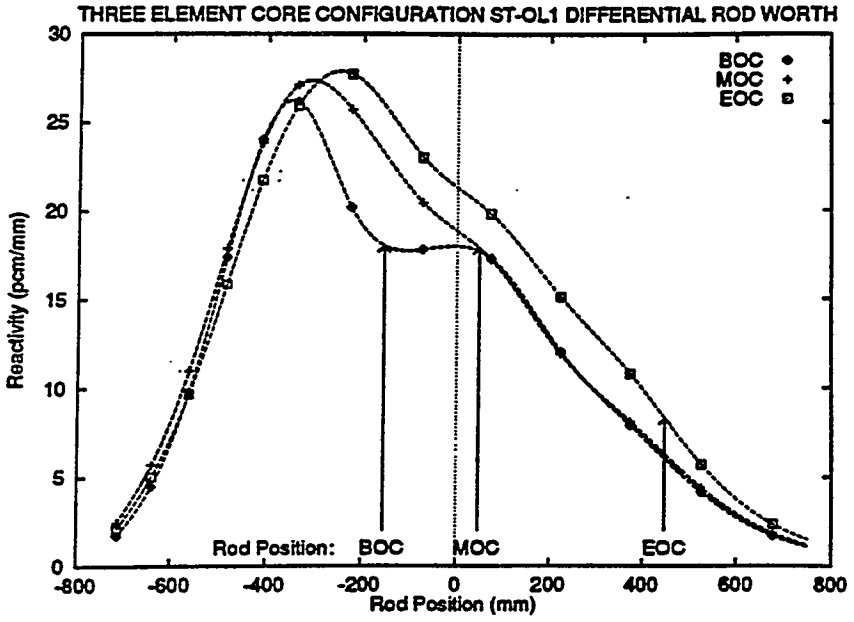

Fig. 4.34. Integral and differential control rod worth curves for three-element core configuration ST-OL1.

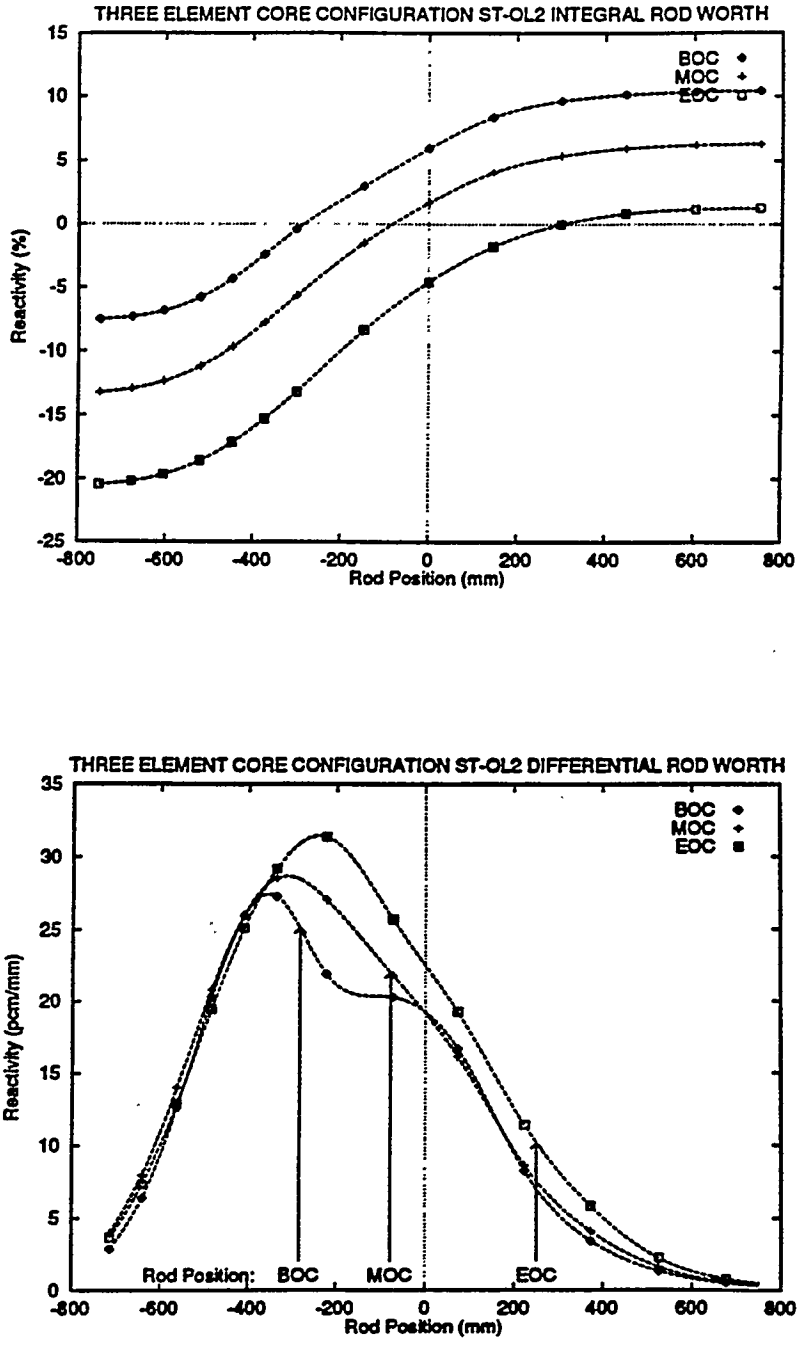

Fig. 4.35. Integral and differential control rod worth curves for three-element core configuration ST-OL2.

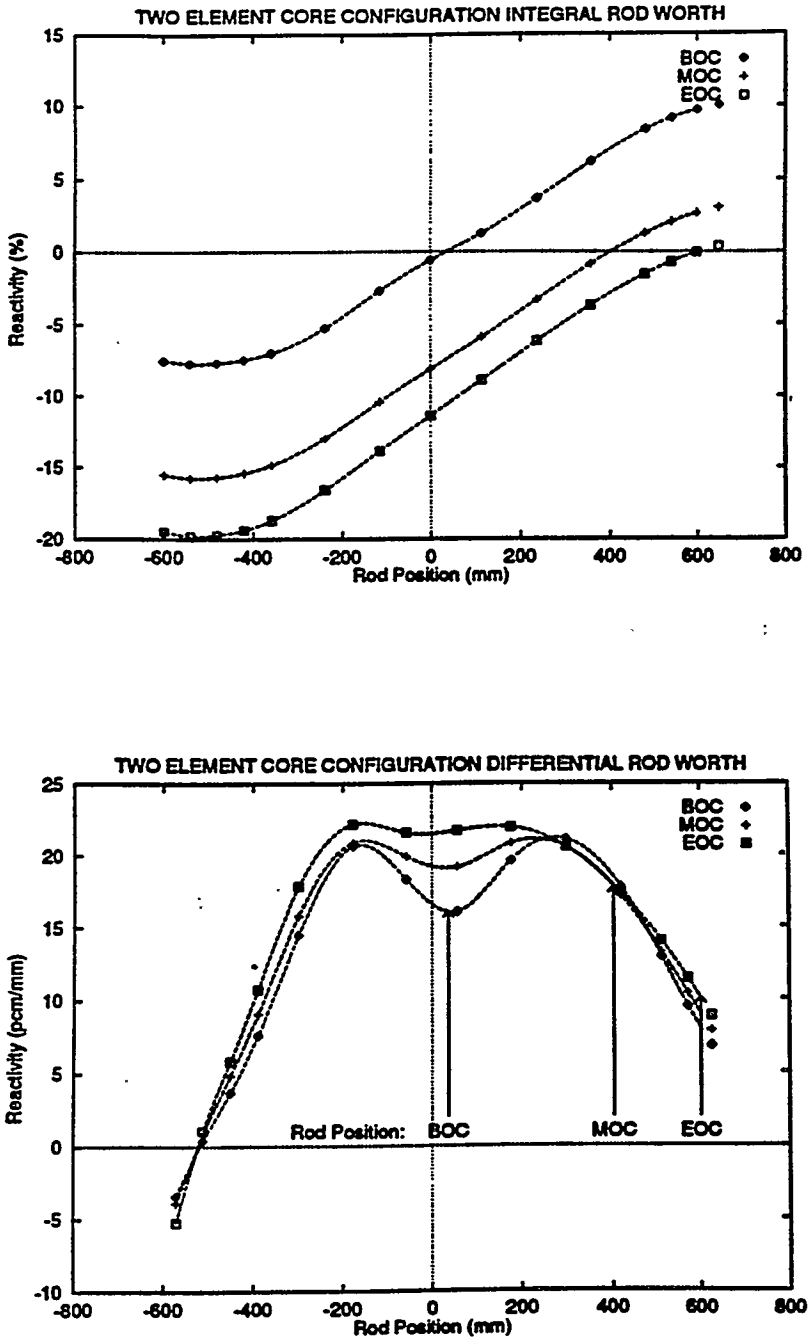

Fig. 4.36. Integral and differential control rod worth curves for two-element conceptual core configuration.

Table 4.1. Summary of results for the two-element and three-element core configurations

	ST	ST-MOD	SB	SB-MOD	MT	MB	LT	LB	ST-OL1	ST-OL2	Two-element core
Fuel density (gU/mL)	0.95	0.95	0.95	0.95	0.95	0.95	0.95	0.95	0.95	0.91	1.7
Rod position (mm from MP)											
BOC	11.6	84.0	–185.5	–220.5	76.0	–301.0	89.4	–201.1	–138.2	–277.0	54.8
EOC	750.0	750.0	750.0	750.0	707.0	750.0	748.4	750.0	684.6	603.9	600.0
B-10 loading (g)											
BOC	17.56	17.52	14.62	14.62	16.77	13.68	17.43	15.69	17.56	17.02	12.76
EOC	.14	.14	.27	.33	.16	.31	.24	.26	0.49	0.38	.22
Component reactivity worth(%)											
BOC	–5.4	–5.8	–5.0	–4.7	–6.9	–5.5	–8.3	–6.9	–6.3	–7.2	–10.5
EOC	–6.7	–6.6	–5.8	–5.6	–7.1	–6.3	–7.7	–7.6	–7.4	–7.5	–10.6
Peak thermal flux (10^{19} m^{-2} s^{-1})											
BOC	5.15	5.10	6.07	6.19	5.10	5.93	5.53	5.52	5.23	5.75	6.44
MOC	5.30	5.30	5.94	6.15	5.51	6.14	5.78	5.93	5.77	6.09	6.67
EOC	5.65	5.68	5.76	5.72	5.79	5.80	5.77	5.72	6.08	6.42	6.83
Thermal flux at beam tube tip (r=430 mm, z=0)											
BOC	4.58	4.67	4.33	4.26	5.08	4.59	5.48	5.00	5.06	5.45	6.11
MOC	5.14	5.15	5.13	4.97	5.46	5.19	5.74	5.44	5.56	5.60	6.45
EOC	5.24	5.20	5.32	5.32	5.51	5.75	5.50	5.67	6.05	6.29	6.46
Thermal/fast flux ratio at beam tube tip (r = 430 mm, z = 0)											
BOC	382	412	415	469	107	121	40	42	72	42	191
MOC	375	419	378	434	114	120	44	45	75	48	188
EOC	414	466	409	457	127	121	52	50	81	51	200
Thermal flux at cold source center (r= 750 mm, z = 25 mm)											
BOC	2.76	2.78	2.70	2.67	2.99	2.82	3.22	3.03	3.01	3.10	3.34
MOC	2.97	2.98	2.97	2.91	3.15	3.05	3.37	3.24	3.15	3.18	3.48
EOC	3.12	3.11	3.11	3.10	3.26	3.29	3.36	3.40	3.40	3.48	3.55
Thermal flux at hot source center (r = 1000 mm, z = 0)											
BOC	1.71	1.72	1.73	1.71	1.78	1.76	1.88	1.82	1.80	1.83	1.97
MOC	1.81	1.81	1.84	1.83	1.86	1.88	1.96	1.93	1.87	1.88	2.03
EOC	1.89	1.89	1.89	1.89	1.94	1.96	1.98	2.00	1.99	2.02	2.08

Table 4.2. Thermal flux and thermal-to-fast flux ratio for three-element core configurations at midplane and best beam-tube location

Configuration	Radius (mm)	Height (mm)	BOC	MOC	EOC	Cycle avg.
ST	430	0	4.83/382[a]	5.46/375	5.61/414	5.11/379
ST-MOD	430	0	4.96/412	5.49/419	5.56/466	5.10/423
SB	430	0	4.56/414	5.43/378	5.64/409	5.10/381
SB-MOD	430	0	4.46/468	5.21/434	5.62/456	5.02/430
MT	430	0	5.45/107	5.86/113	5.91/127	5.43/114
MB	430	0	4.85/121	5.52/120	6.12/120	5.28/118
LT	430	0	5.96/ 39	6.25/ 44	5.95/ 51	5.65/ 44
LB	430	0	5.36/ 41	5.87/ 45	6.13/ 49	5.49/ 44
ST-OL1	430	0	5.06/ 72	5.53/ 75	6.06/ 81	5.59/ 75
ST-OL2	430	0	5.45/ 43	5.61/ 47	6.29/ 51	5.71/ 47
ST	430	26	4.77/376	5.44/364	5.68/396	5.11/366
ST-MOD	430	99	4.72/311	5.46/293	5.84/310	5.14/294
SB	434	–193	5.63/122	6.19/134	5.05/192	5.49/141
SB-MOD	436	–199	5.65/120	6.23/129	5.10/186	5.55/138
MT	434	78	5.40/122	5.87/124	6.10/137	5.48/125
MB	451	–204	5.76/122	6.35/124	5.64/157	5.77/129
LT	485	16	5.81/121	6.08/134	5.85/156	5.51/135
LB	466	–183	5.77/122	6.28/125	5.74/149	5.68/128
ST-OL1	430	–110	5.17/173	5.69/173	5.90/188	5.66/174
ST-OL2	467	–170	5.66/122	5.97/128	6.18/145	5.96/130

[a]Thermal flux (10^{19} m^{-2} s^{-1})/thermal-to-fast flux ratio.

Table 4.3. Reactivity insertion rates (pcm/mm)

Configuration	BOC	MOC	EOC
ST	15.0	10.0	6.3
ST-MOD	14.3	11.0	7.0
SB	17.7	9.8	8.8
SB-MOD	19.5	10.2	8.3
MT	21.1	14.9	6.8
MB	23.6	16.9	5.0
LT	17.8	13.8	8.0
LB	22.0	15.0	4.7
ST-OL1	18.0	17.9	6.7
ST-OL2	25.1	27.0	8.1
2-element	16.0	17.7	10.0

Table 4.4. Control rod insertion (mm) from critical position required for one dollar of negative reactivity
(Effective delayed neutron fraction = 0.0077)

Configuration	BOC	MOC	EOC
ST	50	77	108
ST-MOD	48	70	100
SB	42	74	85
SB-MOD	38	69	88
MT	35	49	102
MB	32	44	126
LT	42	54	91
LB	34	49	130
ST-OL1	42	40	108
ST-OL2	31	36	65
Two-element	45	41	66

Table 4.5. Fuel-element criticality parameters (BOC, clean elements)

	ST			ST-MOD			Two-element	
Element	Small	Medium	Large	Small	Medium	Large	Small	Large
Volume (L)	23.4	29.3	29.9	20.8	28.4	33.6	28.4	39.2
^{235}U (kg)	4.88	6.11	6.25	4.34	5.92	7.02	8.74	14.86
^{10}B (g)	5.44	6.89	5.25	4.86	6.64	6.02	6.73	6.03
k_{eff}	1.062	1.149	1.210	1.054	1.144	1.209	1.160	1.288

5. SUMMARY AND RECOMMENDATIONS

Calculations of several important neutronic parameters have been performed for ten different three-element configurations considered for the ANS. Six of these configurations (ST, SB, MT, MB, LT, and LB) are the result of the permutations of the same three elements, two configurations (ST-MOD and SB-MOD) have the same element configuration as their base core designs (ST and SB) but have slightly different element dimensions, and two configurations (ST-OL1 and ST-OL2) have two elements that overlap to increase the neutron fluxes in the reflector. Descriptions of all of the configurations are given in Chap. 2, and descriptions of the calculational models are given in Chap. 3. For each configuration, along with the conceptual two-element design, fuel cycle calculations were performed along with calculations required to obtain unperturbed fluxes. Element power densities, neutron flux as a function of position throughout the cycle, fast flux and fast-to-thermal flux ratios, irradiation and production region fluxes, and control rod worth curves were presented in Chap. 4. The effective multiplication factor for each individual fuel element was also computed to assess the impact that changing to a three-element design has on fuel-element criticality issues that must be addressed during refueling procedures.

The determination of the best configuration requires careful examination of the results presented in Chap. 4 because some of the configurations perform better in some areas. To assist in the decision process, a comparison chart of the calculated parameters is given in Table 5.1. In this chart a score ranging from one to five was given to each configuration in each category, with a score of one indicating good performance and a score of five indicating poor performance. The scores were then combined using an equal weighting to give a single, representative number. As the comparison chart shows, the ST core configurations have the best scores with the fully overlapping core configuration ST-OL2 having the best overall score by a considerable margin. Therefore, this fully overlapping configuration is recommended for further consideration for a three-element ANS reactor core.

The ranking processes described previously are somewhat arbitrary in the sense that a single number has been used to indicated the performance over relatively broad categories. Such a process is based on the overall view of the results presented in each section of Chap. 4 and can vary depending on how the importance of particular quantities are viewed. Other considerations, such as thermal-hydraulics, safety, and engineering, which are not directly related to the core neutronic performance must be weighed before a final design is chosen.

In comparison with the two-element conceptual design, the only major area in which the ST-OL2 configuration is significantly worse is the reflector neutron fluxes. The three-element configuration, however, has the advantage of a lower fuel density requirement and lower average power densities.

Table 5.1. Three-element configuration comparison chart
The score for each category ranges from one to five, with one being the best score

Configuration	Fuel cycle (power) score	Reflector neutron flux score	Materials irradiation/isotope production flux score	Control rod insertion rate score	Total score
ST	1	4	2	2	9
ST-MOD	1	4	2	2	9
SB	5	3	2	1	11
SB-MOD	5	2	2	1	10
MT	1	4	4	2	11
MB	5	2	5	3	15
LT	3	4	3	1	11
LB	5	3	3	3	14
ST-OL1	1	2	4	2	9
ST-OL2	2	1	1	1	5

6. REFERENCES

1. *ANS Conceptual Design Report Summary,* ORNL/TM-12184, Martin Marietta Energy Systems, Inc., Oak Ridge Natl. Lab., Oak Ridge, TN, September 1992.

2. R. A. Bari, H. Ludewig, and J. Weeks, *Advanced Neutron Source Enrichment Study,* BNL-52433, Brookhaven National Laboratory, Upton, NY, December 1994.

3. E. E. Alston, J. C. Gehin, C. D. West, *Fuel Density, Uranium Enrichment, and Performance Studies for the Advanced Neutron Source Reactor,* ORNL/TM-12775, Martin Marietta Energy Systems, Inc., Oak Ridge Natl. Lab., Oak Ridge, TN, June 1994.

4. C. D. West, *Optimization of PS-2 Core Configuration for the ANS Reactor,* ORNL/M-898, Martin Marietta Energy Systems, Inc., Oak Ridge Natl. Lab., Oak Ridge, TN, 1989.

5. G. L. Copeland et al., *Advanced Neutron Source Final Preconceptual Reference Core Design,* ORNL/TM-11234, Martin Marietta Energy Systems, Inc., Oak Ridge Natl. Lab., Oak Ridge, TN, 1989.

6. D. R. Vondy, T. B. Fowler, and G. W. Cunningham, *The BOLD VENTURE Computation System for Nuclear Reactor Core Analysis, Version III,* ORNL-5711, Union Carbide Corporation, Oak Ridge Natl. Lab., Oak Ridge, TN, June 1981.

7. N. M. Green, W. E. Ford, III, L. M. Petrie, and J. W. Arwood, *AMPX-77: A Modular Code System for Generating Couple Multigroup Neutron-Gamma Cross Section Libraries from ENDF/B-IV and/or ENDF/B-V,* ORNL/CSD/TM-283, Martin Marietta Energy Systems, Inc., Oak Ridge Natl. Lab., Oak Ridge, TN, October 1992.

8. *SCALE 4.1, A Modular Code System for Performing Standardized Computer Analysis for Licensing Evaluation,* CCC-545, Radiation Shielding Information Center, Martin Marietta Energy Systems, Inc., Oak Ridge Natl. Lab., Oak Ridge, TN, July 1992.

9. W. E. Ford, III, *ANSL-V: ENDF/B-V Based Multigroup Cross-Section Libraries for Advanced Neutron Source (ANS) Reactor Studies,* ORNL-6681, Martin Marietta Energy Systems, Inc., Oak Ridge Natl. Lab., Oak Ridge, TN, September 1990.

10. J. F. Briesmeister, ed., *MCNP - A General Monte Carlo Code for Neutron and Photon Transport, Version 3B,* LA-7396-M, Rev. 2, Los Alamos Natl. Lab., Los Alamos, NM, April 1991.

11. L. A. Smith and J-P. Renier, *Implementation of CTRLPOS, A VENTURE Module for Control Rod Position Criticality Searches, Control Rod Worth Curve Calculations, and General Criticality Searches,* ORNL/TM-12746, Martin Marietta Energy Systems, Inc., Oak Ridge Natl. Lab., Oak Ridge, TN, June 1994.

INTERNAL DISTRIBUTION

1. B. R. Appleton
2–3. J. H. Campbell
4. J. E. Cleaves
5. F. X. Gallmeier
6–10. J. C. Gehin
11. R. M. Harrington
12. D. T. Ingersoll
13. R. A. Lillie
14. T. J. McManamy
15. J. P. Renier
16. R. B. Rothrock
17. D. L. Selby
18. C. D. West
19–23. B. A. Worley
24. G. L. Yoder
25. CPED Reports Office
26. ORNL Patent Office
27. Central Research Library Document Reference Section
28–29. Laboratory Records Dept.
30. Laboratory Records, ORNL-RC

EXTERNAL DISTRIBUTION

31. J. M. Ryskamp, Idaho National Engineering Laboratory, P.O. Box 1625, Idaho Falls, ID 83415
32. C. A. Wemple, Idaho National Engineering Laboratory, P.O. Box 1625, Idaho Falls, ID 83415
33. ANS Project Office, U.S. Department of Energy, Oak Ridge Field Office, P.O. Box 2009, FEDC, MS-8218, Oak Ridge, TN 37831-8218
34. Office of Assistant Manager for Energy Research and Development, Department of Energy, Oak Ridge Field Office, P.O. Box 2001, Oak Ridge, TN 37831-2001.
35–36. Office of Scientific and Technical Info., P.O. Box 62, Oak Ridge, TN 37831